A Systematic Procedure to Determine Controller Parameters for MMC-VSC Systems

by

Arunprasanth Sakthivel

A dissertation submitted to the Faculty of Graduate Studies of

The University of Manitoba

in partial fulfillment of the requirements for the degree of

Doctor of Philosophy

Department of Electrical and Computer Engineering

University of Manitoba

Winnipeg, MB, Canada

To my father Sakthivel, mother Jothimani, and wife Shailajah...

Acknowledgement

First of all, my deepest gratitude goes to my advisor, Prof. U.D. Annakkage and my co-advisor, Dr. C. Karawita for their continuous advice, guidance, and encouragement throughout my doctoral studies. It is a privilege for me to work with them and I am grateful for their generosity to share their deep knowledge on this work. I sincerely thank Prof. A.M. Gole for his assistance and advice on this research work. I would also like to thank Prof. N. Sepehri for his encouragement and advice. Without their guidance, this thesis would not have reached the same level as it is today. I must also thank all academic, administrative, and technical staffs at the Department of Electrical and Computer Engineering, especially Erwin Dirks, Traci Gledhill, and Amy Dario for their assistance.

I would like to acknowledge the financial supports received from the University of Manitoba, the Government of Manitoba, the Mitacs accelerate program, and the RTDS Technologies Inc.

I would like to thank the director, Eng. R. Kuffel and my colleagues at the RTDS Technologies Inc. for their technical support. I must also thank all my friends at the Department of Electrical and Computer Engineering for their continuous encouragement and for making my years at the University of Manitoba a pleasant experience.

This acknowledgement would not be complete without thanking my family. Many thanks to my father, mother, brother, and sister for their love and encouragements for all these years. Last but not least, I extend my heartfelt gratitude to my wife for her understanding and encouragements during my hard times.

Abstract

Modular multilevel converter type voltage source converter (MMC-VSC) is a potential candidate for present and future HVdc projects. The d-q decoupled control system is widely used to control MMC-VSC systems. Selection of PI-controller parameters for MMC-VSC systems is a challenging task as control loops are not completely decoupled. Since there is no widely accepted method to tune these control loops, the industry practice is to use the trial and error approach that requires a great amount of time. Therefore, it is required to develop a systematic procedure to tune PI-controllers considering necessary system dynamics and also to propose guidelines for control system design.

This thesis introduces a systematic procedure to determine PI-controller parameters for the d-q decoupled control system. A linearized state-space model of an MMC-VSC system is developed to calculate the frequency-domain attributes. The controller tuning problem is formulated as an optimization problem which is general and any meta-heuristic method can be used to solve the problem. In this thesis, the simulated annealing is applied to solve the problem. The efficacy of the tuned parameters is tested on the electromagnetic transient model of the test system on the real-time digital simulators (RTDS). In addition, it is shown that the proposed method is suitable to tune PI-controller parameters for MMC-VSC systems connected to strong as well as weak ac networks.

Further, this thesis investigates the effects of d-q decoupled controller parameters, phase-locked loop (PLL) gains, and measuring delays on the stability and performance of the MMC-VSC test system. It is shown that the converter controllers have greater influence on the system stability and the impact of PLL gains is negligible unless very high PLL gains are used. In addition, the negative impact of measuring de-

lays in instantaneous currents and voltages is also analysed by performing eigenvalue and sensitivity analysis. Finally, a set of guidelines for control design of MMC-VSC systems is summarized.

In general, the proposed controller tuning procedure would be useful for the industry to tune PI-controllers of MMC-VSC systems. Furthermore, the proposed methodology is generic and can be adapted to tune of any dynamic device in power systems.

List of Principal Symbols

t	time
ω_0	Base angular frequency of a power system
ω	Angular frequency of a power system
λ	Eigenvalue
f, ζ	Frequency and damping of a mode of system
v, i	Fundamental ac voltage and ac current
V, I	Phasor quantities of v, i
$\hat{v}$	Peak value of voltage v
$v_{(l-l)}$	Line to line value of voltage v
$v_{(l-g)}$	Line to ground value of voltage v
v_t, i_t	Instantaneous voltage and current at the converter terminal
V_t, P_t, Q_t	RMS values of voltage, active power, and reactive power
r_s, L_s, r_p	Thévenin equivalent impedance (RRL format)
v_s	Thévenin equivalent voltage
v_i	Internal voltage of the converter ac terminal
r_{arm}, L_{arm}	Arm impedance
r_{SM}, C_{SM}	Sub-module (SM) resistor and capacitor values
r_{dc}, L_{dc}, C_{dc}	DC transmission line parameters
v_{dc}, i_{dc}	DC voltage and current
$v_{dc(p-p)}$	peak to peak value of the dc voltage
N	Number of SMs per arm
δ	Actual voltage phase angle of v_t
δ_m	PLL measured voltage phase angle of v_t
K_P, K_I	Proportional and integral gains of a PI-controller
T	Time-constant of a single pole delay block
v_o	Voltage order from the control system
Subscript (r)	Reference value
Subscript (m)	Measured value
Subscripts R, I	Real and imaginary components
Subscripts d, q	Direct and quadrature components
Subscripts $1, 2$	Converter 1 and 2
Subscript 0	Denotes the initial value

Acronyms

AC	Alternative Current
APF	Active Power Filter
CSC	Current Sourced Converter
DC	Direct Current
EMT	Electro-Magnetic Transient
FACTS	Flexible Alternative Current Transmission System
HVDC	High Voltage Direct Current
IGBT	Insulated Gate Bi-polar Transistor
MLC	Multi-Level Converter
MMC	Modular Multi-level Converter
OEMT	Optimization-enabled EMT
PI	Proportional Integral
PLL	Phase-Locked Loop
PMU	Phasor Measurement Unit
PSO	Particle Swarm Optimization
PSS	Power System Stabilizer
RMS	Root Mean Square
RTDS	Real-Time Digital Simulators
SCR	Short Circuit Ratio
SRF-PLL	Synchronous Reference Frame PLL
SS	Small-Signal
STATCOM	Static Compensator
TCSC	Thyristor Controlled Series Capacitor
VSC	voltage Sourced Converter

Contents

1 Introduction 1
1.1 Background . . . 1
1.1.1 History of DC Transmission . . . 3
1.1.2 Voltage Source Converter Technology . . . 3
1.1.3 Review of Previous Works on Control System Modelling and Tuning . . . 6
1.1.4 Sensitivities of VSC System Stability . . . 11
1.2 Research Objectives . . . 12
1.3 Thesis Outline . . . 13

2 Modelling of a Point-to-Point MMC-VSC System 15
2.1 Electromagnetic Transient Modelling of Test System . . . 15
2.2 Development of Linearized Model . . . 17
2.2.1 AC Network Model . . . 19
2.2.2 DC Network Model . . . 21
2.2.3 Phase-Locked Loop Model . . . 24
2.2.4 Converter Model . . . 25
2.2.5 Control System Model . . . 27
2.2.6 Measurement Filter Model . . . 36
2.2.7 Axis Transformation . . . 38
2.2.8 Overall State-Space Model . . . 41
2.3 Validation of Linearized Model . . . 43
2.3.1 Validation of AC System and PLL Models . . . 43
2.3.2 Validation of Complete Linearized Model of VSC System . . . 45
2.4 Chapter Summary . . . 49

3 Small-Signal Stability Assessment of MMC-VSC System 50
3.1 Small-Signal Stability Assessment . . . 51
3.1.1 Eigenvalues and System Stability . . . 51
3.1.2 Modes . . . 52
3.1.3 Eigenvectors . . . 53
3.1.4 Participation Factors . . . 54
3.2 Eigenvalue Analysis of Test System . . . 55
3.3 Participation Factor Analysis of Test System . . . 56
3.4 Sensitivity Analysis . . . 59
3.4.1 Effect of AC System Strength . . . 59
3.4.2 Effects of PLL Gains . . . 60
3.4.3 Effects of Measuring Delays . . . 62
3.5 Chapter Summary . . . 69

4 Generalized Frequency-Domain Controller Tuning Procedure 70
4.1 Application of Linear Control Techniques . . . 71
4.2 Development of Generalized Frequency Domain Controller Tuning Procedure . . . 72
4.2.1 Penalty Functions . . . 73
4.3 Simulated Annealing . . . 75
4.3.1 Physical Annealing Process . . . 76
4.3.2 Simulated Annealing Optimization Technique . . . 77
4.4 Application of the Simulated Annealing Optimization Method to Solve the Optimization Problem . . . 77
4.5 Application of the Proposed Controller Tuning Procedure to the Test System . . . 81
4.5.1 Performance Criteria to Solve the Optimization Problem . . . 81
4.5.2 Selection of Initial Values for Controller Parameters . . . 82
4.5.3 Discussion on Tuned Controller Parameters . . . 83
4.5.4 Performance Evaluation of Tuned Parameters . . . 85
4.6 Steps to Tune Controllers of an MMC-VSC System . . . 91
4.7 Chapter Summary . . . 92

5 Important Aspects of Controller Tuning of MMC-VSC Systems 93
5.1 Impact of AC System Strength . . . 93
5.1.1 Short Circuit Ratio Estimation . . . 95
5.1.2 Tuning of Controllers Considering Weak to Strong AC Systems 101
5.1.3 Performance of Tuned Controller Gains with Weak AC Systems 101
5.1.4 Performance Comparison of Tuned Controller Gains for Weak to Strong AC Systems . . . 105
5.1.5 Tuning of Controllers Considering both Strong and Weak AC Systems . . . 107
5.2 Impact of Measuring Delays . . . 112
5.2.1 Quick Power Reversal . . . 113
5.2.2 Three Phase to Ground Fault . . . 115
5.3 Discussion on Computation Time for Controller Tuning . . . 116
5.4 Guidelines for MMC-VSC Control System Design . . . 117
5.5 Chapter Summary . . . 118

6 Conclusions, Contributions, and Future Work 120
6.1 General Conclusions . . . 120
6.2 Contributions . . . 122
6.3 Future Work . . . 123

A Additional Information 125
A.1 Generation of AC Voltage Using Voltage Source Converters 125
A.2 Introduction to the RTDS Simulators 126
A.3 Open Loop Test on PLL Gains 127

List of Figures

1.1 Control block diagram of an MMC (r-reference, m-measured, and o-order) . . . 6
1.2 d-q decoupled control system (r-reference, m-measured, and o-order) . 7

2.1 Point-to-point MMC-VSC test system . . . 16
2.2 Circuit diagram of the ac network . . . 20
2.3 DC system representation . . . 22
2.4 PLL block diagram (a) R-I voltages and (b) SRF-PLL . . . 24
2.5 Generation of ac voltage using MMC . . . 26
2.6 Block diagram of the d-q decoupled control system (r-reference, m-measurement, and o-order) . . . 28
2.7 Functional block diagram of the current limiter . . . 29
2.8 Block diagram of the PI-controller . . . 29
2.9 Block diagram of the single-pole measurement filter . . . 36
2.10 R-I to d-q transformation . . . 39
2.11 27th order small-signal model of the point-to-point MMC-VSC system 42
2.12 Test system used to validate the ac network and PLL models . . . 44
2.13 Disturbance applied to the Thévenin voltage magnitude . . . 45
2.14 Simulation results comparison for a sinusoidal disturbance with (a) 20 Hz and (b) 200 Hz applied to the Thévenin voltage magnitude . . . 46
2.15 Disturbance applied to the Thévenin voltage phase angle . . . 46
2.16 Simulation results comparison for a sinusoidal disturbance with (a) 20 Hz and (b) 200 Hz applied to the Thévenin voltage phase angle . . . 47
2.17 Changes in variables for a small pulse applied at 0.2 s to (a) the dc voltage reference of terminal1 and (b) the power reference of terminal2 48
2.18 Changes in variables for a small pulse applied at 0.2 s to the ac voltage reference of (a) terminal1 and (b) terminal2 . . . 49

3.1 Participation factors associated with Mode 5 . . . 57
3.2 Participation factors associated with the ac network modes (State numbers are given in Table 3.3) . . . 58
3.3 Participation factors associated with the controller modes (State numbers are given in Table 3.3) . . . 59
3.4 Loci of critical modes for the change in ac system strength . . . 60
3.5 Loci of critical modes for a change in MMC1 (dc voltage controlling) PLL gains . . . 61
3.6 Loci of critical modes for a change in MMC2 (power controlling) PLL gains . . . 62
3.7 Inner-loop of d-q decoupled controller with measuring delay models . 63
3.8 35th order small-signal model of the point-to-point MMC-VSC system 64
3.9 Block diagram of the measuring delay model . . . 65

3.10 Participation factors of states to measurement delay modes (state numbers are given in Table 3.5) 67
3.11 Loci of critical modes for a change in rectifier (dc voltage controlling) side PLL gains 68
3.12 Loci of critical modes for a change in inverter (power controlling) side PLL gains 68
3.13 Variation of dc voltage for a step change in PLL gain of MMC2 (power controlling converter) 69

4.1 Flow chart to explain the simulated annealing algorithm 79
4.2 Variations of values of objective function with the iteration number . 84
4.3 Variations of active power, dc current, ac voltage, and dc voltage for a step change in dc voltage reference at 0.2 s 86
4.4 Variations of active power, dc current, ac voltage, and dc voltage for a step change in active power reference at 0.2 s 87
4.5 Variations of active power, dc current, ac voltage, and dc voltage for a power order change at 0.2 s 88
4.6 Variations of active power, dc current, ac voltage, and dc voltage for a three phase fault on terminal1 at 0.2 s 89
4.7 Variations of active power, dc current, ac voltage, and dc voltage for a three phase fault on terminal2 at 0.2 s 90

5.1 Variations of ac and dc quantities for changes in ac system strength . 94
5.2 A simple electric circuit 97
5.3 Variations of active power, dc current, ac voltage, and dc voltage for a step change in reference power of terminal2 at 0.2 s (SCR1=SCR2=1.5) 103
5.4 Variations of active power, dc current, ac voltage, and dc voltage for a three phase fault at terminal2 at 0.2 s (SCR1=SCR2=1.5) 104
5.5 Variations of active power, dc current, ac voltage, and dc voltage for a step change in dc voltage of terminal1 at 0.2 s 106
5.6 Variations of active power, dc current, ac voltage, and dc voltage for a power order change to terminal2 applied at 0.2 s 107
5.7 EMT simulation results of dc current, active power, ac voltage, and dc voltage for quick power reversal (C1: case-1, C2: case-2, C3: case-3, and C4: case-4) 110
5.8 EMT simulation results of ac voltage, dc voltage, active power, and reactive power for a three phase fault at terminal2 (C1: case-1, C2: case-2, C3: case-3, and C4: case-4) 112
5.9 EMT simulation results of dc current, active power, ac voltage, and dc voltage for quick power reversal (C1: case-1, C2: case-2, C3: case-3, and C4: case-4) 115

5.10 EMT simulation results of ac voltage, dc voltage, active power, and reactive power for a three phase fault at terminal2 (C1: case-1, C2: case-2, C3: case-3, and C4: case-4) 116

A.1 Evolution of VSC technology 126
A.2 Model of SRF-PLL for open loop test 128
A.3 Response of PLL for step changes in input frequency 128

List of Tables

1.1 Comparison between VSC and LCC 5

2.1 Parameters of the Test System 16
2.2 State variables of the system 41
2.3 Control inputs of the system 41
2.4 Parameters of the simple power system 44
2.5 State variables and control inputs of the simple power system 44
2.6 PI-controller gains 47

3.1 PI-controller gains 55
3.2 Frequency and damping of system modes for different SCR values . . 56
3.3 System state numbers of the 27th order model 57
3.4 Classification of modes 58
3.5 System state numbers of the 35th order model 65
3.6 Measurement filter time-constants 66
3.7 Interested oscillatory modes after the inclusion of measuring delays . 66

4.1 Analogy between physical annealing and simulated annealing optimization 78
4.2 Optimization parameters 82
4.3 Operating points considered for controller tuning 83
4.4 Initial and tuned controller gains 84

5.1 Steady state phasor measurements 97
5.2 Maximum percentage error in SCR estimation with constant Thévenin voltage 99
5.3 Maximum percentage error in SCR estimation considering fluctuation in Thévenin voltage 100
5.4 Tuned PI-controller gains for different SCR 102
5.5 Tuned PI-controller gains for different cases 109
5.6 Tuned PI-controller gains for different cases considering the measuring delays 114
5.7 Average computation time 117

Chapter 1

Introduction

1.1 Background

Present power systems have already accepted plenty of renewable energy generation such as wind and solar in order to cater for the rapid increase in electrical energy demand. As a result, the existing transmission systems are heavily loaded and experience additional stress [1]. To supply the increase in electricity demand, the existing transmission system has to be upgraded with new transmission lines. In addition, the intermittent nature of renewable energy sources can cause undesirable oscillations in transmitted power. Therefore, additional power electronic devices known as the flexible ac transmission system (FACTS) devices are needed to control the power through those ac transmission lines [2]. Moreover, a relatively large corridor is required to build an ac transmission line. Considering the aforementioned challenges and to facilitate the integration of renewable energy generation, dc transmission systems that are capable of transmitting bulk power and able to provide better control of power are being built to strengthen the transmission system [3]. High-voltage dc (HVdc) transmission technology developments have taken place over the past half century and, at

present, it is the best technology available for long-distance bulk power transmission. With the advancement of technology, dc transmission is preferred for a handful of reasons [4, 5, 6, 7]:

- Economical for long-distance power transmission as it has less losses compared to an equivalent ac line and no reactive power compensation is required.
- Connection of asynchronous ac power systems to facilitate power trade and stability enhancement.
- Environmentally friendly as it requires a lower number of conductors (less space), it causes no ionic motion in cables, and it does not induce currents in sheaths of the conductor.
- Relaxed protection requirements as it produces less stress for the same voltage level of the ac transmission system.
- Improved stability and power quality to the power system as the power flow can be controlled to (a) improve the damping of poorly damped oscillations and (b) provide emergency power support for rotor angle stability enhancement.

The ac-dc converter technology has seen evolutions such as mercury arc valve based current sourced converter (CSC), thyristor based CSC, conventional (2-level and 3-level) voltage sourced converter (VSC), multi-level converter (MLC), and modular multi-level converter (MMC). Control methods, switching techniques, and protection schemes have also evolved to support this technology [8]. At present, the MMC-VSC technology is considered as a viable option for dc transmission systems below 2000 MW rating and the thyristor based CSC systems are still being used for bulk power transmission above 2000 MW rating [9, 10].

1.1.1 History of DC Transmission

The direct current (dc) was the first commercial form of electricity generation (in 1879) by the famous inventor Thomas Alva Edison. Then, inventions such as ac machines and ac transformers dominated the developments of dc and led the power industries to favour ac transmission. However, the slow and steady improvements in dc transmission technology over a period of 50 years (1879-1930) created opportunities to consider the use of dc power for transmission across long distances [11].

Research on HVdc dates back to 1930s and numerous contributions were made by researchers from Germany, Sweden, Switzerland, France and United States. However, it required about 20 years of research and development to step on the ground and build the first HVdc system. The world's first commercial HVdc transmission system was the Gotland-1 point-to-point HVdc link commissioned in 1954. The contributions made by Dr. August Uno Lamm to the Gotland-1 project and the HVdc developments around the world were immense. Due to his interests and involvements, Dr. Lamm is known as the father of HVdc transmission [12]. The Gotland-1 HVdc was an undersea transmission system to transfer 20 MW of power from Vastervik on the mainland to Ygne on the island of Gotland at 100 kV dc. The initial converters were made using mercury arc valves and were upgraded with thyristor valves in 1970. However, after commissioning of Gotland-2 (in 1983) and Gotland-3 (in 1985), the Gotland-1 HVdc link was decommissioned in 1986 [13]. The successful operation of Gotland-1 HVdc system gave confidence to build HVdc systems around the world.

1.1.2 Voltage Source Converter Technology

Voltage source converters (VSCs) were popular for many years in motor drive applications as the insulated-gate bi-polar transistor (IGBT) technology was well established.

The invention of high power IGBTs created opportunities to build VSCs that are capable for power system applications such as static compensator (STATCOM) and active power filters (APF). Later, the advantages of VSC technology over the LCC technology led the power industries to consider VSCs for HVdc applications [14]. VSC based HVdc transmission was a research topic for many years. The practical implementation of VSC-HVdc took place in 1997 with the test transmission system built in Hellsjön, Sweden with the rating of 3 MW [15]. Then, within two decades after the first practical implementation, many VSC-HVdc systems have been implemented around the world. Lists of VSC-HVdc systems that are either commissioned or in the planning stage can be found in [14, 16].

An overview of VSC-HVdc transmission systems is presented in [17] and it discusses about the fundamentals of VSC technology, VSC topologies, modelling and control of VSCs, HVdc circuit breakers, and finally the practical implementations of VSC-HVdc systems. Advantages of VSC are compared against the LCC in Table 1.1. Unlike in LCC, the power transmitted by a VSC can be reversed by reversing the direction of the current (i.e: without changing the voltage polarity). This facility has motivated researchers to think about multi-terminal dc (MTdc) systems.

Modular multilevel converter (MMC) is a specially designed VSC to support high voltage applications. In addition to the advantages offered by VSCs, there are unique advantages associated with MMCs and a few are listed below [18, 19],

- Scalable to support very high voltages due to its modular structure.
- Good harmonic performance so that no filtering is needed.
- Improved switching losses as each IGBT in sub-modules is switched at a rate close to the ac fundamental frequency.

Table 1.1: Comparison between VSC and LCC

Voltage source converter (VSC)	**Line commutated converter (LCC)**
Constructed using IGBT valves	Constricted using Thyristor valves
Avoids commutation failure	Can result in commutation failures due to disturbances in the ac voltage
Provides independent control of active and reactive powers	Independent control of active and reactive powers is not possible
Does not require reactive power compensation	Requires reactive power compensation (around 60 % of the rated power)
Power can be reversed by current reversal	Current reversal is not possible and the power reversal is done by reversing the dc voltage
Can connect to weak or dead ac networks	Difficult to connect to the weak ac connections

The interest on MMC-VSC technology for HVdc implementations has led many researchers to perform simulation studies of such systems. This include, studies of MMC-VSC systems with different types of sub-modules, converter topologies, grounding schemes, protection techniques, and control methods. However, a relatively greater effort is being spent on control development as it is the heart of HVdc transmission. The vector control method developed based on the d-q reference frame quantities is widely used in MMC-VSC applications as it provides decoupling between active and reactive powers [20, 21]. In addition to the vector control, different supplementary controls, such as the voltage margin control, voltage droop control, frequency droop control, negative sequence current control, power oscillation damping control, and circulation current control are used to enhance the performance of MMC-VSC systems [22, 23]. Moreover, manufacturers use complicated techniques to control and balance the voltages among the sub-module capacitors [24].

1.1.3 Review of Previous Works on Control System Modelling and Tuning

The control system with primary controls of an MMC is shown in Figure 1.1. The control variables (V, P, Q) are measured at the terminal bus and the terminal voltage phase angle is tracked using a suitable phase-locked loop (PLL). Typically, MMC-VSC systems are controlled using the d-q decoupled control system. Then, the controller output voltage orders are sent to the firing pulse generator that will generate the required firing signals for IGBT switches in the converter.

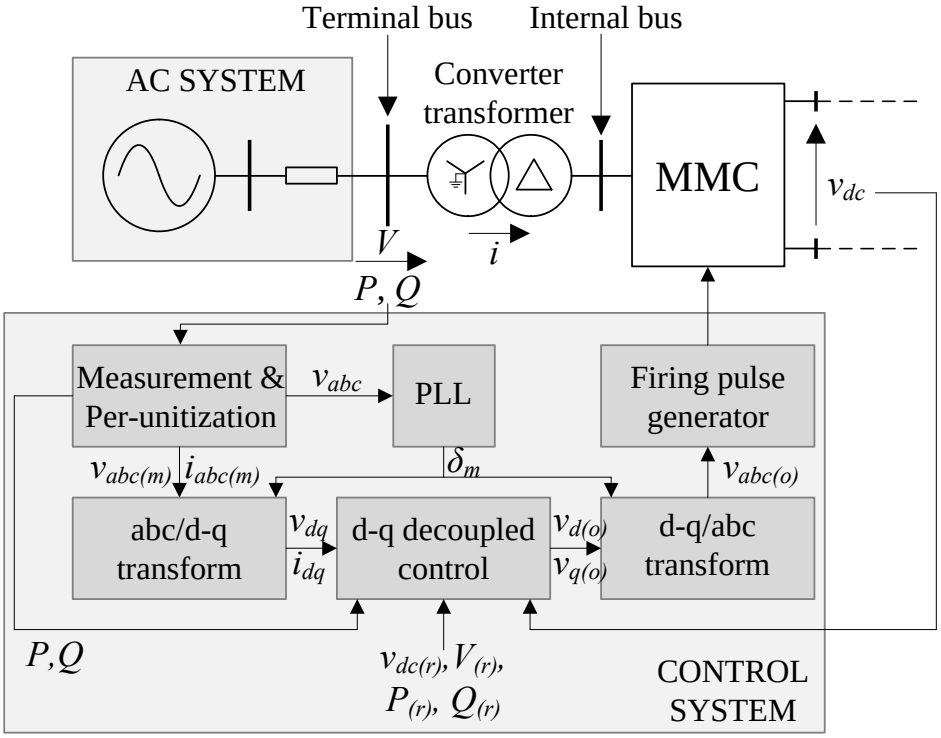

Figure 1.1: Control block diagram of an MMC (r-reference, m-measured, and o-order)

The d-q decoupled control system was first proposed in [25] and it consists of double closed loop PI-controllers as shown by Figure 1.2. In the outer-loop, the dc voltage (v_{dc}) or the active power (P) is chosen as the controlled parameter to produce

the d-axis current reference ($i_{d(r)}$). Similarly, either the ac voltage (V) or the reactive power (Q) is chosen to generate the q-axis current reference ($i_{q(r)}$). The inner-loop current controllers regulate d-axis and q-axis currents to meet the reference currents. Then, the output of the inner-loop controllers are combined with the decoupling terms and measured voltages to produce the voltage orders that are used to generate switching signals for the converter [8, 25].

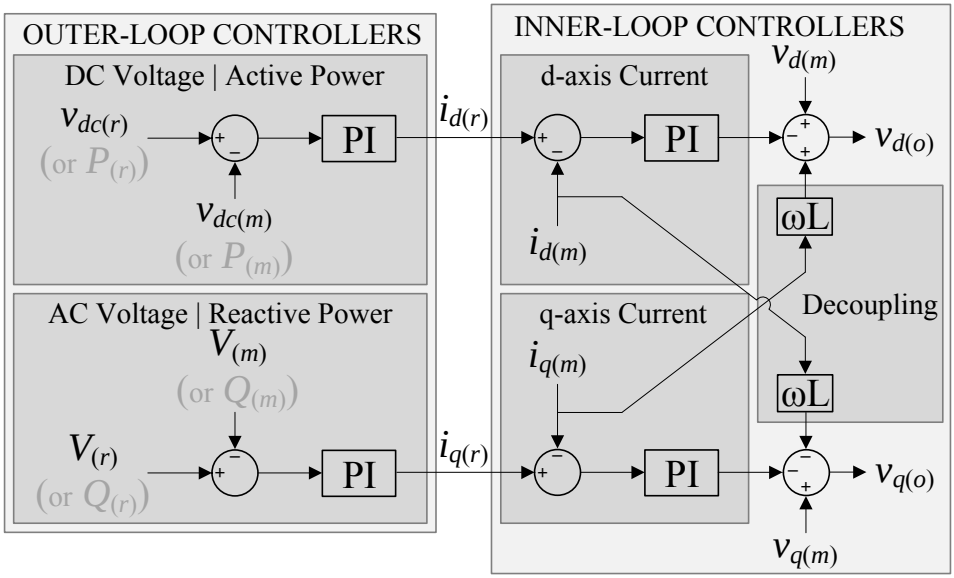

Figure 1.2: d-q decoupled control system (r-reference, m-measured, and o-order)

Although the d-q decoupled control system uses simple PI-controllers, determining control parameters is a challenging task. This is because the control system at each converter station consists of at least five PI-controllers including the one used in the PLL. In addition, the gain tuning problem will become more complicated when the number of converters increases. There are few technical publications available on determining controller parameters for specific VSC systems. The methods reported in literature to tune the d-q decoupled control loops can be categorized into three groups as described below.

Trial and Error Approach

The first step in this method is to develop a non-linear EMT simulation model of the test system. Then, disturbances such as step changes are applied to the reference settings of the EMT model one at a time. Based on the step responses, the PI-controller parameters are selected by trial and error [26]. Although this method of tuning is done by engineering experts who have many years of experience in this field, the tuned gains cannot guarantee the optimum performance. In addition, it is a tedious and time consuming task.

Transfer Function Approach

This method deduces equivalent transfer functions based on assumptions such as the inner-loop controllers are faster than its outer-loop controllers, converters are fully decoupled, and the dc voltage is always a constant. Then, a linear control technique such as Bode method, root-locus, or Nyquist technique is used to tune PI-controller parameters. It is well known that the above design tools can only be used to tune PI-controllers one at a time. Therefore, in research articles based on transfer function approach, it is assumed that the converters in a VSC system do not interact with each other. This assumption localizes the controller tuning problem of VSC system to a single VSC. The inner-loop controllers are tuned in the first step by ignoring the outer-loop controllers assuming that the inner-loop is faster than its outer-loop. After the tuned values are applied to the inner-loop controllers, the outer-loop controllers are tuned [23, 27, 28]. In [29], the bacterial forging algorithm is applied to the simplified transfer functions of VSC system to tune controllers. In short, because of assumptions and simplifications used in the transfer function approach, the performance under all possible operating conditions cannot be guaranteed.

Optimization of Time-domain Objective Functions

The optimization method of controller tuning has become popular in recent years as the researchers have understood that the control loops are not fully decoupled and also the converters interact through the dc system. In this method, the gain tuning problem is formulated as a time-domain optimization problem and solved using a suitable optimization algorithm. The optimization-enabled EMT (OEMT) simulation to tune the controllers of an LCC-HVdc system is presented in [30]. The same technique is used in [22, 31, 32] to tune VSC control loops. In [22], it is stated that this method is computationally intensive even with the use of average models of converters. In addition, the authors of [30] have recommended the simplex method of optimization when the number of variables to be tuned is less than 10. Due to the requirement of high computational effort and the limitation of number of variables that can be optimized using simplex method, the application of OEMT method based on simplex to simultaneously tune converters in a dc grid is challenging. As a solution to the above two problems, a recent literature [33] proposes a parallel multi-model optimization algorithm to tune VSC controllers. However, still it is computationally intensive as it uses a specially designed computer with 60-core processor. The objective functions used in the OEMT methods in literature [22, 31, 32, 33] consider only the outer-loop controllers and the the inner-loop current controllers are not optimized to save the computational time. A method to tune the PI-controller parameters for VSC systems using the particle swarm optimization (PSO) is presented in [34]. This method assumes complete decoupling between control loops even during transients and also assumes no interactions between converters. In [35], a VSC controller tuning method based on the standard infinite time quadratic performance index is explained and solved using the 'fmincon' function available in MATLAB software. The same

method is also used in [36], where the time-domain objective function is minimized using genetic algorithm. However, the performance evaluation presented are not adequate to show the advantages of this method. In addition, the development of soft-computing techniques are also being applied to tune the VSC control loops. A fuzzy supervised variable gain PI-controllers for VSC-HVdc systems are studied in [37] and [38]. However, from the industry's point of view, a variable gain PI-controller is not an attractive solution.

In addition to the above three categories, linear control techniques are applied to tune power system controllers such as power system stabilizers (PSS) [39, 40, 41] and thyristor controlled series capacitors (TCSC) [42, 43]. However, there is not much published literature available on the application of linear control methods to tune the control loops of VSC systems. To make use of the available linear control theories to tune the VSC control loops, it is required to develop the linearized model of the power system including VSC systems. However, small-signal stability programs that can be used to model power systems consisting of VSC systems are not readily available to researchers. Therefore, researchers have to develop their own linearized models to apply linear control techniques. In addition, the amount of details included in the linearized model depends on the researcher. Moreover, the efficacy of the linear analysis depends on the accuracy of the model. The linearized model of VSC systems reported in literature lack in modelling one or more of the important dynamics such as ac system, dc system, converters, converter transformers, converter losses, arm inductors, control loops, PLL, and measuring delays [23, 44, 45]. Generally, the linearized model of a power system is developed by linearizing the non-linear dynamic equation around an operating point [46]. Therefore, it is essential to validate the linearized model against a non-linear simulation model of the same system. The usual

practice in power system studies is to validate the linearized model against a non-linear model developed using an EMT simulation program. However, most linearized models reported in the literature are used for small-signal stability assessment without proper validations [45, 47, 48]. The ac power system configuration is not fixed and the system strength of the ac system connected to the VSC can change. The analysis presented in [22] shows that the ac system will influence the stability of a VSC system. Therefore, it is essential to have a method to estimate the ac system strength. Then, that information can be incorporated to the controller tuning technique.

1.1.4 Sensitivities of VSC System Stability

It is reported in literature that the performance of VSC systems depend on PLL gains, PI-controller parameters, ac system strength, and dc system dynamics [44, 22, 49, 47, 50, 51, 52]. The influence of ac system strength on the stability of VSC systems is studied in [22, 49] and it is showed that the control of VSC system is challenging when the ac system becomes weak. In [44], it is stated that the stability of VSC systems connected to weak ac systems is guaranteed only if very low PLL gains are used. The stability of dc system is investigated in [50] and it is showed that the dc system resonance can cause instabilities. In addition, it is also showed that converters interact through the dc system [53, 47].

Review of previous work indicated that the stability of VSC systems depend on various parameters including ac system strength, dc system dynamics, and controller parameters. As previously mentioned, the control loops of a VSC are not completely decoupled and converters in a dc grid interact through the dc system. Therefore, it is required to simultaneously tune the PI-controller parameters by considering the entire VSC system including all important dynamics of the system. When a point-

to-point MMC-VSC system is considered there are 10 PI-controllers to be tuned and these controllers need to be tuned simultaneously as they interact through the dc transmission system. Therefore, for a point-to-point system there are 20 parameters to be tuned and this number will increase by 10 when each time a converter is added to the MMC-VSC system.

1.2 Research Objectives

Unavailability of a widely accepted controller tuning procedure for VSC systems and the availability of numerous linear and non-linear control techniques are the motivations behind selecting this as the research area to be explored. The principal objective of this research is to develop a systematic procedure to simultaneously tune PI-controller parameters for MMC-VSC systems. This research utilizes the linear control techniques, optimization methods, and EMT simulations. It is necessary to use a generic test system to produce general conclusions that are applicable to any given MMC-VSC system while minimizing the number of modelling assumptions. The main objective of this thesis led to a list of additional objectives as given below:

1. To develop a detailed non-linear EMT simulation model of a point-to-point MMC-VSC system with generic controllers to use as the base case for the research.
2. To model a small-signal stability model (linearized model) of the test system and validate it against the EMT simulation model in order to use it for small-signal stability assessment.
3. To develop a systematic procedure to simultaneously tune all PI-controllers of a given MMC-VSC system.

4. To evaluate the performance of the controller tuning procedure by applying the tuned PI-controller parameters to the EMT simulation model.
5. To analyze the effects of power network and control system parameters to the controller tuning and to the stability of the system.
6. To propose a list of key points that need to be considered with care when planning, modelling, and assessing the stability of a given MMC-VSC system.

1.3 Thesis Outline

This thesis introduces a systematic procedure to simultaneously tune PI-controllers in a given MMC-VSC system. The controller tuning problem is formulated as a frequency-domain optimization problem. The frequency domain stability related attributes are calculated using the small-signal model of an MMC-VSC system developed in this research. The remainder of the thesis is organized as follows,

The modelling details of a generic point-to-point MMC-VSC system is presented in **Chapter 2**. Initially, the development of the EMT model of the test system is briefly discussed. Then, the development of linearized models are explained. After that, the aggregation of developed linearized models to form the complete state-space model of the test system is explained. Finally, the validation results of the small-signal model against the non-linear EMT simulation model of the test are presented.

Chapter 3 presents the small-signal stability assessment of the system. The sensitivity analysis of the control system parameters to the overall stability of the test system is presented. To investigate the effects of measuring delays in instantaneous quantities, the linerized model developed in **Chapter 2** is extended to cover the dynamics of measuring delays. Then, a small-signal stability assessment is performed using the upgraded linearized model.

Chapter 4 is dedicated to present the development of the systematic procedure to simultaneously tune the PI-controllers of a given MMC-VSC system. Initially, the gain tuning problem is formulated as a frequency-domain optimization problem that can be solved using any suitable optimization technique. Then, followed by a brief introduction to the simulated annealing optimization technique, the steps to solve the gain tuning problem using simulated annealing is presented. The performance of proposed systematic controller tuning procedure is verified using the EMT simulation model of the test system. To show the robustness of the tuned controller gains, simulation results for a wide range of disturbances are presented.

Chapter 5 investigates the effect of proposed controller tuning method for different ac system strengths and measuring delays. Initially, a stability evaluation of the test system for changes in short circuit ratio (SCR) is presented. Then, a method to estimate the SCR is presented. After that, the optimized controller gains for the MMC-VSC test system with different ac systems ranging from weak ac grid (SCR=1.5) to very strong ac grid (SCR=20.0) are discussed. Later, the performance evaluation of tuned controller gains is done by means of EMT simulations for different disturbances to claim the efficacy and robustness of the tuning method. In addition, tuning of controllers considering measuring delays in instantaneous quantities is also presented. Finally, based on the findings of this research, a list of key points that need to be considered with care when modelling and performing stability analysis of MMC-VSC systems is presented.

The conclusions, contributions, and suggestions for future work are presented in **Chapter 6**.

Chapter 2

Modelling of a Point-to-Point MMC-VSC System

Electro-magnetic transient (EMT) simulations are widely used to analyze the power system transients because of the accuracy in modelling and the use of very small integration time-steps. A detailed analysis including the effect of non-linearities can be performed in the time-domain using EMT simulation tools. The small-signal analysis produces frequency domain stability attributes that are very important for stability studies and control design. This thesis utilizes both the real-time EMT simulation method and the small-signal stability assessment method for simulation studies. This chapter provides details about developing EMT and small-signal models of the test system. The validation of linearized models is also presented.

2.1 Electromagnetic Transient Modelling of Test System

A point-to-point MMC-VSC system shown in Figure 2.1 is used as the test system and parameters of the system are given in Table 2.1.

Table 2.1: Parameters of the Test System

Parameter	**Value**
HVdc system type	Symmetrical mono-pole MMC-VSC
Rated power	500 MW
Rated dc voltage	500 kV
Rated ac voltage	230 kV (L-L RMS) at 60 Hz on both sides
AC system strength	SCR range: 1.5 to 20 at 84°
Converter transformer ratio	230 kV:250 kV
Converter transformer impedance	0.18 p.u. on 575 MVA
Sub-module type	250 half-bridge sub-modules per arm
Sub-module capacitor	10000 μF
Arm inductor	50 mH
DC transmission system	400 km overhead transmission line
DC line parameters	7.17 Ω, 0.74 H, 5 μF

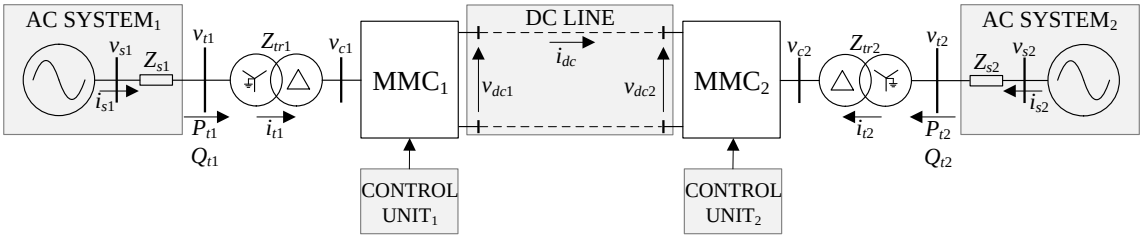

Figure 2.1: Point-to-point MMC-VSC test system

The real-time digital simulator (RTDS) is selected as the EMT simulation platform for this study and a brief introduction to the RTDS simulator is given in the **Appendix A.2**. Standard library models and user defined control components are utilized to model the test system. The real-time simulation of the test system requires four advanced type (GPC or PB5) processor cards on an RTDS rack. The RTDS simulators are capable of simulating power systems in two different integration time-steps to keep the accuracy at a high-level. In this thesis, the MMCs and the dc

transmission system are simulated using small integration time-step ($\sim 2\ \mu$s) and the ac systems and control components are simulated using larger integration time-step (50 μs). The control system is modelled in per-unit.

2.2 Development of Linearized Model

Small-signal stability of a power system is defined as "the ability of the power system to maintain synchronism when subjected to small disturbances". A disturbance is considered as small, if linearized equations are valid to analyze the stability of the system for that disturbance [46].

A dynamic system can be defined by a set of first order non-linear differential equations. Equation (2.1) shows the general state-space representation of a system with n number of state variables and r number of inputs.

$$\dot{\mathbf{X}} = f(\mathbf{X}, \mathbf{U}) \tag{2.1}$$

Where,

$$\mathbf{X} = [X_1, X_2, \ldots, X_n]^T \qquad \mathbf{U} = [U_1, U_2, \ldots, U_r]^T \qquad f = [f_1, f_2, \ldots, f_n]^T$$

At an equilibrium point (i.e: at a steady state operating condition), Equation (2.1) can be written as shown in Equation (2.2).

$$\dot{\mathbf{X}}_0 = f(\mathbf{X}_0, \mathbf{U}_0) = 0 \tag{2.2}$$

Consider disturbing the system given in Equation (2.1), by a small amount from the above mentioned steady state operating point. Substituting $\mathbf{X} = \mathbf{X}_0 + \Delta\mathbf{X}$ and $\mathbf{U} = \mathbf{U}_0 + \Delta\mathbf{U}$ in Equation (2.1) results in Equation (2.3).

$$\dot{\mathbf{X}} = f[(\mathbf{X}_0 + \Delta\mathbf{X}), (\mathbf{U}_0 + \Delta\mathbf{U})] \tag{2.3}$$

Consider the ith non-linear equation shown in (2.4),

$$\dot{X}_i = f_i[(\mathbf{X}_0 + \Delta\mathbf{X}), (\mathbf{U}_0 + \Delta\mathbf{U})] \tag{2.4}$$

The linearization of the non-linear Equation (2.4) can be obtained using the Taylor series expansion and neglecting 2nd and higher order terms of ΔX and ΔU as shown in Equation (2.5).

$$\dot{X}_i = f_i(\mathbf{X}_0, \mathbf{U}_0) + \left(\frac{\partial f_i}{\partial X_1}\Delta X_1 + \ldots + \frac{\partial f_i}{\partial X_n}\Delta X_n\right) + \left(\frac{\partial f_i}{\partial U_1}\Delta U_1 + \ldots + \frac{\partial f_i}{\partial U_r}\Delta U_r\right) \tag{2.5}$$

Since $f_i(\mathbf{X}_0, \mathbf{U}_0) = 0$ and $\dot{X}_i = \Delta\dot{X}_i$, Equation (2.5) can be simplified as given in Equation (2.6) and can be written in a compact form shown by Equation (2.7)

$$\Delta\dot{X}_i = \left(\frac{\partial f_i}{\partial X_1}\Delta X_1 + \ldots + \frac{\partial f_i}{\partial X_n}\Delta X_n\right) + \left(\frac{\partial f_i}{\partial U_1}\Delta U_1 + \ldots + \frac{\partial f_i}{\partial U_r}\Delta U_r\right) \tag{2.6}$$

$$\Delta\dot{X}_i = \sum_{j=1}^{n} \frac{\partial f_i}{\partial X_j}\Delta X_j + \sum_{j=1}^{r} \frac{\partial f_i}{\partial U_j}\Delta U_j \tag{2.7}$$

Similarly, all linearized equations can be combined to form the state-space model of the system given Equation (2.8). The partial derivatives are evaluated at the steady state equilibrium point.

$$\Delta\dot{\mathbf{X}} = \mathbf{A}\Delta\mathbf{X} + \mathbf{B}\Delta\mathbf{U} \tag{2.8}$$

Where,

$$\begin{aligned}
\Delta\mathbf{X} &= [\Delta X_1, \Delta X_2, ..., \Delta X_n]^T \\
\Delta\mathbf{U} &= [\Delta U_1, \Delta U_2, ..., \Delta U_r]^T \\
\mathbf{A} &= \begin{bmatrix} \frac{\partial f_1}{\partial X_1} & \cdots & \frac{\partial f_1}{\partial X_n} \\ \vdots & \ddots & \vdots \\ \frac{\partial f_n}{\partial X_1} & \cdots & \frac{\partial f_n}{\partial X_n} \end{bmatrix} \\
\mathbf{B} &= \begin{bmatrix} \frac{\partial f_1}{\partial U_1} & \cdots & \frac{\partial f_1}{\partial U_r} \\ \vdots & \ddots & \vdots \\ \frac{\partial f_n}{\partial U_1} & \cdots & \frac{\partial f_n}{\partial U_r} \end{bmatrix}
\end{aligned}$$

The above linearization technique is used to obtain the small-signal model of the MMC-VSC test system and the important steps of the linearization process are given in Sections 2.2.1 to 2.2.8.

2.2.1 AC Network Model

The ac network connected to MMC terminal is represented using the Thévenin equivalent model, that comprises a voltage source and an RRL type impedance as shown in Figure 2.2. The ac side of the converter model consists of the converter transformer and the arm inductor. Dynamic phasors are used to write the analytical equations of the ac system to maintain the modelling accuracy at a high-level [54]. By applying Kirchoff's voltage law to the circuit shown in Figure 2.2, the dynamic equations for the ac system can be written as shown in Equations (2.9) to (2.11).

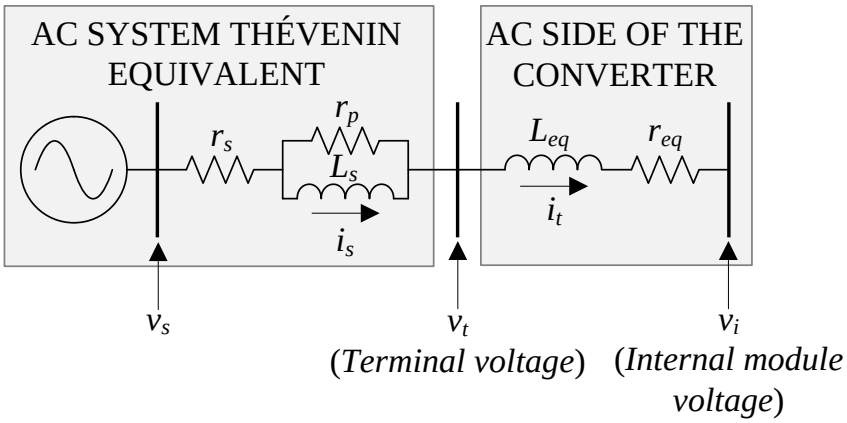

Figure 2.2: Circuit diagram of the ac network

$$L_s\frac{di_s}{dt} = -j\omega L_s i_s + -r_s i_t + v_s - v_t \tag{2.9}$$

$$L_{eq}\frac{di_t}{dt} = -j\omega L_{eq} i_t - r_{eq} i_t + v_t - v_i \tag{2.10}$$

$$L_s\frac{di_s}{dt} = -j\omega L_s i_s + r_p\left(i_t - i_s\right) \tag{2.11}$$

The state-space model of the ac system given by Equation (2.12) can be obtained by combining Equations (2.9)-(2.11) and by substituting with the R-I reference frame quantities for voltages and currents. Let I_{sR} and I_{sI} be real and imaginary components of current i_s. Therefore, current i_s can be written as I_s=I_{sR}+jI_{sI} in phasor domain. Similarly, I_t=I_{tR}+jI_{tI}, V_s=V_{sR}+jV_{sI}, and V_i=V_{iR}+jV_{iI}.

$$\Delta\dot{\mathbf{X}}_{ac} = \mathbf{A}_{ac}\Delta\mathbf{X}_{ac} + \mathbf{B}_{ac}\Delta\mathbf{U}_{ac} + \mathbf{E}_{ac}\Delta\mathbf{V}_i \tag{2.12}$$

Where,

$$\Delta\mathbf{X}_{ac} = \left[\Delta I_{sR}, \Delta I_{sI}, \Delta I_{tR}, \Delta I_{tI}\right]^T$$

$$\Delta\mathbf{U}_{ac} = \left[\Delta V_{sR}, \Delta V_{sI}\right]^T$$

$$\Delta\mathbf{V}_i = \left[\Delta V_{iR}, \Delta V_{iI}\right]^T$$

$$\mathbf{A}_{ac} = \begin{bmatrix} -k_s r_p & \omega_0 & k_s r_p & 0 \\ -\omega_0 & -k_s r_p & 0 & k_s r_p \\ k_{eq} r_p & 0 & -k_{eq}(r_p + r_s + r_{eq}) & \omega_0 \\ 0 & k_{eq} r_p & -\omega_0 & -k_{eq}(r_p + r_s + r_{eq}) \end{bmatrix}$$

$$\mathbf{B}_{ac} = \begin{bmatrix} 0 & 0 \\ 0 & 0 \\ k_{eq} & 0 \\ 0 & k_{eq} \end{bmatrix}$$

$$\mathbf{E}_{ac} = \begin{bmatrix} 0 & 0 \\ 0 & 0 \\ -k_{eq} & 0 \\ 0 & -k_{eq} \end{bmatrix}$$

with,

$$r_{eq} = r_t + \frac{r_{arm}}{2}, \quad L_{eq} = L_t + \frac{L_{arm}}{2}, \quad k_s = \frac{\omega_0}{L_s}, \quad k_{eq} = \frac{\omega_0}{L_{eq}} \tag{2.13}$$

2.2.2 DC Network Model

The dc network consists of the dc transmission system and the equivalent sub-module capacitances seen from the dc side. The dc network is represented using a Π-model as shown in Figure 2.3. The capacitors (C_{dc1} and C_{dc2}) are modelled to reflect the combined effects of the equivalent sub-module capacitance and the transmission line shunt capacitances.

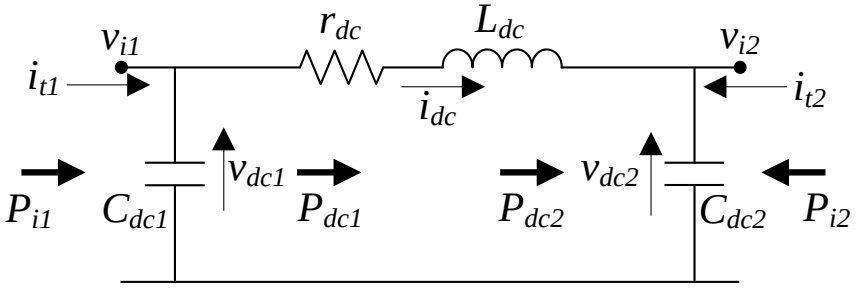

Figure 2.3: DC system representation

The dynamics of capacitors are modelled by writing the power balance as shown in Equations (2.14) and (2.15). The dynamic equation of the dc line inductor is written as given in Equation (2.16).

$$C_{dc1}\frac{dv_{dc1}}{dt} = P_{i1} - P_{dc1} - P_{loss1} \tag{2.14}$$

$$C_{dc2}\frac{dv_{dc2}}{dt} = P_{i2} + P_{dc2} - P_{loss2} \tag{2.15}$$

$$L_{dc}\frac{di_{dc}}{dt} = -r_{dc}i_{dc} + v_{dc1} - v_{dc2} \tag{2.16}$$

Where,

$$P_{ik} = v_{ik}i_{tk}, \quad P_{dck} = v_{dck}i_{dc}, \quad P_{lossk} = r_{ck}\left(\frac{i_{dc}}{3}\right)^2 + r_{ck}\left(\frac{i_{tk}}{2}\right)^2$$

$$r_{eqk} = N_k r_{SMk}, \quad C_{eqk} = 3\frac{C_{SMk}}{N_k}, \quad C_{dck} = C_{eqk} + \frac{C_{dck}}{2}, \quad k = 1, 2$$

The state-space model of the dc network can be written as shown in Equation (2.17) by linearizing Equations (2.14)-(2.16) and then by substituting with the real and imaginary components of the voltage and currents..

$$\Delta\dot{\mathbf{X}}_{dc} = \mathbf{A}_{dc}\Delta\mathbf{X}_{dc} + \mathbf{A^*}_{dc}\Delta\mathbf{X}_{ac12} + \mathbf{E}_{dc}\Delta\mathbf{V}_{i12} \tag{2.17}$$

Where,

$$\begin{aligned}
\Delta\mathbf{X}_{dc} &= [\Delta v_{dc1}, \Delta v_{dc2}, \Delta i_{dc}]^T \\
\Delta\mathbf{X}_{ac12} &= [\Delta I_{t1R}, \Delta I_{t1I}, \Delta I_{t2R}, \Delta I_{t2I}]^T \\
\Delta\mathbf{V}_{i12} &= [\Delta V_{i1R}, \Delta V_{i1I}, \Delta V_{i2R}, \Delta V_{i2I}]^T \\
\mathbf{A}_{dc} &= \begin{bmatrix} -i_{dc0} & 0 & -k_{dc1}\left(9v_{dc0} + 2r_{c1}i_{dc0}\right) \\ 0 & k_{dc2}i_{dc0} & k_{dc2}\left(9v_{dc0} + 2r_{c2}i_{dc0}\right) \\ k_{dc3} & -k_{dc3} & -k_{dc3}r_{dc} \end{bmatrix} \\
\mathbf{A^*}_{dc} &= \begin{bmatrix} a_{11}^* & a_{12}^* & 0 & 0 \\ 0 & 0 & a_{23}^* & a_{24}^* \\ 0 & 0 & 0 & 0 \end{bmatrix} \\
\mathbf{E}_{ac} &= \begin{bmatrix} k_{dc1}S_bI_{tR10} & k_{dc1}S_bI_{t1I0} & 0 & 0 \\ 0 & 0 & k_{dc2}S_bI_{tR20} & k_{dc2}S_bI_{t2I0} \\ 0 & 0 & 0 & \end{bmatrix}
\end{aligned}$$

with,

$$\begin{aligned}
a_{11}^* &= S_bk_{dc1}\left(V_{i1R0} - \frac{r_{eq1}}{2Z_b}I_{t1R0}\right), \qquad a_{12}^* = S_bk_{dc1}\left(V_{i1I0} - \frac{r_{eq1}}{2Z_b}I_{t1I0}\right), \\
a_{23}^* &= S_bk_{dc2}\left(V_{i2R0} - \frac{r_{eq2}}{2Z_b}I_{t2R0}\right), \qquad a_{24}^* = S_bk_{dc2}\left(V_{i2I0} - \frac{r_{eq2}}{2Z_b}I_{t2I0}\right), \\
k_{dc1} &= \frac{1}{9C_{dc1}v_{dc10}}, \qquad k_{dc2} = \frac{1}{9C_{dc2}v_{dc20}}, \qquad k_{dc3} = \frac{1}{L_{dc}}
\end{aligned}$$

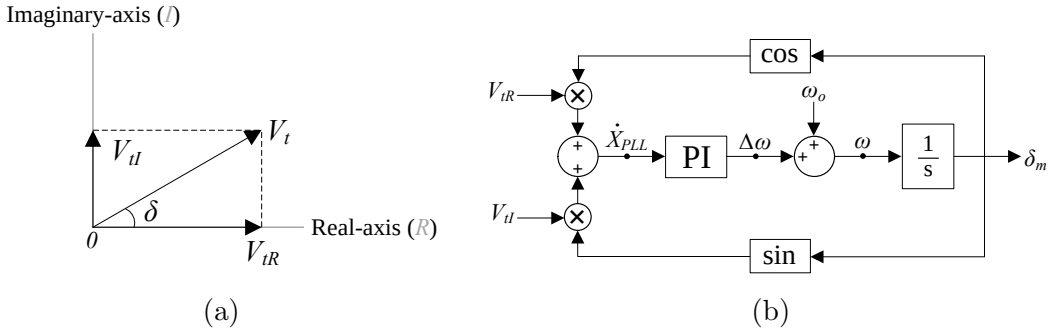

Figure 2.4: PLL block diagram (a) R-I voltages and (b) SRF-PLL

2.2.3 Phase-Locked Loop Model

Phase-locked loops (PLLs) are used in power system devices to measure the phase angle of the control bus voltage. The synchronous reference frame (SRF) PLL is commonly used in power system applications for control system design purposes and the same model is used in this thesis. The control block diagram of an SRF-PLL is shown in Figure 2.4. Per-unitized real and imaginary components (V_{tR} and V_{tI}) of the terminal voltage (V_t) are given as inputs to the PLL to produce the reference voltage phase angle (δ_m) that is used in the control system. The PLL dynamic equations are given by Equations (2.18) and (2.19).

$$\dot{X}_{PLL} = sin\,(\delta - \delta_m) \tag{2.18}$$

$$\dot{\delta}_m = K_{P(PLL)} sin\,(\delta - \delta_m) + K_{I(PLL)} X_{PLL} \tag{2.19}$$

The state-space model of the PLL given by Equation (2.20) can be obtained by linearizing the dynamic Equations (2.18) and (2.19).

$$\Delta\dot{\mathbf{X}}_{pll} = \mathbf{A}_{pll}\Delta\mathbf{X}_{pll} + \mathbf{E}_{pll}\Delta\mathbf{V}_t \tag{2.20}$$

Where,

$$\mathbf{A}_{pll} = \begin{bmatrix} 0 & -1 \\ K_{I(PLL)} & -K_{P(PLL)} \end{bmatrix}$$

$$\mathbf{E}_{pll} = \begin{bmatrix} -k_{pll}^2 V_{tI0} & k_{pll}^2 V_{tR0} \\ -k_{pll}^2 K_{P(PLL)} V_{tI0} & k_{pll}^2 K_{P(PLL)} V_{tR0} \end{bmatrix}$$

With,

$$k_{pll} = \frac{1}{\sqrt{V_{tR0}^2 + V_{tI0}^2}}$$

Typically, VSC systems are controlled using the *d-q* decoupled control that is based on synchronous (*d-q*) reference frame. The main advantage of using *d-q* control technique is that the time varying ac quantities in *abc* reference frame will become dc quantities in *d-q* reference frame. Therefore, these quantities can be easily controlled using PI-controllers. In state-space modelling, the ac systems are modelled on *R-I* reference frame and the converter controls are modelled on *d-q* reference frame. The relationship between *R-I* and *d-q* reference frame is presented in Section 2.2.7.

2.2.4 Converter Model

The block diagram of the converter is shown in Figure 2.5 and the basic ac-dc voltage relation of a VSC is given by Equation (2.21). This relationship is used to relate the voltage orders (v_o) from control system to the converter internal ac voltage (v_i) as given by Equations (2.22) and (2.23). It was observed through EMT simulations that the MMC does not introduce any noticeable delay in producing ac voltages. Therefore, the converter is modelled by assuming no delay.

$$\hat{v}_{i(l-g)} = \frac{m}{2} v_{dc(p-p)} \tag{2.21}$$

where m is the modulation index.

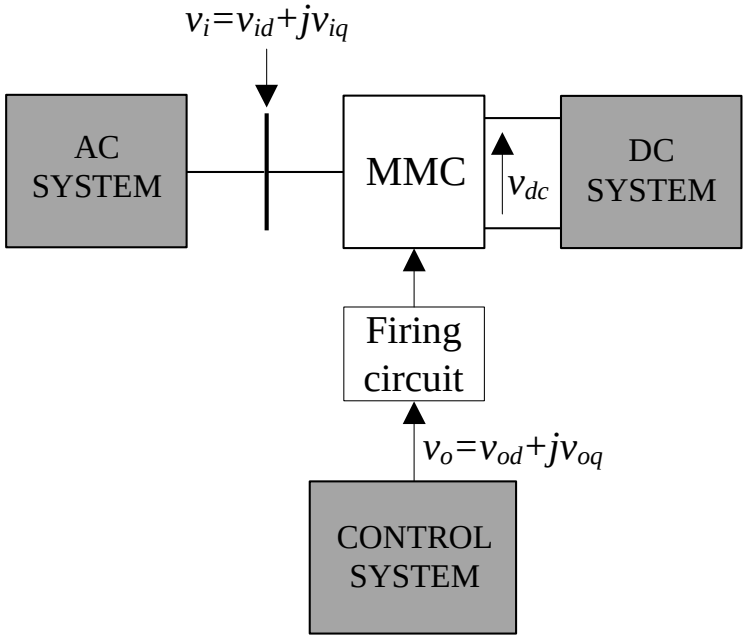

Figure 2.5: Generation of ac voltage using MMC

$$v_{id} = \frac{1}{2}\left(\frac{\sqrt{3}v_{od}}{\sqrt{2}}\right) v_{dc} \tag{2.22}$$

$$v_{iq} = \frac{1}{2}\left(\frac{\sqrt{3}v_{oq}}{\sqrt{2}}\right) v_{dc} \tag{2.23}$$

The algebraic model of the MMC given in Equation (2.24) can be obtained by combining Equations (2.22) and (2.23).

$$\Delta \mathbf{V}_i^{dq} = \mathbf{C}_m \Delta v_{dc} + \mathbf{D}_m \Delta \mathbf{V}_o^{dq} \tag{2.24}$$

Where,

$$\begin{aligned} \Delta \mathbf{V}_i^{dq} &= [\Delta v_{id}, \Delta v_{iq}]^T \\ \Delta \mathbf{V}_o^{dq} &= [\Delta v_{od}, \Delta v_{oq}]^T \end{aligned}$$

$$\begin{aligned} \mathbf{C}_m &= \begin{bmatrix} k_m v_{od0} \\ k_m v_{oq0} \end{bmatrix} \\ \mathbf{D}_m &= \begin{bmatrix} k_m v_{dc0} & 0 \\ 0 & k_m v_{dc0} \end{bmatrix} \end{aligned}$$

With,

$$k_m = \frac{\sqrt{3}}{2\sqrt{2}}$$

Note that the dynamics of the sub-module capacitances have already been considered in modelling of the dc transmission system.

2.2.5 Control System Model

The commonly used d-q decoupled control scheme is adopted in this thesis to control each MMC converter. The functional block diagram of the MMC is shown in Figure 2.6. This control scheme consists of cascaded PI-control loops referred to as outer-loop (power-loop) controllers and inner-loop (current-loop) controllers. The outer-loop controllers are responsible to produce the reference values for the d-q frame currents that are controlled at the inner-loop. In the outer-loop, either the dc voltage or the active power is selected as the control variable to produce d-axis current reference.

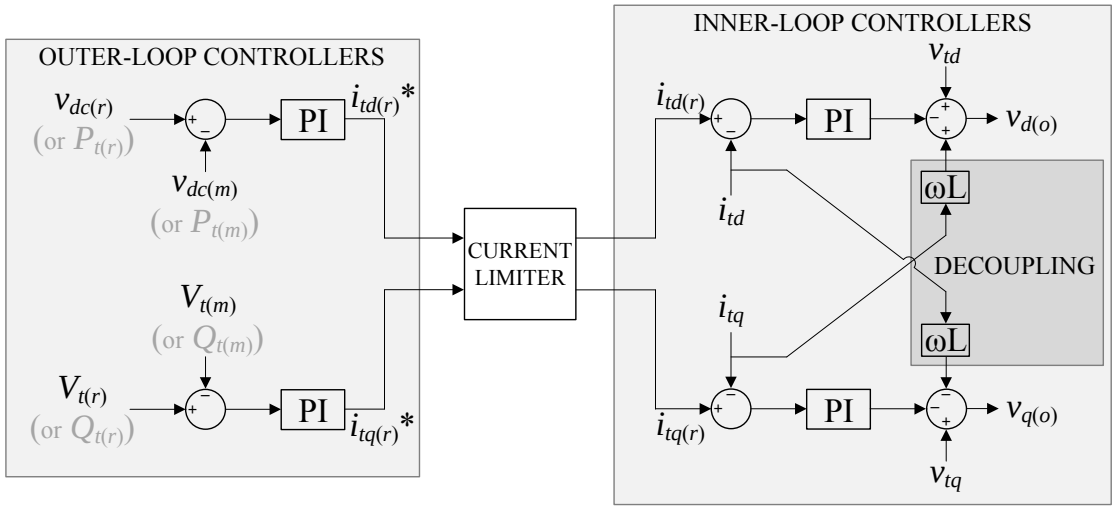

Figure 2.6: Block diagram of the d-q decoupled control system (r-reference, m-measurement, and o-order)

Similarly, either ac voltage or reactive power is selected as the q-axis control variable. Then, at the inner-loop, the measured d-q currents are regulated to meet the reference currents.

To make it general, the control system in both EMT and small-signal models are modelled using per-unit quantities. The current limiter in the above control system can be modelled in different ways depending on the application of the converter [8, 55, 56]. However, the typical way of modelling is to limit the magnitude while preserving its phase angle [8]. This typical current limiter model is used in the EMT model of the test system and the functional block diagram is shown in Figure 2.7. Initially, the d-q reference currents generated by the outer-loop controllers are converted into magnitude and angle. Then, the magnitude is limited to a pre-defined maximum (I_{max}). The resultant current magnitude is then converted back to d-q quantities using the original phase angle (θ). The value of I_{max} is selected such that the ratings of devices such as converter transformer and converter are not exceeded. Typically, the small-signal models are used to assess the stability around a steady

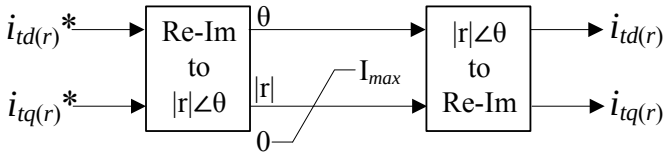

Figure 2.7: Functional block diagram of the current limiter

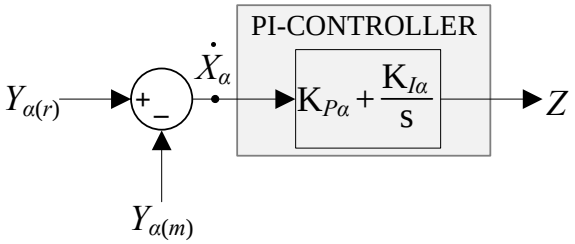

Figure 2.8: Block diagram of the PI-controller

state operating condition. Therefore, the current limiters are not included in the small-signal model.

The dynamic equations of each PI-controller of the above control scheme are written for the model shown in Figure 2.8. The error between desired value ($Y_{\alpha(r)}$) and measured value ($Y_{\alpha(m)}$) is regulated through the PI-controller. The dynamic and linear equations of the PI-controller are given by Equations (2.25) and (2.26).

$$\dot{X}_\alpha = \left(Y_{\alpha(r)} - Y_{\alpha(m)}\right) \tag{2.25}$$

$$Z = K_{P\alpha}\left(Y_{\alpha(r)} - Y_{\alpha(m)}\right) + K_{I\alpha}X_\alpha \tag{2.26}$$

The dynamic equations for outer-loop controllers on both sides are obtained by substituting Y_α in Equation (2.25) with v_{dc1}, P_{t2}, V_{t1}, and V_{t2}. The resulting dynamic equations are given by Equations (2.27)-(2.30).

$$\dot{X}_{v_{dc1}} = \left(v_{dc1(r)} - v_{dc1(m)}\right) \tag{2.27}$$

$$\dot{X}_{P_{t1}} = \left(P_{t1(r)} - P_{t1(m)}\right) \tag{2.28}$$

$$\dot{X}_{V_{t1}} = \left(V_{t1(r)} - V_{t1(m)}\right) \tag{2.29}$$

$$\dot{X}_{V_{t2}} = \left(V_{t2(r)} - V_{t2(m)}\right) \tag{2.30}$$

The outputs of outer-loop controller are the reference currents for the inner-loop current controllers. The output equations are written by substituting the parameter Z in Equation (2.26) with $i_{t1d(r)}$, $i_{t2d(r)}$, $i_{t1q(r)}$, and $i_{t2q(r)}$ and the corresponding equations are given below.

$$i_{t1d(r)} = K_{P(v_{dc1})}\left(v_{dc1(r)} - v_{dc1(m)}\right) + K_{I(v_{dc1})}X_{v_{dc1}} \tag{2.31}$$

$$i_{t2d(r)} = K_{P(P_{t1})}\left(P_{t1(r)} - P_{t1(m)}\right) + K_{I(P_{t1})}X_{P_{t1}} \tag{2.32}$$

$$i_{t1q(r)} = K_{P(V_{t1})}\left(V_{t1(r)} - V_{t1(m)}\right) + K_{I(V_{t1})}X_{V_{t1}} \tag{2.33}$$

$$i_{t2q(r)} = K_{P(V_{t2})}\left(V_{t2(r)} - V_{t2(m)}\right) + K_{I(V_{t2})}X_{V_{t2}} \tag{2.34}$$

The inner-loop controller equations are written by assuming no measurement delays. The state equations corresponding to inner-loop controllers on both sides of MMCs are given by Equations (2.35)-(2.38)

$$\dot{X}_{i_{t1d}} = \left(i_{t1d(r)} - i_{t1d}\right) \tag{2.35}$$

$$\dot{X}_{i_{t2d}} = \left(i_{t2d(r)} - i_{t2d}\right) \tag{2.36}$$

$$\dot{X}_{i_{t1q}} = \left(i_{t1q(r)} - i_{t1q}\right) \tag{2.37}$$

$$\dot{X}_{i_{t2q}} = \left(i_{t2q(r)} - i_{t2q}\right) \tag{2.38}$$

The linear equations from outer-loop controllers are used to replace the reference currents of the above equations to obtain the final dynamic equations. The state-space models of control system can be obtained by linearizing the controller dynamic equations and by combining them into the state-space form as shown in Equation (2.39).

For terminal1,

$$\Delta\dot{\mathbf{X}}_{c1} = \mathbf{A}_{c1}\Delta\mathbf{X}_{c1} + \mathbf{A^*}_{c1}\Delta\mathbf{X}_{ms1} + \mathbf{B}_{c1}\Delta\mathbf{U_{c1}} + \mathbf{E}_{c1}\Delta\mathbf{I}_{t1}^{dq} \tag{2.39}$$

Where,

$$\begin{aligned}
\Delta\mathbf{X}_{c1} &= \left[\Delta X_{v_{dc1}}, \Delta X_{V_{t1}}, \Delta X_{i_{t1d}}, \Delta X_{i_{t1q}}\right]^T \\
\Delta\mathbf{I}_{t1}^{dq} &= \left[\Delta i_{t1d}, \Delta i_{t1q}\right]^T \\
\Delta\mathbf{X}_{m1} &= \left[\Delta v_{dc1(m)}, \Delta V_{t1(m)}\right]^T \\
\Delta\mathbf{U}_{r1} &= \left[\Delta v_{dc1(r)}, \Delta V_{t1(r)}\right]^T
\end{aligned}$$

$$\mathbf{A}_{c1} = \begin{bmatrix} 0 & 0 & 0 & 0 \\ 0 & 0 & 0 & 0 \\ K_{I(v_{dc1})} & 0 & 0 & 0 \\ 0 & K_{I(V_{t1})} & 0 & 0 \end{bmatrix}$$

$$\mathbf{A^*}_{c1} = \begin{bmatrix} -1 & 0 \\ 0 & -1 \\ -K_{P(v_{dc1})} & 0 \\ 0 & -K_{P(V_{t1})} \end{bmatrix}$$

$$\mathbf{B}_{c1} = \begin{bmatrix} 1 & 0 \\ 0 & 1 \\ K_{P(v_{dc1})} & 0 \\ 0 & K_{P(V_{t1})} \end{bmatrix}$$

$$\mathbf{E}_{c1} = \begin{bmatrix} 0 & 0 \\ 0 & 0 \\ -1 & 0 \\ 0 & -1 \end{bmatrix}$$

For terminal2,

$$\Delta\dot{\mathbf{X}}_{c2} = \mathbf{A}_{c2}\Delta\mathbf{X}_{c2} + \mathbf{A^*}_{c2}\Delta\mathbf{X}_{ms2} + \mathbf{B}_{c2}\Delta\mathbf{U_{c2}} + \mathbf{E}_{c2}\Delta\mathbf{I}_{t2}^{dq} \tag{2.40}$$

Where,

$$\Delta\mathbf{X}_{c2} = \left[\Delta X_{P_{t2}}, \Delta X_{v_{t2}}, \Delta X_{i_{t2d}}, \Delta X_{i_{t2q}}\right]^T$$

$$\Delta\mathbf{I}_{t2}^{dq} = \left[\Delta i_{t2d}, \Delta i_{t2q}\right]^T$$

$$
\begin{aligned}
\Delta\mathbf{X}_{(m)2} &= \left[\Delta P_{t2(m)}, \Delta V_{t2(m)}\right]^T \\
\Delta\mathbf{U}_{c2} &= \left[\Delta P_{t2(r)}, \Delta V_{t2(r)}\right]^T \\
\mathbf{A}_{c2} &= \begin{bmatrix} 0 & 0 & 0 & 0 \\ 0 & 0 & 0 & 0 \\ K_{I(P_{t2})} & 0 & 0 & 0 \\ 0 & K_{I(V_{t2})} & 0 & 0 \end{bmatrix} \\
\mathbf{A^*}_{c2} &= \begin{bmatrix} -1 & 0 \\ 0 & -1 \\ -K_{P(P_{t2})} & 0 \\ 0 & -K_{P(V_{t2})} \end{bmatrix} \\
\mathbf{B}_{c2} &= \begin{bmatrix} 1 & 0 \\ 0 & 1 \\ K_{P(P_{t2})} & 0 \\ 0 & K_{P(V_{t2})} \end{bmatrix} \\
\mathbf{E}_{c2} &= \begin{bmatrix} 0 & 0 \\ 0 & 0 \\ -1 & 0 \\ 0 & -1 \end{bmatrix}
\end{aligned}
$$

The output signals of the inner-loop controllers are combined with terminal voltage measurements and decoupling terms to produce the voltage orders (v_o) as shown in Figure 2.1. The voltage order equations for terminal1 and terminal2 are given by Equations (2.41) and (2.42) respectively.

For terminal1,

$$\Delta \mathbf{V}_{o1}^{dq} = \mathbf{C}_{o1}\Delta \mathbf{X}_{c1} + \mathbf{C^*}_{o1}\Delta \mathbf{X}_{ms1} + \mathbf{D}_{o1}\Delta \mathbf{U}_{c1} + \mathbf{K}_{o1}\Delta \mathbf{V}_{t1}^{dq} + \mathbf{L}_{o1}\Delta \mathbf{I}_{t1}^{dq} \tag{2.41}$$

Where,

$$\begin{aligned}
\Delta \mathbf{V}_{o1}^{dq} &= \left[\Delta v_{1d(o)}, \Delta v_{1q(o)}\right]^T \\
\Delta \mathbf{X}_{c1} &= \left[\Delta X_{v_{dc1}}, \Delta X_{V_{t1}}, \Delta X_{i_{t1d}}, \Delta X_{i_{t1q}}\right]^T \\
\Delta \mathbf{X}_{ms1} &= \left[\Delta v_{dc1(m)}, \Delta V_{t1(m)}\right]^T \\
\Delta \mathbf{U}_{c1} &= \left[\Delta v_{dc1(r)}, \Delta V_{t1(r)}\right]^T \\
\Delta \mathbf{V}_{t1}^{dq} &= [\Delta v_{t1d}, \Delta v_{t1q}]^T \\
\Delta \mathbf{I}_{t1}^{dq} &= [\Delta i_{t1d}, \Delta i_{t1q}]^T \\
\mathbf{C}_{o1} &= \begin{bmatrix} -K_{P(i_{t1d})}K_{I(v_{dc1})} & 0 & -K_{I(i_{t1d})} & 0 \\ 0 & -K_{P(i_{t1q})}K_{I(V_{t1})} & 0 & -K_{I(i_{t1q})} \end{bmatrix} \\
\mathbf{C^*}_{o1} &= \begin{bmatrix} K_{P(v_{dc1})}K_{P(i_{t1d})} & 0 \\ 0 & K_{P(V_{t1})}K_{P(i_{t1q})} \end{bmatrix} \\
\mathbf{D}_{o1} &= \begin{bmatrix} -K_{P(v_{dc1})}K_{P(i_{t1d})} & 0 \\ 0 & -K_{P(V_{t1})}K_{P(i_{t1q})} \end{bmatrix} \\
\mathbf{K}_{o1} &= \begin{bmatrix} 1 & 0 \\ 0 & 1 \end{bmatrix} \\
\mathbf{L}_{o1} &= \begin{bmatrix} K_{P(i_{t1d})} & \omega L_{eq} \\ -\omega L_{eq} & K_{P(i_{t1q})} \end{bmatrix}
\end{aligned}$$

For terminal2,

$$\Delta \mathbf{V}_{o2}^{dq} = \mathbf{C}_{o2}\Delta \mathbf{X}_{c1} + \mathbf{C^*}_{o1}\Delta \mathbf{X}_{ms2} + \mathbf{D}_{o2}\Delta \mathbf{U}_{c2} + \mathbf{K}_{o2}\Delta \mathbf{V}_{t2}^{dq} + \mathbf{L}_{o2}\Delta \mathbf{I}_{t2}^{dq} \tag{2.42}$$

Where,

$$\begin{aligned}
\Delta \mathbf{V}_{o2}^{dq} &= \left[\Delta v_{2d(o)}, \Delta v_{2q(o)}\right]^T \\
\Delta \mathbf{X}_{c2} &= \left[\Delta X_{P_{t2}}, \Delta X_{V_{t2}}, \Delta X_{i_{t2d}}, \Delta X_{i_{t2q}}\right]^T \\
\Delta \mathbf{X}_{ms2} &= \left[\Delta P_{t2(m)}, \Delta V_{t2(m)}\right]^T \\
\Delta \mathbf{U}_{c2} &= \left[\Delta P_{t2(r)}, \Delta V_{t2(r)}\right]^T \\
\Delta \mathbf{V}_{t2}^{dq} &= \left[\Delta v_{t2d}, \Delta v_{t2q}\right]^T \\
\Delta \mathbf{I}_{t2}^{dq} &= \left[\Delta i_{t2d}, \Delta i_{t2q}\right]^T \\
\mathbf{C}_{o2} &= \begin{bmatrix} -K_{P(i_{t2d})}K_{I(P_{t2})} & 0 & -K_{I(i_{t2d})} & 0 \\ 0 & -K_{P(i_{t2q})}K_{I(V_{t2})} & 0 & -K_{I(i_{t2q})} \end{bmatrix} \\
\mathbf{C^*}_{o2} &= \begin{bmatrix} K_{P(P_{t2})}K_{P(i_{t2d})} & 0 \\ 0 & K_{P(V_{t2})}K_{P(i_{t2q})} \end{bmatrix} \\
\mathbf{D}_{o1} &= \begin{bmatrix} -K_{P(P_{t2})}K_{P(i_{t2d})} & 0 \\ 0 & -K_{P(V_{t2})}K_{P(i_{t2q})} \end{bmatrix} \\
\mathbf{K}_{o1} &= \begin{bmatrix} 1 & 0 \\ 0 & 1 \end{bmatrix} \\
\mathbf{L}_{o1} &= \begin{bmatrix} K_{P(i_{t2d})} & \omega L_{eq} \\ -\omega L_{eq} & K_{P(i_{t2q})} \end{bmatrix}
\end{aligned}$$

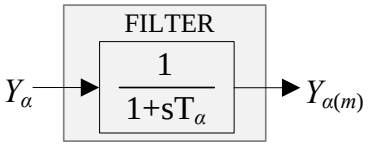

Figure 2.9: Block diagram of the single-pole measurement filter

2.2.6 Measurement Filter Model

Typically, the outer-loop control variables are filtered using measurement filters to remove the noise. It is reported in literature [22] that measurement filters have considerable effect on the stability of VSC systems. Therefore, it is very important to model the dynamics of these filters. A first order measurement filter model shown in Figure 2.9 is used to filter the outer-loop controller parameters. The dynamic equation of the filter model is given by Equation (2.43).

$$\dot{Y}_{\alpha(m)} = \frac{1}{T_\alpha}\left(Y_\alpha - Y_{\alpha(m)}\right) \tag{2.43}$$

The equations representing measurement dynamics of four outer-loop quantities are given by Equations (2.44)-(2.47).

$$\dot{v}_{dc1(m)} = \frac{1}{T_{v_{dc1}}}\left(v_{dc1} - v_{dc1(m)}\right) \tag{2.44}$$

$$\dot{P}_{t1(m)} = \frac{1}{T_{P_{t1}}}\left(P_{t1} - P_{t1(m)}\right) \tag{2.45}$$

$$\dot{V}_{t1(m)} = \frac{1}{T_{V_{t1}}}\left(V_{t1} - V_{t1(m)}\right) \tag{2.46}$$

$$\dot{V}_{t2(m)} = \frac{1}{T_{V_{t2}}}\left(V_{t2} - V_{t2(m)}\right) \tag{2.47}$$

By substituting P_{t2}, V_{t1}, and V_{t2} in-terms of the $R-I$ frame quantities of voltages and currents and by linearizing the equations, the state-space models of measurement delays are obtained as given by Equations (2.48) and (2.49).

For terminal1,

$$\Delta\dot{\mathbf{X}}_{ms1} = \mathbf{A}_{ms1}\Delta\mathbf{X}_{ms1} + \mathbf{A^*}_{ms1}\Delta v_{dc1} + \mathbf{F}_{ms1}\Delta\mathbf{I}_{t1} \tag{2.48}$$

Where,

$$\begin{aligned}
\Delta\mathbf{X}_{ms1} &= \left[\Delta v_{dc1(m)}, \Delta V_{t1(m)}\right]^T \\
\Delta\mathbf{V}_{t1} &= \left[\Delta V_{t1R}, \Delta V_{t1I}\right]^T \\
\mathbf{A}_{ms1} &= \begin{bmatrix} -k_{ms1} & 0 \\ 0 & -k_{ms2} \end{bmatrix} \\
\mathbf{A^*}_{ms1} &= \begin{bmatrix} k_{ms1} \end{bmatrix} \\
\mathbf{F}_{ms1} &= \begin{bmatrix} 0 & 0 \\ k_{ms2}d_1V_{t1R0} & k_{ms2}d_1V_{t1I0} \end{bmatrix}
\end{aligned}$$

with

$$k_{ms1} = \frac{1}{T_{v_{dc1}}}, \qquad k_{ms2} = \frac{1}{T_{V_{t1}}}, \qquad d_1 = \frac{1}{\sqrt{V_{t1R0}^2 + V_{t1I0}^2}}$$

Similarly, for terminal2,

$$\Delta\dot{\mathbf{X}}_{ms2} = \mathbf{A}_{ms2}\Delta\mathbf{X}_{ms2} + \mathbf{A^*}_{ms2}\Delta\mathbf{I}_{t2} + \mathbf{E}_{ms2}\Delta\mathbf{V}_{t2} \tag{2.49}$$

Where,

$$\begin{aligned}
\Delta\mathbf{X}_{ms2} &= \left[\Delta P_{t2(m)}, \Delta V_{t2(m)}\right]^T \\
\Delta\mathbf{I}_{t2} &= \left[\Delta I_{t2R}, \Delta I_{t2I}\right]^T \\
\Delta\mathbf{V}_{t2} &= \left[\Delta V_{t2R}, \Delta V_{t2I}\right]^T \\
\mathbf{A}_{ms2} &= \begin{bmatrix} -k_{ms3} & 0 \\ 0 & -k_{ms4} \end{bmatrix} \\
\mathbf{A^*}_{ms2} &= \begin{bmatrix} k_{ms3}V_{t2R0} & k_{ms3}V_{t2I0} \\ 0 & 0 \end{bmatrix} \\
\mathbf{E}_{ms2} &= \begin{bmatrix} k_{ms3}I_{t2R0} & k_{ms3}I_{t2I0} \\ k_{ms4}d_2V_{t1R0} & k_{ms4}d_2V_{t1I0} \end{bmatrix}
\end{aligned}$$

with,

$$k_{ms3} = \frac{1}{T_{P_{t2}}}, \qquad k_{ms4} = \frac{1}{T_{V_{t2}}}, \qquad d_2 = \frac{1}{\sqrt{V_{t2R0}^2 + V_{t2I0}^2}}$$

2.2.7 Axis Transformation

The d-q decoupled control uses synchronous reference (d-q) frame currents and voltages. However, the ac side is modelled using real-imaginary (R-I) frame quantities.

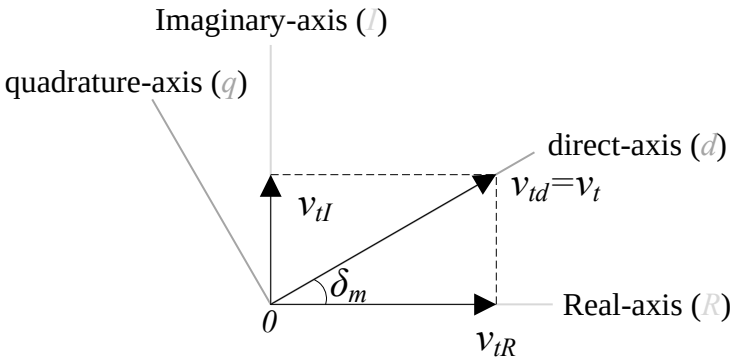

Figure 2.10: R-I to d-q transformation

Therefore, to combine the control system equations and power network equations, the *d-q* to *R-I* transformation shown in Figure 2.10 is used. The angle δ_m is the phase angle of the terminal voltage (v_t) and it is obtained using the PLL as shown in Figure 2.4.

The *d-q* to *R-I* transformation and inverse transformation matrices for a vector X are given by Equations (2.50) and (2.51) respectively.

$$\begin{bmatrix} X_d \\ X_q \end{bmatrix} = \begin{bmatrix} \cos(\delta_m) & \sin(\delta_m) \\ -\sin(\delta_m) & \cos(\delta_m) \end{bmatrix} \begin{bmatrix} X_R \\ X_I \end{bmatrix} \tag{2.50}$$

$$\begin{bmatrix} X_R \\ X_I \end{bmatrix} = \begin{bmatrix} \cos(\delta_m) & -\sin(\delta_m) \\ \sin(\delta_m) & \cos(\delta_m) \end{bmatrix} \begin{bmatrix} X_d \\ X_q \end{bmatrix} \tag{2.51}$$

The linearized equation for transformation and inverse transformation of voltages and currents can be written as given by Equations (2.52) to (2.54).

$$\Delta \mathbf{V}_t^{dq} = \mathbf{K}_v \Delta \mathbf{V}_t + \mathbf{M}_v \Delta \delta_m \tag{2.52}$$

$$\Delta \mathbf{I}_t^{dq} = \mathbf{K}_i \Delta \mathbf{I}_t + \mathbf{M}_i \Delta \delta_m \tag{2.53}$$

$$\Delta \mathbf{V}_i = \mathbf{J}_v \Delta \mathbf{V}_i^{dq} + \mathbf{N}_v \Delta \delta_m \tag{2.54}$$

Where,

$$\begin{aligned}
\Delta \mathbf{V}_t^{dq} &= [\Delta v_{td}, \Delta v_{tq}]^T \\
\Delta \mathbf{V}_t &= [\Delta V_{tR}, \Delta V_{tI}]^T \\
\Delta \mathbf{V}_i^{dq} &= [\Delta v_{id}, \Delta v_{iq}]^T \\
\Delta \mathbf{V}_i &= [\Delta V_{iR}, \Delta V_{iI}]^T \\
\Delta \mathbf{I}_t^{dq} &= [\Delta i_{td}, \Delta i_{tq}]^T \\
\Delta \mathbf{I}_t &= [\Delta I_{tR}, \Delta I_{tI}]^T \\
\mathbf{K}_v &= \begin{bmatrix} cos\left(\delta_{m0}\right) & sin\left(\delta_{m0}\right) \\ -sin\left(\delta_{m0}\right) & cos\left(\delta_{m0}\right) \end{bmatrix} \\
\mathbf{K}_i &= \begin{bmatrix} cos\left(\delta_{m0}\right) & sin\left(\delta_{m0}\right) \\ -sin\left(\delta_{m0}\right) & cos\left(\delta_{m0}\right) \end{bmatrix} \\
\mathbf{J}_v &= \begin{bmatrix} cos\left(\delta_{m0}\right) & -sin\left(\delta_{m0}\right) \\ sin\left(\delta_{m0}\right) & cos\left(\delta_{m0}\right) \end{bmatrix} \\
\mathbf{M}_v &= \begin{bmatrix} -V_{tR0} sin\left(\delta_{m0}\right) + V_{tI0} cos\left(\delta_{m0}\right) \\ -V_{tR0} cos\left(\delta_{m0}\right) - V_{tI0} sin\left(\delta_{m0}\right) \end{bmatrix} \\
\mathbf{M}_i &= \begin{bmatrix} -I_{tR0} sin\left(\delta_{m0}\right) + I_{tI0} cos\left(\delta_{m0}\right) \\ -I_{tR0} cos\left(\delta_{m0}\right) - I_{tI0} sin\left(\delta_{m0}\right) \end{bmatrix} \\
\mathbf{N}_v &= \begin{bmatrix} -v_{id0} sin\left(\delta_{m0}\right) - v_{iq0} cos\left(\delta_{m0}\right) \\ v_{id0} cos\left(\delta_{m0}\right) - v_{iq0} sin\left(\delta_{m0}\right) \end{bmatrix}
\end{aligned}$$

2.2.8 Overall State-Space Model

The complete state-space model given in Equation (2.55) is obtained by combining linearized equations of ac system, dc system, control system, PLL and measurement filters. The matrix combination was computed using MATLAB software. The signal flows between sub-systems are shown in Figure 2.11. This system consists of 27 state variables and 8 control inputs in total as shown in Tables 2.2 and 2.3 respectively.

$$\Delta\dot{\mathbf{X}} = \mathbf{A}\Delta\mathbf{X} + \mathbf{B}\Delta\mathbf{U} \tag{2.55}$$

Table 2.2: State variables of the system

System	**State variables**	
	MMC1	**MMC2**
AC system	ΔI_{s1R}, ΔI_{s1I}, ΔI_{t1R}, ΔI_{t1I}	ΔI_{s2R}, ΔI_{s2I}, ΔI_{t2R}, ΔI_{t2I}
DC system	Δv_{dc1}	Δv_{dc2}
	Δi_{dc}	
Control system	$\Delta X_{(v_{dc1})}$, $\Delta X_{V_{t1}}$, $\Delta X_{i_{t1d}}$, $\Delta X_{i_{t1q}}$	$\Delta X_{P_{t2}}$, $\Delta X_{V_{t2}}$, $\Delta X_{i_{t2d}}$, $\Delta X_{i_{t2q}}$
PLL	X_{PLL1}, $\Delta\delta_{m1}$	ΔX_{PLL2}, $\Delta\delta_{m2}$
Measurements	$\Delta v_{dc1(m)}$, $\Delta V_{t1(m)}$	$\Delta P_{t2(m)}$, $\Delta V_{t2(m)}$

Table 2.3: Control inputs of the system

System	**State variables**	
	MMC1	**MMC2**
AC system	ΔV_{s1R}, ΔV_{s1I}	ΔV_{s2R}, ΔV_{s2I}
Control system	$\Delta v_{dc1(r)}$, $\Delta V_{t1(r)}$	$\Delta P_{t2(r)}$, $\Delta V_{t2(r)}$

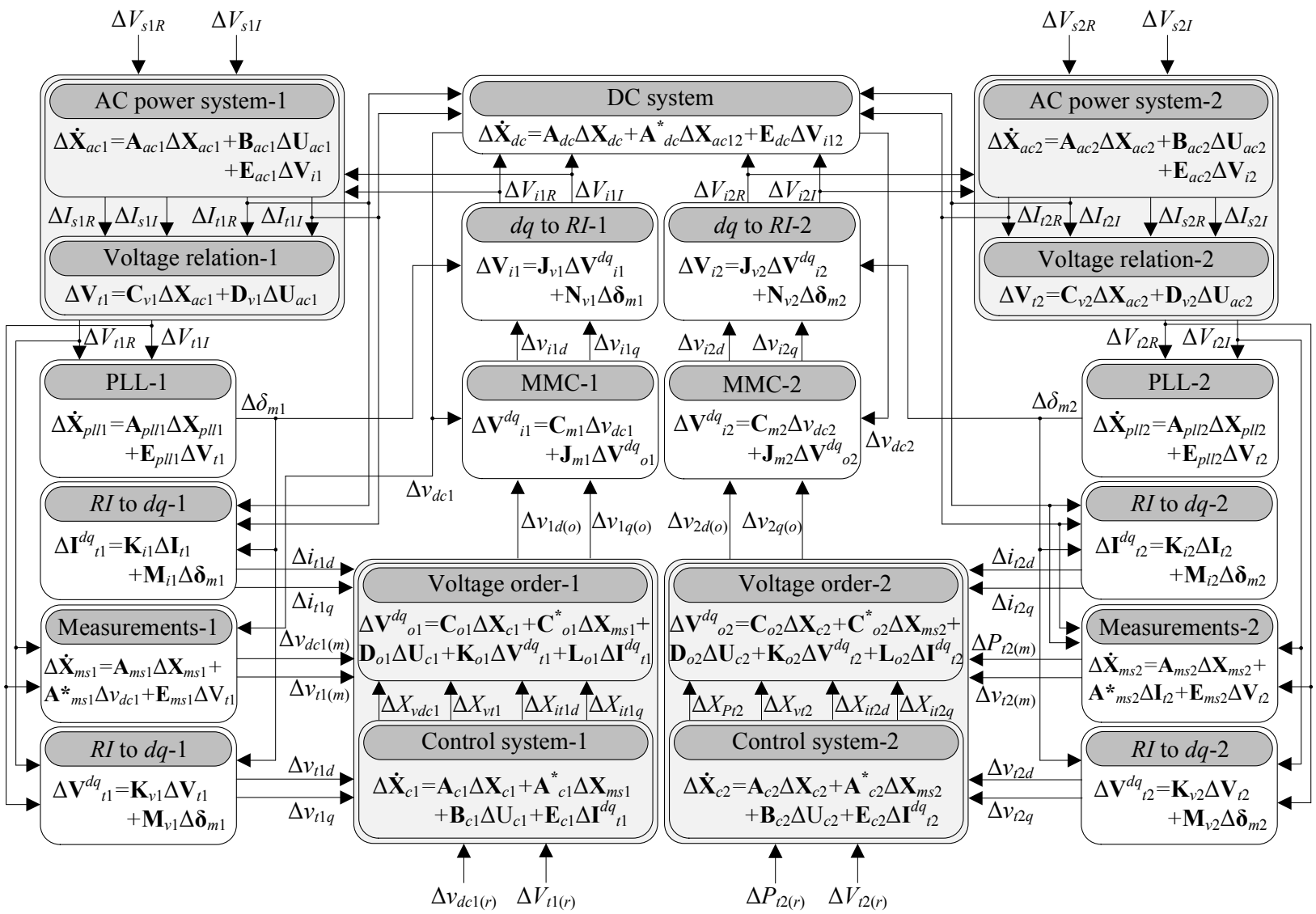

Figure 2.11: 27th order small-signal model of the point-to-point MMC-VSC system

The overall state-space model given by Equation (2.55) can be excited by applying signals to the control inputs. The outputs of the system can be written as linear combinations of states and control inputs as given by Equation (2.56).

$$\Delta \mathbf{Y} = \mathbf{C}\Delta \mathbf{X} + \mathbf{D}\Delta \mathbf{U} \tag{2.56}$$

where $\mathbf{C}$ and $\mathbf{D}$ are user defined matrices to generate required outputs.

2.3 Validation of Linearized Model

Small-signal models of power systems are obtained by linearizing the non-linear equations of power systems. Therefore, it is recommended to validate the small-signal model against a non-linear simulation model before using it for stability assessment. In this thesis, the model validation is performed in two steps as described below.

2.3.1 Validation of AC System and PLL Models

As the first step, the linearized models of ac network and PLL are validated. This validation is performed for the test network shown in Figure 2.12a. The ac network is connected to a series R-L load and the terminal voltage phase angle and the angular frequency are tracked using the SRF-PLL shown in Figure 2.12b. The system parameters are given in Table 2.4. The small-signal model is represented as $\Delta \dot{\mathbf{X}} = \mathbf{A}\Delta \mathbf{X} + \mathbf{B}\Delta \mathbf{U}$ and the state variables and control inputs are given in Table. 2.5.

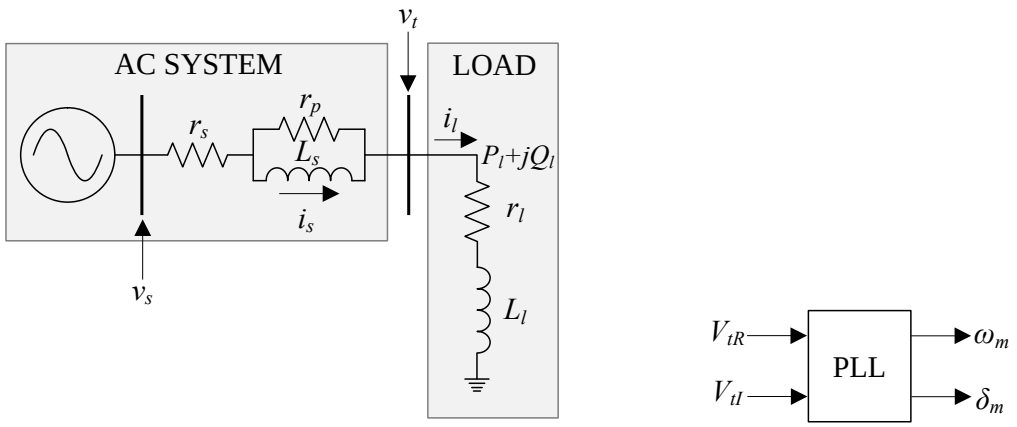

(a) Simple power system (b) Phase-locked loop

Figure 2.12: Test system used to validate the ac network and PLL models

Table 2.4: Parameters of the simple power system

Parameter	**Notation**	**Numerical Value**
Thévenin voltage	v_s	288∠23° kV
Terminal voltage	v_t	230∠0° kV
Load power	$P_l + jQ_l$	500 MW + j100 MVAr
Source Impedance	r_s	3.691 Ω
	L_s	0.1379 H
	r_p	1507 Ω
Load impedance	r_l	20.346 Ω
	L_l	0.269 H

Table 2.5: State variables and control inputs of the simple power system

State Variables	**Control Inputs**
ΔI_{sR}, ΔI_{sI}, ΔI_{tR}, ΔI_{tI}, X_{PLL}, $\Delta\delta_m$	ΔV_{sR}, ΔV_{sI}

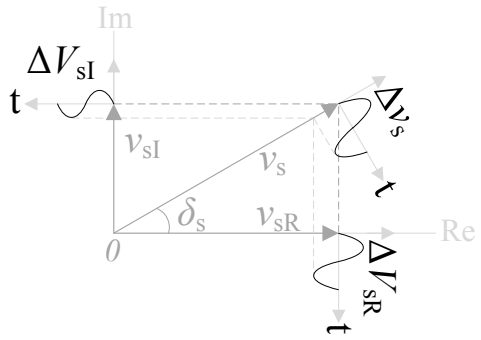

Figure 2.13: Disturbance applied to the Thévenin voltage magnitude

At first, the Thévenin voltage magnitude of the EMT model was changed by a sinusoidal disturbance (Δv_s) as shown in Figure 2.13. Then, the corresponding disturbances (ΔV_{sR}, ΔV_{sI}) were applied to the small-signal model to obtain responses for the same disturbance. The frequencies of the sinusoidal disturbances were selected as 20 Hz and 200 Hz to validate the model for a wide range of frequencies. The results obtained using EMT and small-signal (SS) models are compared in Figs. 2.14a and 2.14b.

Then, the phase angle of the Thévenin voltage was changed by a sinusoidal disturbance (Δv_s), as shown in Figure 2.15. The corresponding changes, ΔV_{sR} and ΔV_{sI} were also applied to the small-signal model. Simulation results from both EMT and SS models are compared in Figs. 2.16a and 2.16b.

It can be observed from the validation results shown in Figures 2.14 and 2.16 that the small-signal models of ac system and PLL are accurate and valid up to a frequency of 200 Hz.

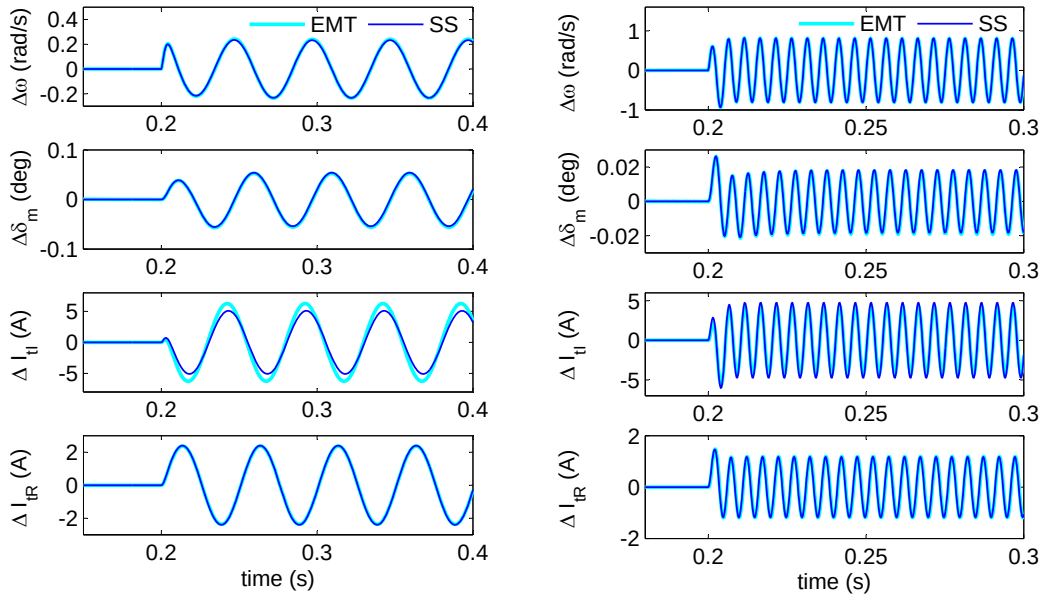

(a) (b)

Figure 2.14: Simulation results comparison for a sinusoidal disturbance with (a) 20 Hz and (b) 200 Hz applied to the Thévenin voltage magnitude

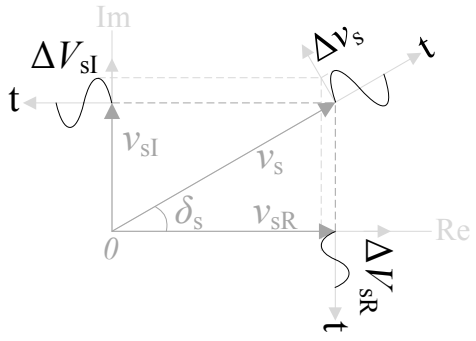

Figure 2.15: Disturbance applied to the Thévenin voltage phase angle

2.3.2 Validation of Complete Linearized Model of VSC System

The complete linearized model of the point-to-point MMC-VSC system is validated against the non-linear EMT simulation. For this validation, the SCR values are selected as 2.0 and the PI-controller parameters are given in Table 2.6. The model

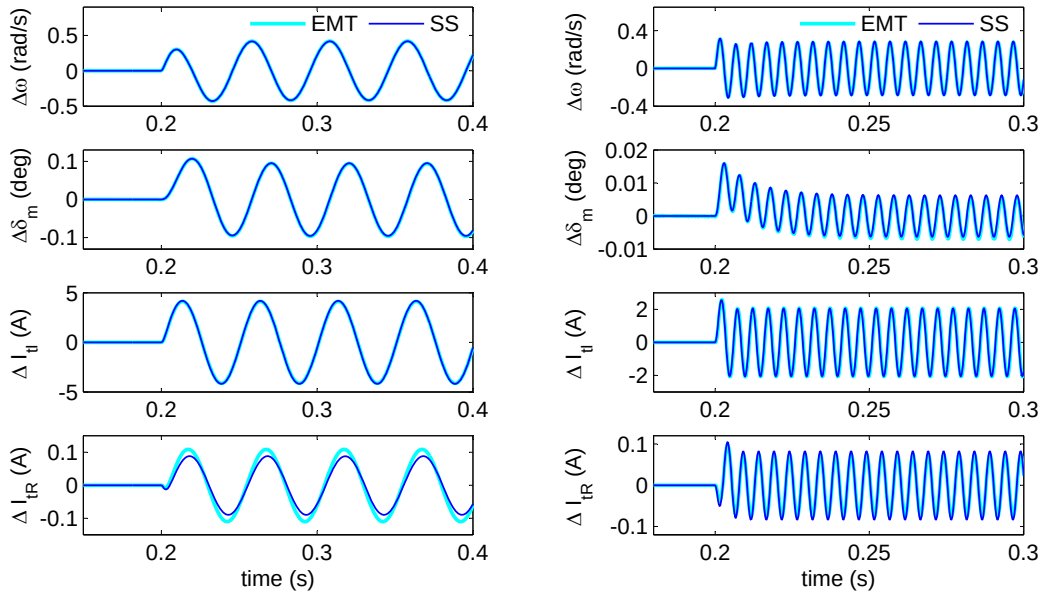

(a) (b)

Figure 2.16: Simulation results comparison for a sinusoidal disturbance with (a) 20 Hz and (b) 200 Hz applied to the Thévenin voltage phase angle

Table 2.6: PI-controller gains

Controller	**Terminal1**		**Terminal2**	
	$\mathbf{K}_P$	$\mathbf{K}_I$	$\mathbf{K}_P$	$\mathbf{K}_I$
PLL	50	250	50	250
DC voltage	2	20	—	—
Active Power	—	—	1	20
AC voltage	1	20	1	20
d-axis current	1	100	1	100
q-axis current	1	100	1	100

validation is performed by changing all four reference settings ($v_{dc1(r)}$, $P_{t2(r)}$, $V_{t1(r)}$, and $V_{t2(r)}$) of the test system one at a time. A small-pulse with a magnitude of 0.03 p.u. and a duration of 100 ms is used as the disturbance to each of the reference settings.

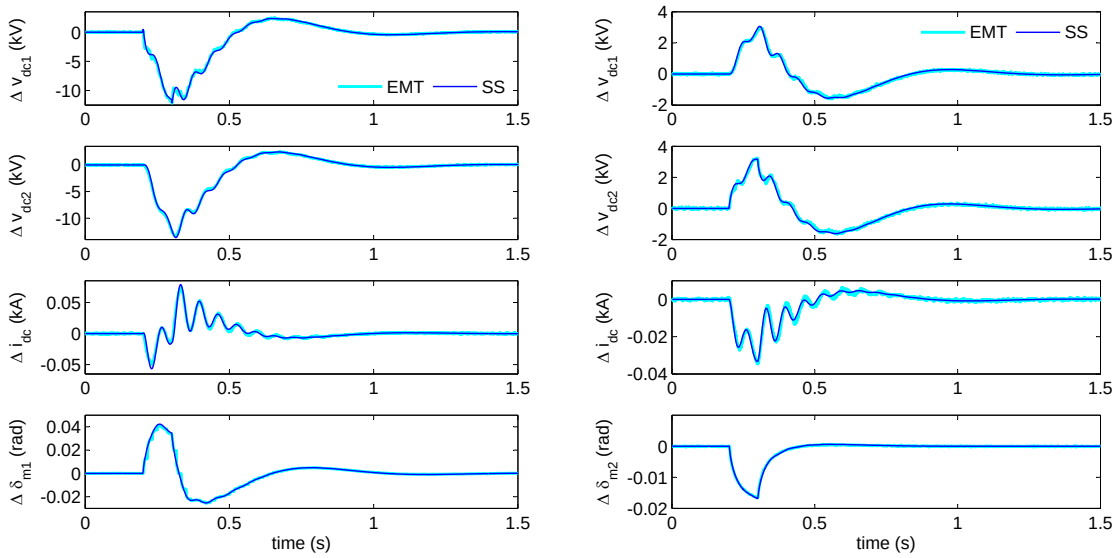

(a) (b)

Figure 2.17: Changes in variables for a small pulse applied at 0.2 s to (a) the dc voltage reference of terminal1 and (b) the power reference of terminal2

Disturbance to DC Voltage Reference

The dc voltage reference of terminal1 was disturbed by applying a small pulse (0.03 p.u. and 100 ms). The simulation results from EMT and small-signal (SS) models are compared in Figure 2.17a.

Disturbance to Power Reference

The active power order of terminal2 was disturbed by applying a small pulse (0.03 p.u. and 100 ms). The simulation results from EMT and small-signal (SS) models are compared in Figure 2.17b.

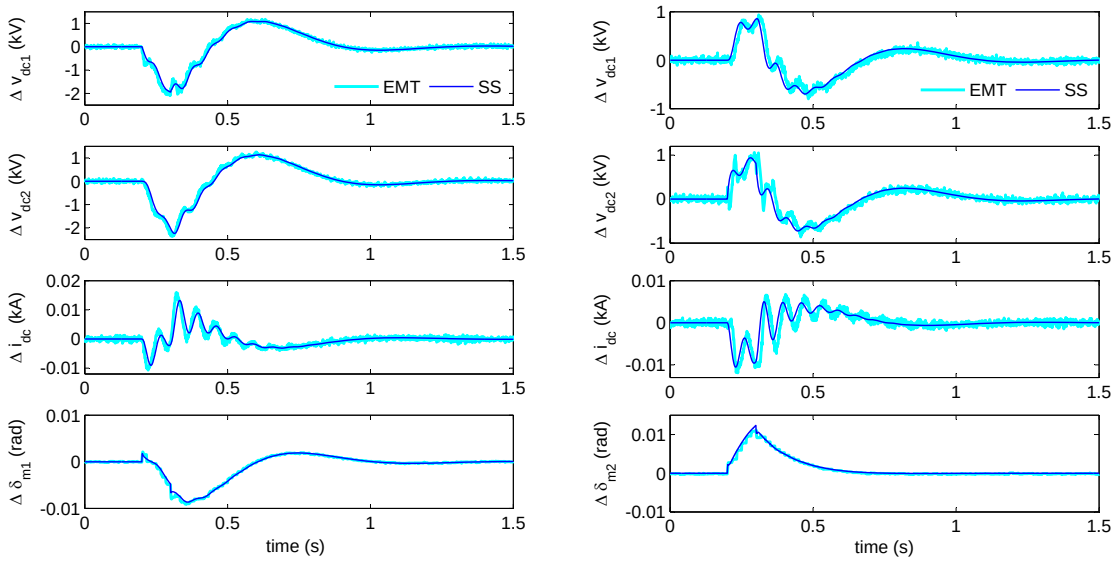

(a) (b)

Figure 2.18: Changes in variables for a small pulse applied at 0.2 s to the ac voltage reference of (a) terminal1 and (b) terminal2

Disturbance to AC Voltage References

The ac voltage references of terminal1 and terminal2 were changed one at a time by applying a small pulse (0.03 p.u. and 100 ms). The simulation results from EMT and small-signal (SS) models are compared in Figs. 2.18a and 2.18b.

The validation results shown in Figures 2.17 and 2.18 confirm that the dynamics of the test system is accurately represented by the small-signal model. The accuracy observed in PLL angle confirms that the PLL model is correctly represented to capture the transients in terminal voltage phase angle. The small-signal model which is developed and validated is used in this thesis to perform small-signal stability assessment and controller tuning.

2.4 Chapter Summary

This chapter explained the development of simulation models of the test system incorporating all important dynamics. The Taylor series expansion is used to linearize the non-linear equations of the test system. The ac system is modelled using dynamic phasors and the validation results presented in this chapter showed that the model is capable of capturing frequencies up to 200 Hz. The validation of the overall state-space model showed a good agreement with the non-linear EMT simulation model of the test system.

Chapter 3

Small-Signal Stability Assessment of MMC-VSC System

Stability of linear continuous-time systems can be analyzed using different methods such as state-space analysis, root-locus, Bode diagram, and Nyquist stability theory. Among those methods, the eigenvalue analysis is powerful and popular in control system studies. It can produce stability related frequency domain attributes such as eigenvalues, modes (frequency and damping), eigenvectors, and participations factors. Therefore, it is more commonly used to assess the stability compared to other linear stability analysis techniques. In addition, the state-space analysis is also commonly used to assess the small-signal stability of non-linear systems such as power systems [57, 46]. In order to perform small-signal assessment, an accurate linarized state-space model of the non-linear system must be used. In this chapter, the small-signal model of the test system that was derived and validated in **Chapter 2** is utilized to perform the stability assessment.

3.1 Small-Signal Stability Assessment

A linearized power system can be represented by Equation (3.1).

$$\Delta\dot{\mathbf{X}} = \mathbf{A}\Delta\mathbf{X} + \mathbf{B}\Delta\mathbf{U} \tag{3.1}$$

Where, $\Delta\mathbf{X}$ is the vector of change in state variables, $\Delta\mathbf{U}$ is the vector of change in control inputs, $\mathbf{A}$ is the system matrix, and $\mathbf{B}$ is the input matrix. The representation in Equation (3.1) allows the user to compute different stability attributes of the system as explained below.

3.1.1 Eigenvalues and System Stability

The eigenvalues of the system matrix can be computed by solving Equation (3.2).

$$det\left(\mathbf{A} - \lambda\mathbf{I}\right) = 0 \tag{3.2}$$

Where, λ denotes the eigenvalues of the system.

If the system has n number of states, the solutions to Equation (3.2) will be n identical eigenvalues (i.e: $\lambda = \lambda_1, \lambda_2, ..., \lambda_n$). The eigenvalues are used to assess the stability of the system around the operating point ("stability in small") at which the system is linearized. The stability criteria explained in [46] is given below and it is based on the Lyapunov's first method [58].

1. "When the eigenvalues have negative real parts, the original system is asymptotically stable."
2. "When at least one of the eigenvalues has a positive real part, the original system is unstable."

3. "When the eigenvalues have real parts equal to zero, it is not possible on the basis of the first approximation to say anything in general."

The "stability in the large"can be assessed using Lyapunav's second method or the direct method [58]. However, such stability studies are out of the scope of this thesis.

3.1.2 Modes

Modes of the system are computed from the eigenvalues of the system. Then, the oscillatory and non-oscillatory modes and their stability properties are identified as explained below.

- "A real eigenvalue corresponds to a non-oscillatory (aperiodic) mode. A negative real eigenvalue represents an aperiodic mode. The larger its magnitude, the faster the decay. A positive real eigenvalue represents aperiodic instability."
- "Complex eigenvalues occur in conjugate pairs and each pair corresponds to an oscillatory mode. A negative real part represents a damped oscillation whereas a positive real part represents oscillation of increasing amplitude."

  If the conjugate eigenvalues are $\sigma \pm j\omega$, the frequency of oscillation is given by Equation (3.3) and the corresponding damping ratio is given by Equation (3.4).

$$f = \frac{\omega}{2\pi} \tag{3.3}$$

$$\zeta = \frac{-\sigma}{\sqrt{\sigma^2 + \omega^2}} \tag{3.4}$$

3.1.3 Eigenvectors

Each eigenvalue (λ_i) of the system is associated with a column vector ($\mathbf{\Phi_i}$) that satisfies the relationship given in Equation (3.5). This vector $\mathbf{\Phi_i}$ is known as the right eigenvector of $\mathbf{A}$ associated with λ_i.

$$\mathbf{A}\mathbf{\Phi_i} = \lambda_i \mathbf{\Phi_i} \tag{3.5}$$

Where,

$$\begin{aligned} \mathbf{\Phi_i} &= [\phi_{1i}, \phi_{2i}, \ldots, \phi_{ni}]^T \\ i &= 1, 2, ..., n \end{aligned}$$

Similarly the row vector ($\mathbf{\Psi_i}$) that satisfies Equation (3.6) is known as the left eigenvector of $\mathbf{A}$ associated with λ_i.

$$\Psi_i \mathbf{A} = \lambda_i \Psi_i \tag{3.6}$$

Where,

$$\begin{aligned} \mathbf{\Psi_i} &= [\psi_{1i}, \psi_{2i}, \ldots, \psi_{ni}] \\ i &= 1, 2, ..., n \end{aligned}$$

Therefore, the right and left eigenvector matrices corresponding to the system matrix ($\mathbf{A}$) can be written as given by Equations (3.7) and (3.8) respectively.

$$\mathbf{\Phi} = [\mathbf{\Phi_1} \quad \mathbf{\Phi_2} \quad \dots \quad \mathbf{\Phi_n}] \tag{3.7}$$

$$\mathbf{\Psi} = \begin{bmatrix} \mathbf{\Psi_1^T} & \mathbf{\Psi_2^T} & \dots & \mathbf{\Psi_n^T} \end{bmatrix} \tag{3.8}$$

3.1.4 Participation Factors

Participation factors form a relationship between the modes and state variables of the system. The participation matrix given in Equation (3.9) combines the right and left eigenvectors [46].

$$\mathbf{P} = [\mathbf{P_1} \quad \mathbf{P_2} \quad \dots \quad \mathbf{P_n}] \tag{3.9}$$

Where,

$$\mathbf{P_i} = \begin{bmatrix} P_{1i} \\ P_{2i} \\ \vdots \\ P_{ni} \end{bmatrix} = \begin{bmatrix} \Phi_{1i}\Psi_{i1} \\ \Phi_{2i}\Psi_{i2} \\ \vdots \\ \Phi_{ni}\Psi_{in} \end{bmatrix}$$

The participation factors are used to study the influence of state variables on modes of the system. In addition, the participation factors are also used to classify system modes into different groups in interaction studies. In ac power systems, participations factor analysis is widely used to identify intra-area and inter-area oscillations and sub-synchronous resonance [46].

Table 3.1: PI-controller gains

Terminal	**Controller**	**SCR=5.0**		**SCR=2.0**		**SCR=1.5**	
		$\mathbf{K}_P$	$\mathbf{K}_I$	$\mathbf{K}_P$	$\mathbf{K}_I$	$\mathbf{K}_P$	$\mathbf{K}_I$
Terminal1	PLL	50	250	50	250	50	250
	DC voltage	2	20	2	20	2	20
	AC voltage	1	20	1	20	1	20
	d-axis current	1	100	1	100	0.5	50
	q-axis current	1	100	1	100	0.5	50
Terminal2	PLL	50	250	50	250	50	250
	Active Power	1	20	1	20	1	20
	AC voltage	1	20	1	20	1	20
	d-axis current	1	100	1	100	0.5	50
	q-axis current	1	100	1	100	0.5	50

3.2 Eigenvalue Analysis of Test System

The point-to-point MMC-VSC system is connected to ac systems with different SCR values. For this stability evaluation, strong ac system (SCR=5.0), moderately strong ac system (SCR=2.0), and weak ac system (SCR=1.5) connections are considered. The controller parameters used for the small-signal stability assessment are given in Table 3.1 and these parameters are obtained by trial and error method. In addition, it must be noted that to achieve a stable system, the inner current controller gains were reduced for the case with SCR=1.5. The oscillatory modes of the system at the rated operating conditions are given in Table 3.2. It can be observed that there are two modes (Mode 5 and 8) with low damping. In addition, it can also be observed that when the ac system strength decreases, the damping of all modes decreases. Moreover, the decrease in damping of mode 8 is significant when the ac system strength becomes low (i.e: SCR=1.5).

Table 3.2: Frequency and damping of system modes for different SCR values

Mode	**SCR=5.0**		**SCR=2.0**		**SCR=1.5**	
	f (Hz)	ζ (%)	f (Hz)	ζ (%)	f (Hz)	ζ (%)
Mode 1	106.09	99.7	474.44	83.0	617.17	66.6
Mode 2	60.30	99.0	431.04	75.1	574.69	53.9
Mode 3	75.08	99.9	111.46	99.6	154.58	99.0
Mode 4	21.78	99.8	57.06	98.7	99.80	97.3
Mode 5	15.52	10.1	15.57	9.5	15.58	9.0
Mode 6	3.06	98.8	3.91	97.4	4.98	95.8
Mode 7	0.67	99.9	3.19	98.6	3.95	98.0
Mode 8	1.27	39.4	1.31	28.6	1.34	21.4
Mode 9	-	-	0.62	92.3	0.97	85.4

3.3 Participation Factor Analysis of Test System

The participation factors are used to track and classify system modes into network and controller modes. For the purpose of explanation, the test system connected to ac systems with SCR of 2.0 are considered. The participation factors corresponding to low damped mode (Mode 5) are shown in Figure 3.1 and the system state numbers are given in Table 3.3.

Although most states of the system show non zero participations in this mode, the major participations are from the dc system states. Therefore, this mode can be identified as the dc network mode. The dc system oscillation are typically the resonance between the transmission line inductor and the equivalent sub-module capacitors. Therefore, mode 5 can be specifically identified as the dc resonance. The

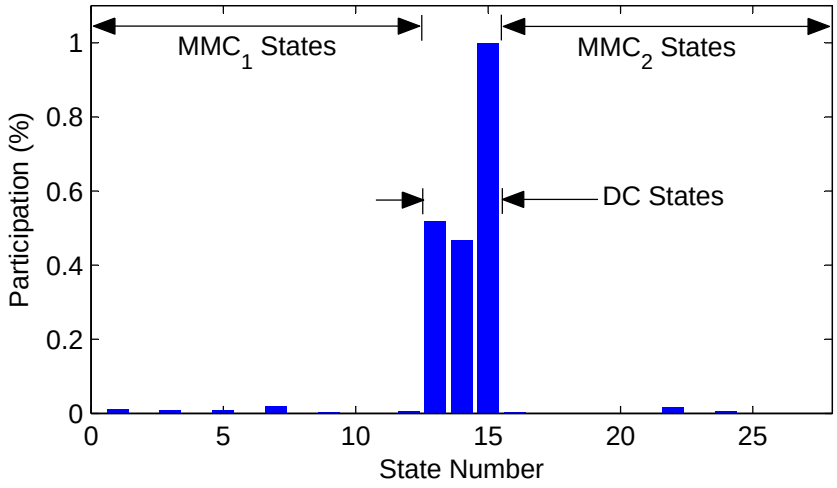

Figure 3.1: Participation factors associated with Mode 5

Table 3.3: System state numbers of the 27th order model

System	**State Numbers**	
	MMC1	**MMC2**
AC system	1-4	16-19
d-q control system	5-8	20-23
Measurement	9-10	24-25
PLL	11-12	26-27
DC voltage	13	15
DC current	14	

participation factors associated with the ac network modes (Modes 1-4) are shown in Figure 3.2. Similarly, the participation factors of control modes (Modes 6-9) are shown in Figure 3.3. The mode classification is given in Table 3.4. It can be seen from Figure 3.3 that modes corresponding to controllers in one converter are influenced by the states of the other converter. This observation verifies the interaction between converters.

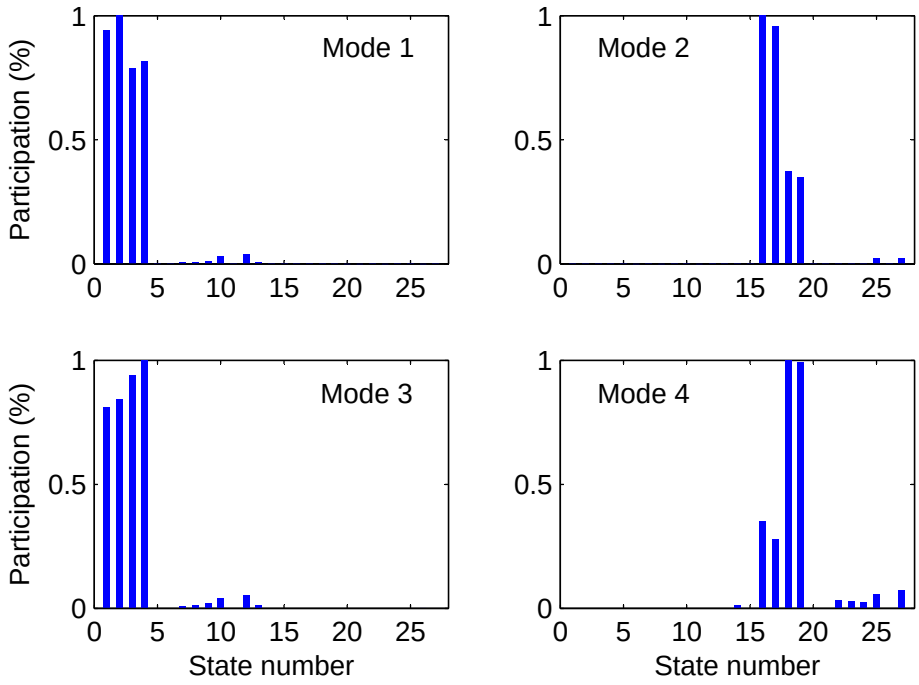

Figure 3.2: Participation factors associated with the ac network modes (State numbers are given in Table 3.3)

Table 3.4: Classification of modes

Modes	**f (Hz)**	ζ (%)	**Classification**	
1	474.44	83.0	MMC1 ac current	network modes
2	431.04	75.1	MMC2 ac current	
3	111.46	99.6	MMC1 ac current	
4	57.06	98.7	MMC2 ac current	
5	15.57	9.5	dc resonance	
6	3.91	97.4	MMC1 current controller	controller modes
7	3.19	98.6	MMC2 current controller	
8	1.31	28.6	MMC1 dc voltage controller	
9	0.62	92.3	MMC2 power controller	

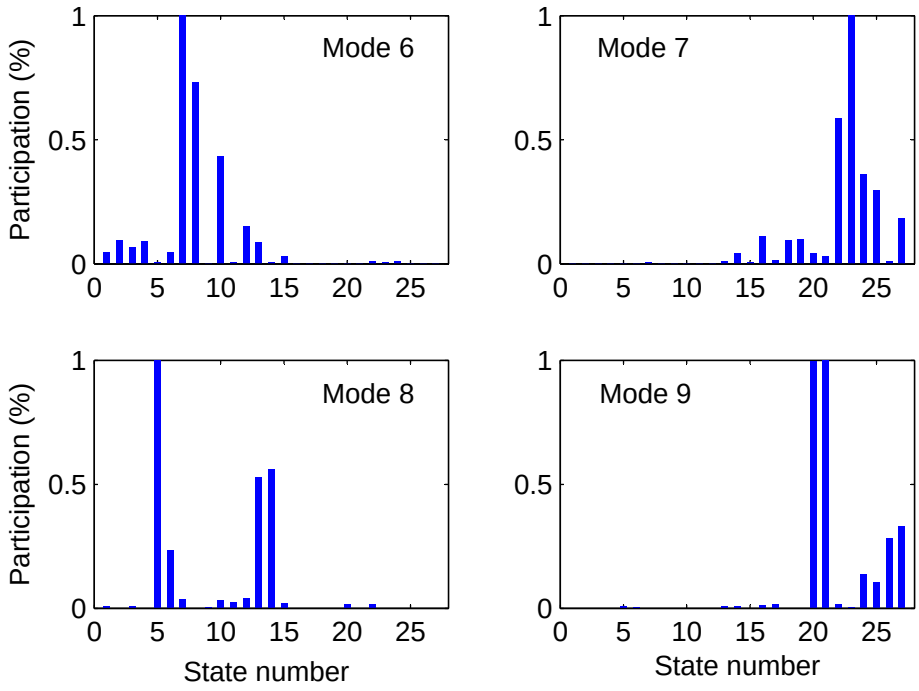

Figure 3.3: Participation factors associated with the controller modes (State numbers are given in Table 3.3)

3.4 Sensitivity Analysis

In this section, the sensitivities of system parameters such as ac system strength, dc line length, sub-module capacitor, PLL gains, and measurement delays to the system stability are investigated by means of the eigenvalue analysis. The effect of PI-controller gains are not investigated one by one as they all impact the stability of the system together. The combined effect is analysed in **Chapter 5** of this thesis.

3.4.1 Effect of AC System Strength

It is reported in literature that the ac system strength is a key factor that affects the stability of VSC systems [22, 44, 49]. To investigate the influence of the ac system strength using the frequency-domain approach, the SCR values of ac systems on both

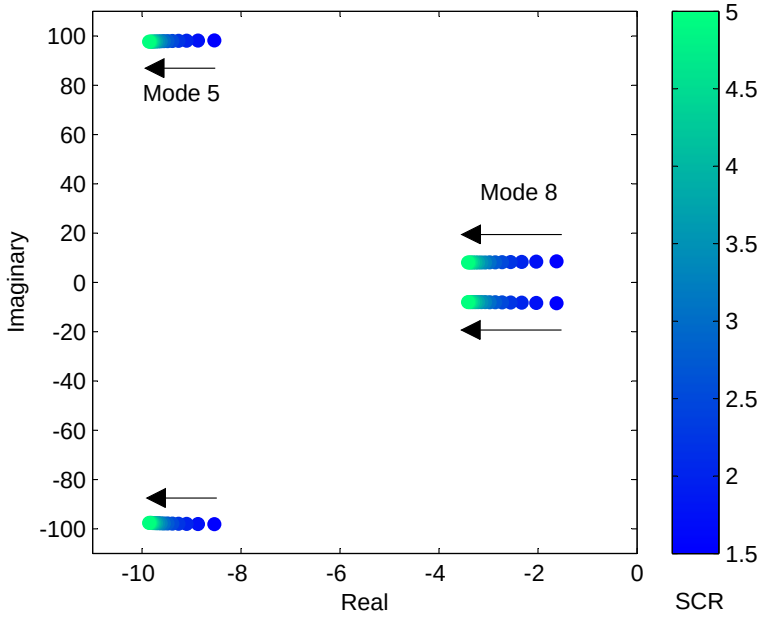

Figure 3.4: Loci of critical modes for the change in ac system strength

ends of the MMC-VSC test system were changed from 1.5 to 5.0 in steps of 0.25 and the system eigenvalue trajectories were observed. The range of SCR values were selected to cover ac systems strength from weak to strong. The loci of low damped modes are shown in Figure 3.4.

It was noted that all eigenvalues moved to more stable region of the complex plane when the SCR was increased. It is clear that for the selected practical range of SCR values, the system becomes more stable when the ac system strength increases.

3.4.2 Effects of PLL Gains

In MMC-VSC systems, the PLL is used to track the terminal ac voltage phase angle for control purposes. To investigate the influence of PLL gains on the small-signal stability of the test system, the MMC-VSC system was connected to weak ac grids (SCR=1.5) on both sides. The PLL gains of each MMC converter is changed one at a time and the eigenvalue trajectories are used to evaluate the stability of the system.

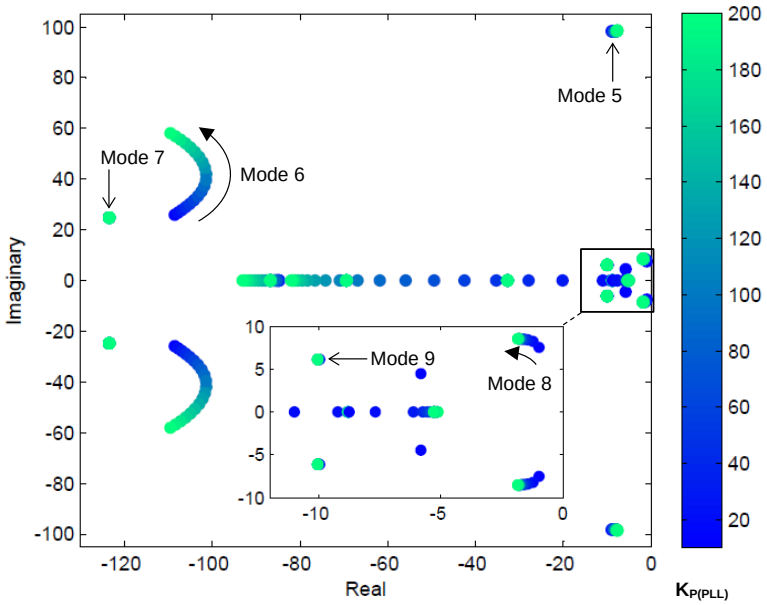

Figure 3.5: Loci of critical modes for a change in MMC1 (dc voltage controlling) PLL gains

Typically, for a PLL, the integral gain is selected to have a value higher than the proportional gain. In this study, the integral gain of the PLL ($K_{I(PLL)}$) is chosen as five times of the proportional gain ($K_{P(PLL)}$).

Initially, the MMC1 (dc voltage controlling side) PLL proportional gain was changed from 10 to 200 in steps of 10 (integral gain from 50 to 1000 in steps of 50) and the loci of critical modes are shown in Figure 3.5. It can be noted that the system eigenvalues move towards more stable region when the PLL gains are increased.

Then, the MMC2 (power controlling side) PLL proportional gain was changed from 10 to 200 in steps of 10 (integral gain from 50 to 1000 in steps of 50) and the loci of critical modes are shown in Figure 3.6. A similar observation is made as eigenvalues move towards the more stable region with the increase of PLL gains. Therefore, it can be said that the small-signal performance of the MMC-VSC system is improved

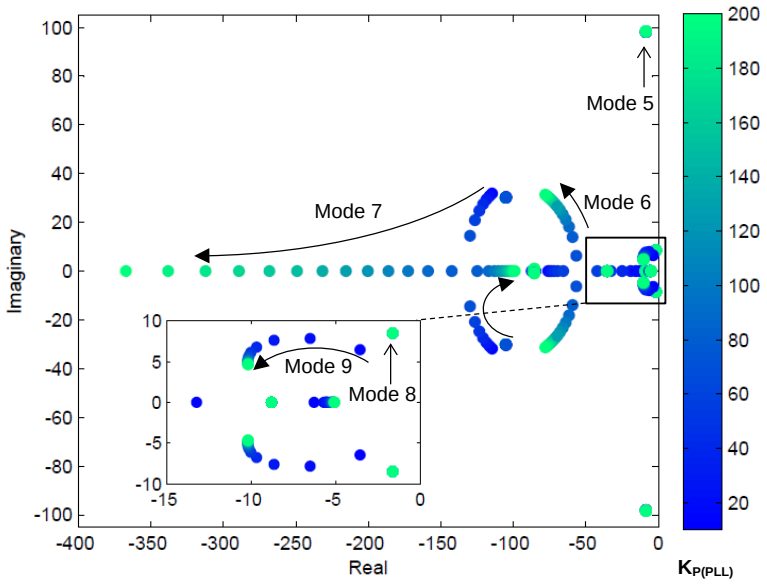

Figure 3.6: Loci of critical modes for a change in MMC2 (power controlling) PLL gains

by high PLL gains. However, the use of high PLL gains can cause instability when the measuring delays in instantaneous quantities are considered in system modelling as described in the following section.

3.4.3 Effects of Measuring Delays

In practical systems, the measurement transducers are used to measure instantaneous voltages and currents. The use of measurement transducers introduce certain delays in measured quantities. These measurement delays are ignored in simulation models available in literature [59, 60, 61, 62]. However, the measurement delays in instantaneous quantities such as voltages and currents can result in serious stability issues as explained in this section.

The small-signal model used so far in this thesis considered the effects of measurement filter models for the outer-loop control variables such as RMS voltages and powers. However, it did not consider the effects of measuring delays in instantaneous

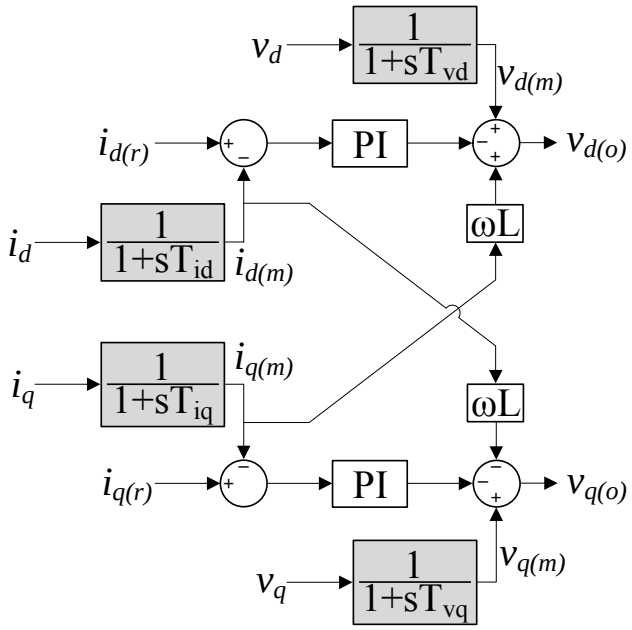

Figure 3.7: Inner-loop of d-q decoupled controller with measuring delay models

voltages and currents. Therefore, the small-signal model of the MMC-VSC system developed in **Chapter 3** is added with the dynamics of measuring delays of d-q voltages and currents. The modified d-q decoupled control system with delay models is shown in Figure 3.7 and the same delay models are incorporated to the EMT model of the test system.

The small-signal model of the test system was added with the first order delay model shown in in Figure 3.9 and the filter dynamic equation is given in Equation (3.10). The parameter α is replaced with i_{t1d}, i_{t1q}, i_{t2d}, i_{t2q} to obtain dynamic equations of current measurements and with v_{t1d}, v_{t1q}, v_{t2d}, v_{t2q} to obtain the dynamic equations of voltage measurements. The addition of 8 dynamic equations increased the order of the small-signal model to 35. The overall small-signal model with signal flow paths is shown in Figure 3.8. The state variables of the system with the corresponding state numbers are given in Table 3.5.

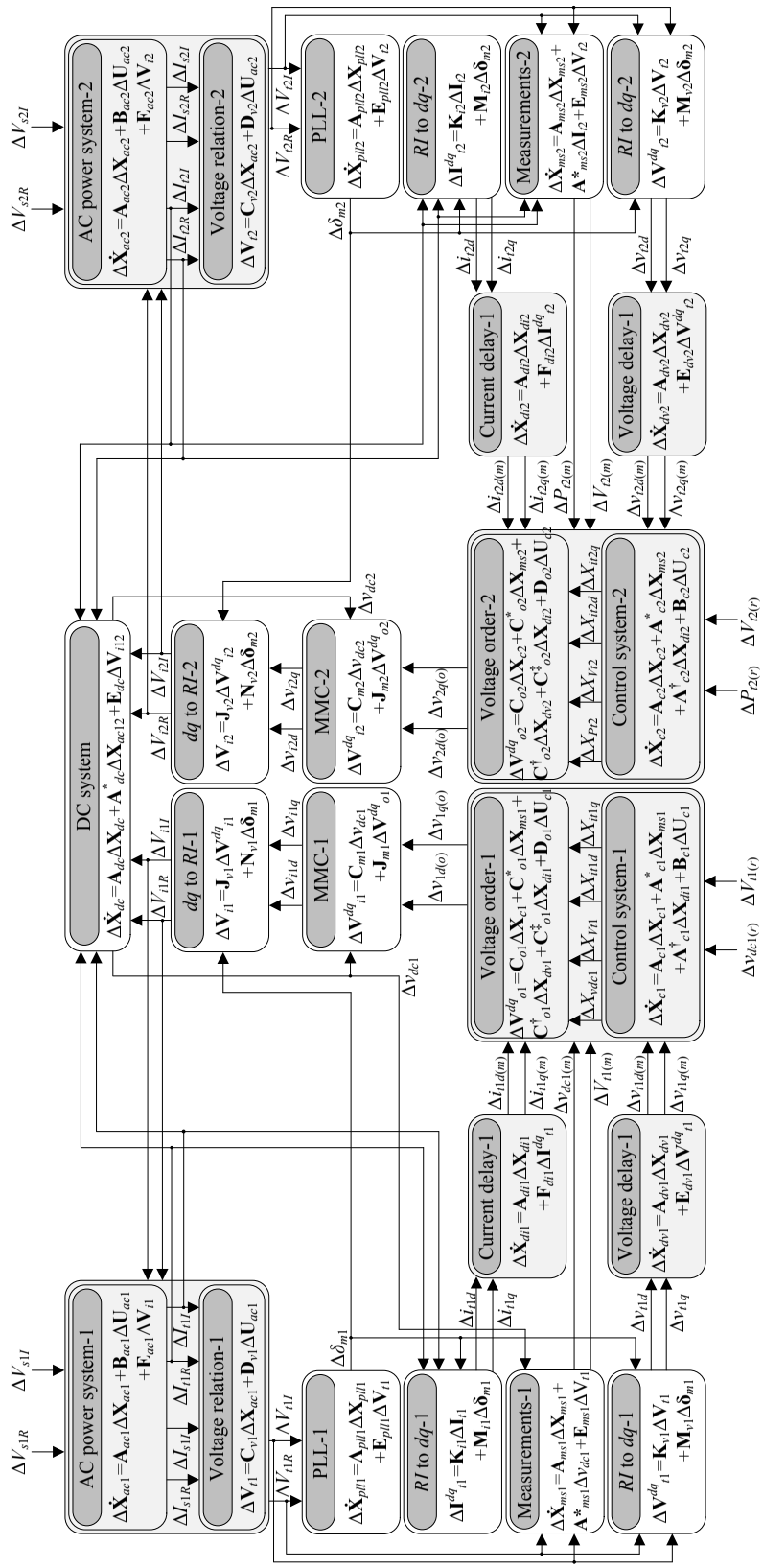

Figure 3.8: 35th order small-signal model of the point-to-point MMC-VSC system

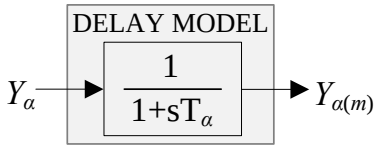

Figure 3.9: Block diagram of the measuring delay model

Table 3.5: System state numbers of the 35th order model

System	**State Numbers**	
	MMC1	**MMC2**
AC system	1-4	20-23
d-q control system	5-8	24-27
dc voltage measurement	9	-
power measurement	-	28
RMS ac voltage measurement	10	29
d-q current measurement delay	11-12	30-31
d-q voltage measurement delay	13-14	32-33
PLL	15-16	34-35
DC voltage	17	19
DC current	18	

$$\dot{Y}_{\alpha(m)} = \frac{1}{T_\alpha}\left(Y_\alpha - Y_{\alpha(m)}\right) \tag{3.10}$$

In actual systems, measurement filters are used to remove the unwanted signals (noise) for control purposes. Typically, a time-constant around one cycle (15-20 ms) is used for slow varying signals such as average powers and RMS voltages. However, the fast varying signals such as instantaneous currents and voltages are measured with fast acting transducers. Therefore, a very small time-constant, such as a quarter cycle, may be used. In addition, the current measurement transducers are faster compared to the voltage transducers. The measuring time-constants used for this

Table 3.6: Measurement filter time-constants

Control-loop	**Filter**	**Time-constant**
outer-loop	DC voltage	0.5 ms
	Average power	20 ms
	RMS ac voltage	20 ms
inner-loop	d-q frame currents	1.5 ms
	d-q frame voltages	5 ms

Table 3.7: Interested oscillatory modes after the inclusion of measuring delays

Mode No	**Frequency**	**Damping**	**Classification**
Mode 2	112.79 Hz	24 %	MMC1 ac current
Mode 4	107.71 Hz	23 %	MMC2 ac current
Mode 10	50.77 Hz	3 %	MMC1 voltage delay
Mode 11	44.17 Hz	6 %	MMC2 voltage delay
Mode 12	14.12 Hz	98 %	MMC2 current delay
Mode 13	12.68 Hz	98 %	MMC1 current delay

investigation are given in Table 3.6. The ac system strength of both sides of the ac systems are set to 1.5 to reflect weak ac networks and oscillatory modes of interest are given in Table 3.7.

It can be noted that the modelling of delays in instantaneous d-q quantities has decreased both frequency and damping of modes 2 and 4. In addition, the modelling of delay also introduced four additional modes and out of which two (modes 10 and 11) are critical as shown in Table 3.7. The damping of other modes (Mode 1, 3, 6, 7, and 9) were adequate.

The participation of system states to the low damped modes (Modes 10 and 11) are shown in Figure 3.10. It can be seen that major participations to these modes are the measured d-q voltages and currents. However, a considerable high participation

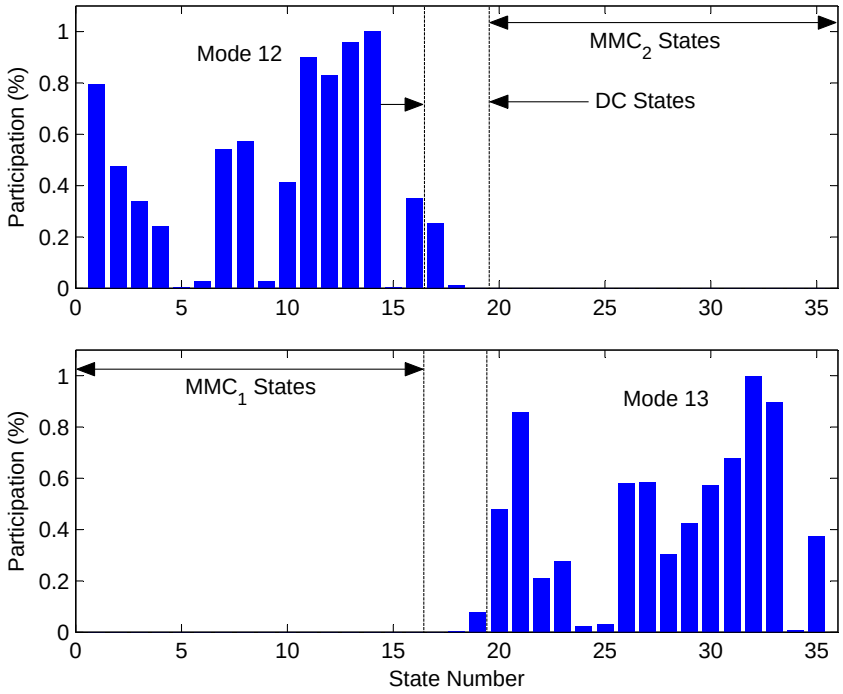

Figure 3.10: Participation factors of states to measurement delay modes (state numbers are given in Table 3.5)

from PLL (states 15, 16) can also be observed. This observation indicates that these measurement delay modes are influenced by PLL gains.

The influence of PLL gains is further investigated using sensitivity analysis by changing PLL gains of both sides one at a time. The PLL proportional gain $K_{P(PLL)}$ was changed from 10 to 200 in steps of 10 and the corresponding $K_{I(PLL)}$ value was changed from 50 to 1000 in steps of 50). The loci of interested modes for the change in PLL gains of dc voltage controlling side (MMC1) and power controlling side (MMC2) are plotted in Figures 3.11 and 3.12 respectively. It can be observed that when the MMC1 side PLL gains are increased, the critical mode (mode 10) moves towards more stable region of the complex plane. In contrast, when the MMC2 side PLL gains are increased, the critical mode (mode 11) moves in the undesirable direction and causes instability for high PLL gains ($K_{P(PLL)}$>100 and $K_{I(PLL)}$>500). It was noted that

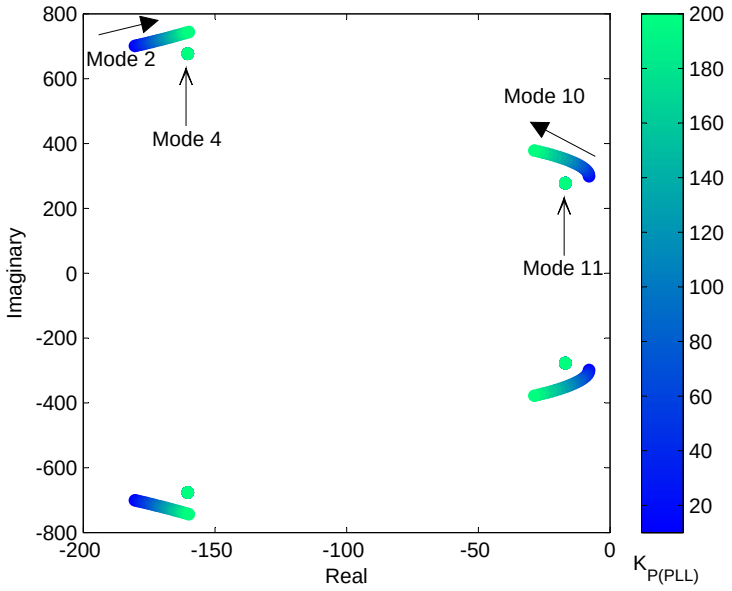

Figure 3.11: Loci of critical modes for a change in rectifier (dc voltage controlling) side PLL gains

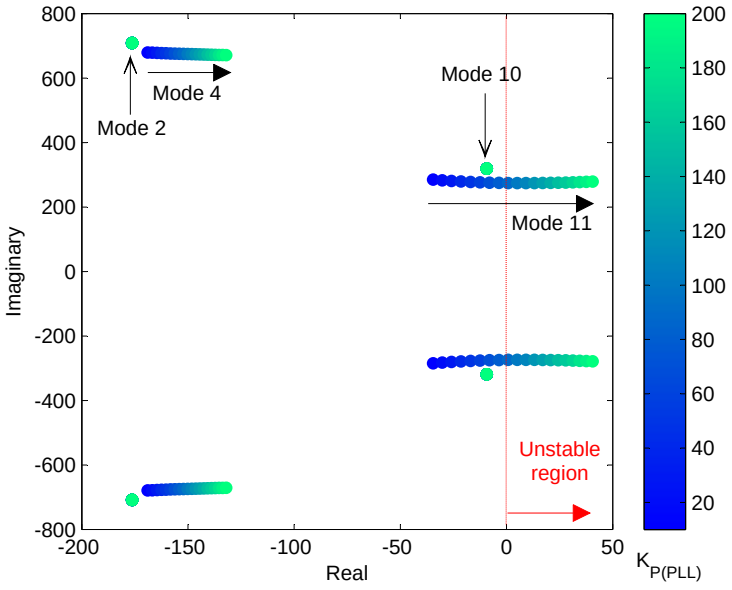

Figure 3.12: Loci of critical modes for a change in inverter (power controlling) side PLL gains

the loci of all other modes reported in Table 3.2 lie in stable region for the above changes in PLL gains.

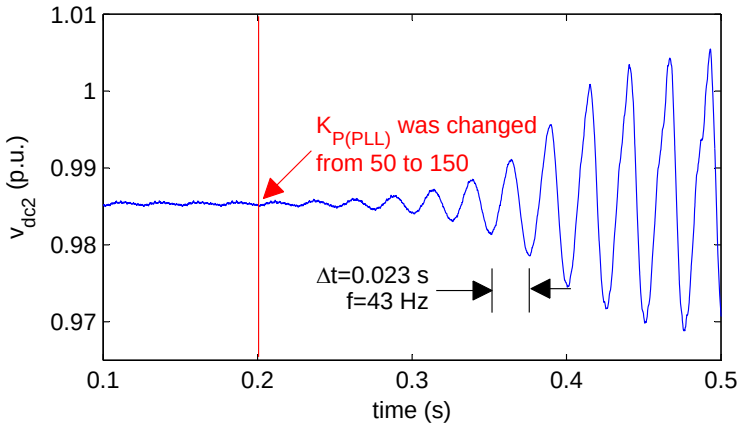

Figure 3.13: Variation of dc voltage for a step change in PLL gain of MMC2 (power controlling converter)

The frequency of the unstable mode (mode 11) seen in Figure 3.12, has a frequency of is 43.45 Hz. This instability was further verified using EMT simulations on RTDS. At steady state, the proportional gain of inverter side PLL was changed from 50 to 150 and the EMT simulation result is shown in Figure 3.13. It can be seen that the growing oscillations in the inverter side dc voltage shows a frequency of 43 Hz, which is close to the unstable mode observed by small-signal stability assessment.

3.5 Chapter Summary

A comprehensive analysis of small-signal stability of the MMC-VSC system has been presented in this chapter. The influence of network and controller parameters to the stability of the system is analysed by means of small-signal stability assessment. It is demonstrated that the change in ac system strength can significantly influence the MMC-VSC system stability. The importance of modelling the delays introduced by measurement transducers is discussed. In addition, it has been shown that the use of very high PLL gains for the MMC that controls the active power can lead the system to instabilities.

Chapter 4

Generalized Frequency-Domain Controller Tuning Procedure

.

The key contribution of this thesis is the development of a generalized frequency-domain controller tuning procedure to tune d-q decoupled controllers used in MMC-VSC systems. The PI-controller tuning problem is formulated as an optimization problem. The objective function is written by incorporating frequency-domain stability attributes. The steps to solve the optimization problem using the simulated annealing optimization technique is described in detail in this chapter. The main advantage of the proposed controller tuning technique is the simultaneous tuning of all PI-controllers in the d-q decoupled control system. In addition, any number of converters in a dc grid can be simultaneously tuned using this technique. The objective function developed for the proposed method is general so that any suitable optimization technique can be used.

4.1 Application of Linear Control Techniques

In general, the linearized state-space model of a non-linear system can be expressed by Equation (4.1).

$$\Delta\dot{\mathbf{X}} = \mathbf{A}\Delta\mathbf{X} + \mathbf{B}\Delta\mathbf{U} \tag{4.1}$$

Where $\Delta\mathbf{X}$ is the state vector that consists of changes in state variables and $\Delta\mathbf{U}$ is the input vector that consists of changes in inputs to the system. Matrices $\mathbf{A}$ and $\mathbf{B}$ are named as system matrix and input matrix respectively. The stability of the test system around a particular operating point is determined by the eigenvalues of the system matrix $\mathbf{A}$. The system is stable only if all eigenvalues lie on the left-half plane of the complex coordinate system [63]. Matrices $\mathbf{A}$ and $\mathbf{B}$ mainly depend on the operating point at which the small-signal model of the non-linear system is obtained. By considering a possible range of operating conditions, it is possible to investigate the impact of controller gains on the overall stability of the system.

The performance of a system during a large disturbance, such as faults, is usually governed by non-linearities such as limits and non-linear gains. However, the recovery of the system after a large disturbance is determined by the modes of the system. A better dynamic performance can be achieved if the oscillatory modes are adequately damped and if the aperiodic modes have adequate large negative values (i.e.: fast decaying time-constants). It was observed through simulations [49] and also reported in literature [47] that converters interact through the dc system. In addition, the system stability is influenced by the ac system strength [22, 49]. When a particular operating point is considered, the controller gains decide positions of eigenvalues. Therefore, the controller tuning method for such systems must consider the dynamics of the entire system including the ac system, dc system, and control system.

4.2 Development of Generalized Frequency Domain Controller Tuning Procedure

In this research, the PI-controller gains of the entire MMC-VSC test system are tuned by considering different operating conditions and ac system strengths. Damping of oscillatory modes will decide the settling speeds of oscillations present after a disturbance. The aperiodic modes or the real eigenvalues will determine the settling times of dc offsets after a disturbance. Based on the understanding of the stability and the dynamic performance of the linearized model of the test system, the objectives of the optimization problem are defined:

- To improve the damping of low damped oscillatory modes while maintaining the damping of well damped oscillatory modes for all considered operating conditions.
- To move all aperiodic modes towards the left side of the negative real axis for all considered operating conditions.

The gain tuning problem is formulated as a constrained optimization problem. The constraints are the minimum and maximum values of the PI-controller gains. Available literature on tuning of d-q decoupled controllers does not provide the range for the PI-controller gains. Therefore, a minimum of a very small value and a maximum of very large value are selected as constraints to cover a wide search space. In order to achieve the aforementioned objectives, an objective function based on frequency-domain attributes of the system is developed as given by Equation (4.2).

$$O = \sum_{i=1}^{I} \left\{ \sum_{j=1}^{J} \left(\alpha P^{\lambda_o(i,j)} + \beta P^{\lambda_r(i,j)} \right) \right\} \tag{4.2}$$

where,

I	is the number of operating conditions
J	is the number of eigenvalues of the system
i	denotes the ith operating condition
j	denotes the jth eigenvalue
P^{λ_o}	penalty function corresponding to oscillatory modes
P^{λ_r}	penalty function corresponding to aperiodic modes
α	is the weight of the penalty function for oscillatory modes
β	is the weight of the penalty function for aperiodic modes

It must be noted that the weights α and β for the penalty functions affects the rate of convergence of the optimization problem. However, the values of α and β will not influence the required stability performance. It is because, at the end upon convergence, the optimized controller parameters will result a objective function value that satisfies the convergence criteria.

4.2.1 Penalty Functions

It is desired to have adequate damping for oscillatory modes and adequately large negative values for aperiodic modes. Therefore, penalty functions with positive values are assigned for each oscillatory mode and aperiodic mode that does not satisfy the performance criteria. The penalty function values for oscillatory modes and aperiodic modes are calculated as shown by Equation (4.3) and (4.4) respectively. It can be seen from the expressions for penalty functions that if the considered mode satisfies

the performance requirement, then the corresponding penalty function is set to zero and if not a positive value is assigned. The ultimate goal of the optimization problem is to minimize the objective function (O), so that all the penalty functions reach zero ensuring that stability performance criteria is met.

$$P^{\lambda_o(i,j)} = \begin{cases} 0 & \text{if } \zeta(i,j) \geq \zeta_d, \\ \zeta_d - \zeta(i,j) & \text{else} \end{cases} \tag{4.3}$$

where,

$\zeta(i,j)$ is the damping of jth (oscillatory) mode at ith operating condition

ζ_d is the desired damping for that oscillatory mode

$$P^{\lambda_r(i,j)} = \begin{cases} 0 & \text{if } \sigma(i,j) \leq \sigma_d, \\ \sigma(i,j) - \sigma_d & \text{else} \end{cases} \tag{4.4}$$

where,

$\sigma(i,j)$ is the value of jth (aperiodic) mode at ith operating condition

σ_d is the desired value for that aperiodic mode

It was observed and reported in **Chapter 3** and in [53] that MMC-VSC systems consists of two sets of oscillatory modes. They are network modes (electrical resonances) that highly depend on the network parameters, and controller modes that

highly depend on controller gains and time-constants. It was observed that the damping improvement of dc resonance through controller gains is limited. In addition, it was noted that any attempt to improve the damping of these modes could adversely affect the performance of the other controller modes. This problem was specifically noticed when the ac grid is weak (SCR=1.5). Therefore, it is very important to identify these electrical resonances before starting to tune the controllers and also it is important to set the required damping of these electrical resonances accordingly.

The objective function in Equation (4.2) is general and any suitable optimization technique can be used to solve for controller gains that give required performance criteria. However, a meta-heuristic optimization technique is desired as they are very powerful compared to other optimization techniques. In this thesis, the simulated annealing optimization technique is successfully applied to solve the optimization problem.

4.3 Simulated Annealing

Simulated annealing is an effective global optimization technique that has been widely applied to find optimal solutions for large combinatorial optimization problems. This optimization technique is developed by using the analogy of the physical annealing process of a substance. There are a number of advantages associated with this optimization technique including the following smart features that are relevant to solve the optimization problem developed in this thesis.

- Flexibility of dealing with a large number of variables.
- Simplicity of constrain handling.
- Ensuring the global optimum solution.

4.3.1 Physical Annealing Process

In thermal physics, the annealing is defined as the process to achieve the minimum energy state of a substance. In this process, a solid is heated to a very high temperature at which it melts into its liquid state and all molecules in that liquid randomly move and arrange in arbitrary positions. Then, the temperature of that substance is slowly reduced until it reaches the thermal equilibrium in the solid state. Slow and steady cooling will ensure that at each temperature, the molecules in the substance achieve the minimum energy state. To ensure this thermal equilibrium, the molecules must be allowed sufficient time at temperatures in the vicinity of the freezing point [64, 65]. If the cooling is not slow enough, then the solid may escape from thermal equilibrium and result in a crystal structure and that process is known as quenching.

The thermal equilibrium at a single temperature of a substance that is in the cooling process can be explained using the Metropolis criteria. At a fixed temperature, the state of a substance is defined by the position of its molecules and it is quantified in terms of the total energy of the substance (E). When a randomly generated small perturbation is applied to a particle, the state of the substance will change and achieve a new state at which the total energy can be different from the pre-disturbance value. Metropolis [66] has defined a criterion for accepting the new state as stated below.

Metropolis Criterion

- *If*, the new state contains lower total energy compared to the previous state, then the new state is accepted.

- *Else*, the new state is accepted with the probability given by Equation (4.5).

$$p(\Delta E) = e^{-\left(\frac{\Delta E}{K_B \times T}\right)} \tag{4.5}$$

where,

ΔE is the change occurred in the total energy of the solid due to the perturbation

K_B is the Boltzmann's constant

T is the temperature of the substance

The Metropolis criteria explains the possibility of achieving the minimum energy state at a given temperature.

4.3.2 Simulated Annealing Optimization Technique

Simulated annealing is inspired by the physical annealing process. Analogies used in this optimization method to mimic the physical annealing process is given in Table 4.1. The parameter known as temperature is set to a very high value at the beginning of the optimization problem to mimic the physical annealing that begins at a heated liquid state. The incorporation of Metropolis criterion will ensure that the objective function escapes from local minima when solving optimization problems. It can also be shown that when temperature becomes low (i.e: when reaching freezing point) the probability of accepting higher energy states becomes less, which guarantees the achievement of global minimum.

4.4 Application of the Simulated Annealing Optimization Method to Solve the Optimization Problem

The simulated annealing optimization method used in this thesis is explained using a flow chart shown in Figure 4.1. There are two loops used in this optimization. The

Table 4.1: Analogy between physical annealing and simulated annealing optimization

Actual	**Analogy**
Thermodynamic system	Optimization problem
Molecules	Variables
Energy	Objective function
Frozen state	Optimal solution

outer loop runs until the objective function becomes less than a threshold value or until the iteration count reaches a maximum ($iter_{1(MAX)}$). The inner loop runs until the optimum solution at each value of temperature (C) is found.

The outer loop is evaluated once at each value of temperature (C) and the inner loop is evaluated based on the Metropolis criterion to find the optimum solution at each value of temperature. At the beginning, the values for maximum iteration counts ($iter_{1(MAX)}$, $iter_{2(MAX)}$) for each loop, minimum ($K_{P(MIN)}$, $K_{I(MIN)}$) and maximum ($K_{P(MAX)}$, $K_{I(MAX)}$) values of gains are chosen. Then, variables such as temperature and PI-controller gains are initialized. Using the initial gains, the value of the objective function is evaluated and stored as the best solution for the first iteration. Then, the temperature is reduced based on the relationship given by Equation (4.6) in which the constant K_c is selected to have a value close to and less than 1 to mimic the physical annealing which is a slow process.

$$C(iter_1) = K_c \times C(iter_1 - 1) \tag{4.6}$$

The inner loop uses the Monte Carlo method to simulate the Metropolis criterion at a fixed value of temperature (C). The inner loop iteration count maximum ($iter_{2(MAX)}$) is chosen according to the Equation (4.7), where $M_1 > M_2$ and C_{cold} is the temperature when the objective function is close to the specified threshold value.

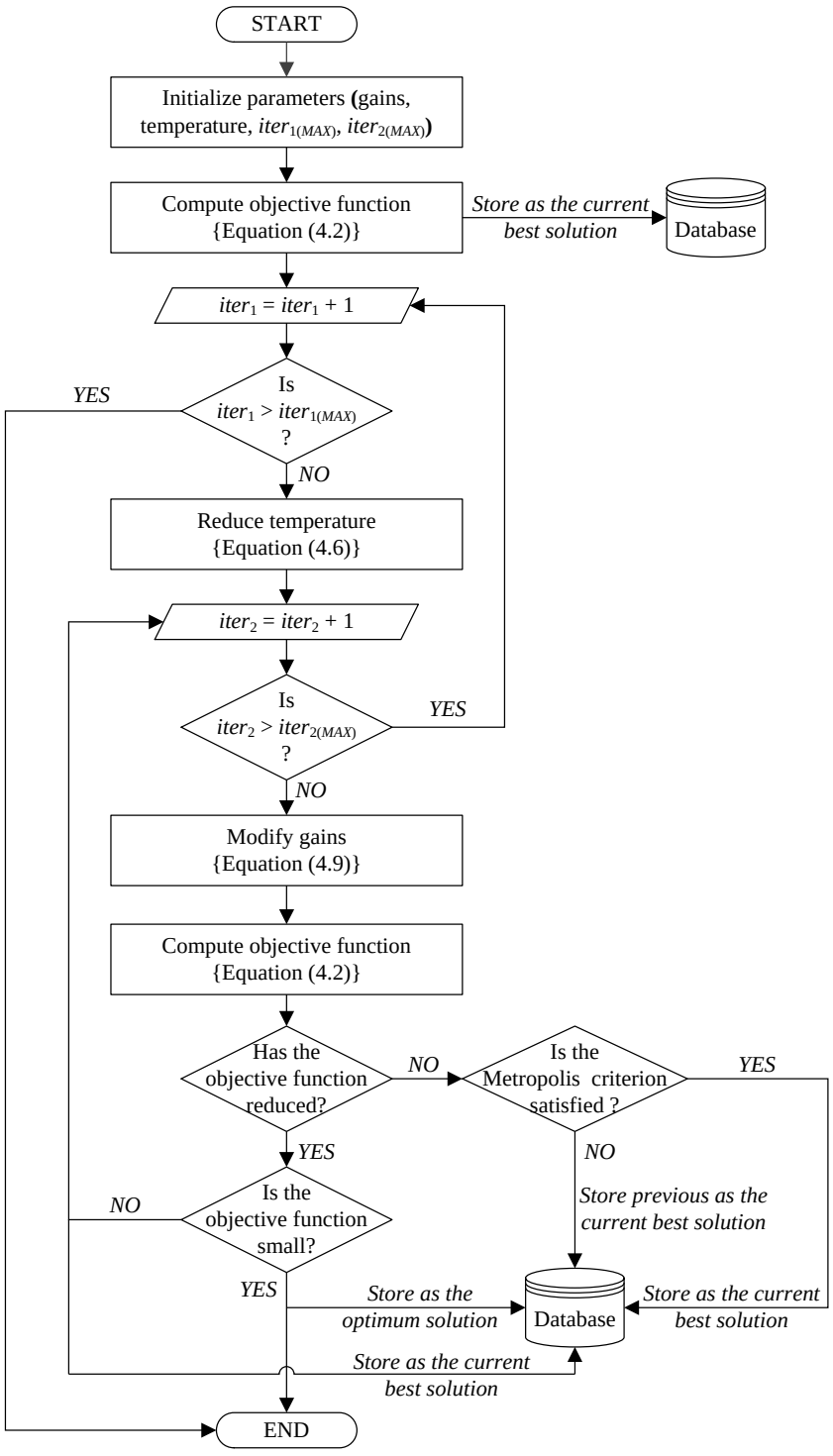

Figure 4.1: Flow chart to explain the simulated annealing algorithm

$$iter_{2(MAX)} = \begin{cases} M_1 & \text{if } C \leq C_{cold}, \\ M_2 & \text{else} \end{cases} \tag{4.7}$$

In the Monte Carlo simulation, if the objective function has reduced, then the new solution is accepted. On the other hand, if the objective function has increased, then the acceptance of the new solution is based on the Metropolis criteria, which is given in Equation (4.8).

$$Newsolution = \begin{cases} accept & \text{if } e^{-\Delta O/K_b C} \geq rand(), \\ discard & \text{else} \end{cases} \tag{4.8}$$

where ΔO is the change in objective function, K_b is the Boltzmann constant, C is the temperature, and $rand()$ is a random number between 0 and 1. In simulated annealing optimization, the Metropolis criteria creates opportunities to escape from local minimum points while solving the optimization problem.

At each iteration of the Monte Carlo simulation, values of the variables (in this case, the PI-controller gains) are changed by a small amount, which is random and calculated as shown by Equation (4.9).

$$\begin{aligned} K_P(iter_2) &= K_P(iter_2 - 1) + frac_P * (rand() - 0.5) \\ K_I(iter_2) &= K_I(iter_2 - 1) + frac_I * (rand() - 0.5) \end{aligned} \tag{4.9}$$

where $rand()$ is a random number between 0 and 1, $frac_P$ and $frac_I$ are defined to scale the change applied to proportional and integral gains of PI-controllers. Upon convergence, the algorithm returns the best gains for the PI-controllers that meet specified performance requirements defined by the user.

4.5 Application of the Proposed Controller Tuning Procedure to the Test System

The application of proposed controller tuning procedure to the MMC-VSC test system is discussed below in detail. The performance of the tuned controller gains are evaluated by applying them to the EMT model of the test system. The strengths of ac systems connected to MMC-VSC test system are set to reflect moderately strong ac connections (SCR=2.0).

4.5.1 Performance Criteria to Solve the Optimization Problem

The MMC-VSC system consists of two sets of oscillatory modes: electrical resonances and controller modes. The damping improvement of electrical resonances through controller gains is limited. Therefore, the required damping for electrical resonances is set to 20 %. The damping requirements for controller modes are set to 80 %. In addition, the requirement for aperiodic modes is set to -5. The other parameters used for the optimization problem are given in Table 4.2. To cover the complete operating region of the test system, 17 operating points shown in Table 4.3 are considered for the controller tuning. The first five operating points are to consider different power levels at rated ac and dc voltage conditions to cover the normal operating conditions. The next eight ac voltage operating points (four per each side) are selected to cover ac voltage variations between 0.9 p.u. and 1.1 p.u. The final four operating points use different dc voltage settings from 0.9 p.u. to 1.1 p.u.

Table 4.2: Optimization parameters

Parameter	**Value**
ζ_d for electrical modes	20 %
ζ_d for controller modes	80 %
σ_d	-5
I (No of operating points)	17
J (No of eigenvalues)	27
$iter_{1(MAX)}$	20000
$Tolerance$	0.00001
M_1, M_2	10, 3
C_{cold}	0.001
K_c	0.98
K_B	1
α, β	1, 1
$frac_P$, $frac_I$	0.01, 0.1

4.5.2 Selection of Initial Values for Controller Parameters

Selection of the initial controller parameters is an important step in many controller tuning methods based on optimization techniques. However, in this study, it was made sure that the initial parameters must be easily selected with very little knowledge on the d-q decoupled control system. Simply, two norms given below were used to select initial gains in Table 4.4.

1. DC voltage controller has to be faster than the active power controller to maintain the dc voltage stability.

2. Inner-loop controllers have to be faster than the outer-loop controllers for the overall system stability.

Table 4.3: Operating points considered for controller tuning

Operating	**Terminal1**			**Terminal2**		
Points	v_{dc1}	V_{t1}	Q_{t1}	P_{t2}	V_{t2}	Q_{t2}
OP-01	1.00 p.u.	1.00 p.u.	-0.18 p.u.	-1.00 p.u.	1.00 p.u.	-0.17 p.u.
OP-02	1.00 p.u.	1.00 p.u.	0.03 p.u.	-0.75 p.u.	1.00 p.u.	-0.08 p.u.
OP-03	1.00 p.u.	1.00 p.u.	0.07 p.u.	-0.50 p.u.	1.00 p.u.	-0.02 p.u.
OP-04	1.00 p.u.	1.00 p.u.	0.14 p.u.	-0.25 p.u.	1.00 p.u.	0.00 p.u.
OP-05	1.00 p.u.	1.00 p.u.	0.17 p.u.	0.00 p.u.	1.00 p.u.	0.00 p.u.
OP-06	1.00 p.u.	1.10 p.u.	-0.37 p.u.	-1.00 p.u.	1.00 p.u.	-0.17 p.u.
OP-07	1.00 p.u.	1.05 p.u.	-0.27 p.u.	-1.00 p.u.	1.00 p.u.	-0.17 p.u.
OP-08	1.00 p.u.	0.95 p.u.	-0.11 p.u.	-1.00 p.u.	1.00 p.u.	-0.17 p.u.
OP-09	1.00 p.u.	0.90 p.u.	-0.04 p.u.	-1.00 p.u.	1.00 p.u.	-0.17 p.u.
OP-10	1.00 p.u.	1.00 p.u.	-0.18 p.u.	-1.00 p.u.	1.10 p.u.	-0.36 p.u.
OP-11	1.00 p.u.	1.00 p.u.	-0.18 p.u.	-1.00 p.u.	1.05 p.u.	-0.26 p.u.
OP-12	1.00 p.u.	1.00 p.u.	-0.18 p.u.	-1.00 p.u.	0.95 p.u.	-0.10 p.u.
OP-13	1.00 p.u.	1.00 p.u.	-0.18 p.u.	-1.00 p.u.	0.90 p.u.	-0.03 p.u.
OP-14	1.10 p.u.	1.00 p.u.	-0.18 p.u.	-1.00 p.u.	1.00 p.u.	-0.17 p.u.
OP-15	1.05 p.u.	1.00 p.u.	-0.18 p.u.	-1.00 p.u.	1.00 p.u.	-0.17 p.u.
OP-16	0.95 p.u.	1.00 p.u.	-0.18 p.u.	-1.00 p.u.	1.00 p.u.	-0.17 p.u.
OP-17	0.90 p.u.	1.00 p.u.	-0.18 p.u.	-1.00 p.u.	1.00 p.u.	-0.17 p.u.

4.5.3 Discussion on Tuned Controller Parameters

The tuned gains in Table 4.4 were obtained by applying the proposed tuning method to achieve the damping performances given in Section 4.5.1. Note that the idea of the proposed tuning method is to meet the design specification and not to obtain the most optimum solution. The values of objective function against iteration numbers are plotted in Figure 4.2. The pattern of convergence shown in Figure 4.2 confirms that the simulated annealing method of optimization is capable to escape from local minima. It can be seen from Table 4.4 that the dc voltage controller gain has increased

Table 4.4: Initial and tuned controller gains

Controller	**Gain**	**MMC1**		**MMC2**	
		Initial	**Optimized**	**Initial**	**Optimized**
PLL	K_P	50	50.9	50	50.8
	K_I	250	249.4	250	249.5
DC Voltage	K_P	2	9.4	1	0.6
Active Power	K_I	20	40.9	20	12.7
AC Voltage	K_P	1	2.7	1	1.1
	K_I	20	23.8	20	12.7
d-axis	K_P	1	1.2	1	0.8
Current	K_I	100	101.8	100	92.9
q-axis	K_P	1	1.3	1	0.9
Current	K_I	100	102.8	100	98.9

to improve both dc mode and dc resonance (modes 5 and 8). The terminal1 ac voltage controller proportional gain has increased to improve other oscillatory modes. In contrast, the PLL gains haven't changed from the initial values. Therefore, it can be said that the PI-controller gains of the d-q decoupled controller have greater impact on the system stability compared to the influence of the PLL gains on the stability.

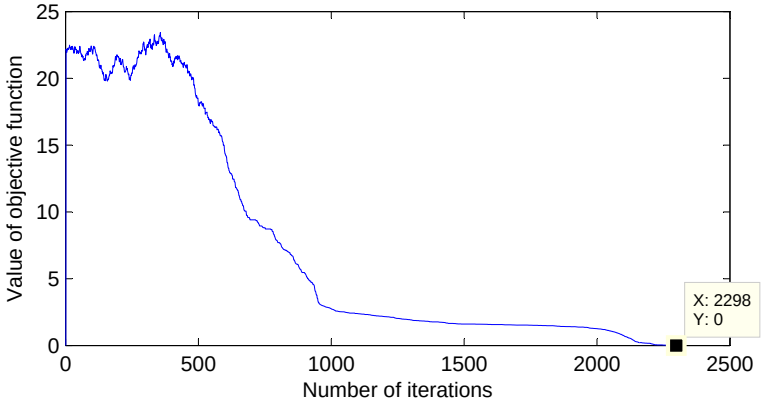

Figure 4.2: Variations of values of objective function with the iteration number

4.5.4 Performance Evaluation of Tuned Parameters

The tuned gains were applied to the EMT simulation model of the test system and different disturbances such as step changes, power ramp-up, and three phase faults were applied to the system. Simulation results with initial and tuned gains are compared for each disturbance to show the efficacy of the controller tuning method.

Step Change in DC Voltage

The test system was set to deliver 500 MW (1 p.u.) to the ac system connected to terminal2 at rated ac voltages and 0.95 p.u. dc voltage. At steady state, a step change of 0.05 p.u. was applied to the terminal1 dc voltage reference at 0.2 s. The EMT simulation results obtained using both initial and tuned controller gains are compared in Figure 4.3.

It can be observed that the low frequency oscillations seen in active power, dc current, and both ac and dc voltages are well damped by the tuned controller gains. In addition, the settling time is significantly improved. Although the overshoot seen in active power and dc current has slightly increased, the overall performance of the system with the tuned parameters is improved compared to that with the pre-optimized gains.

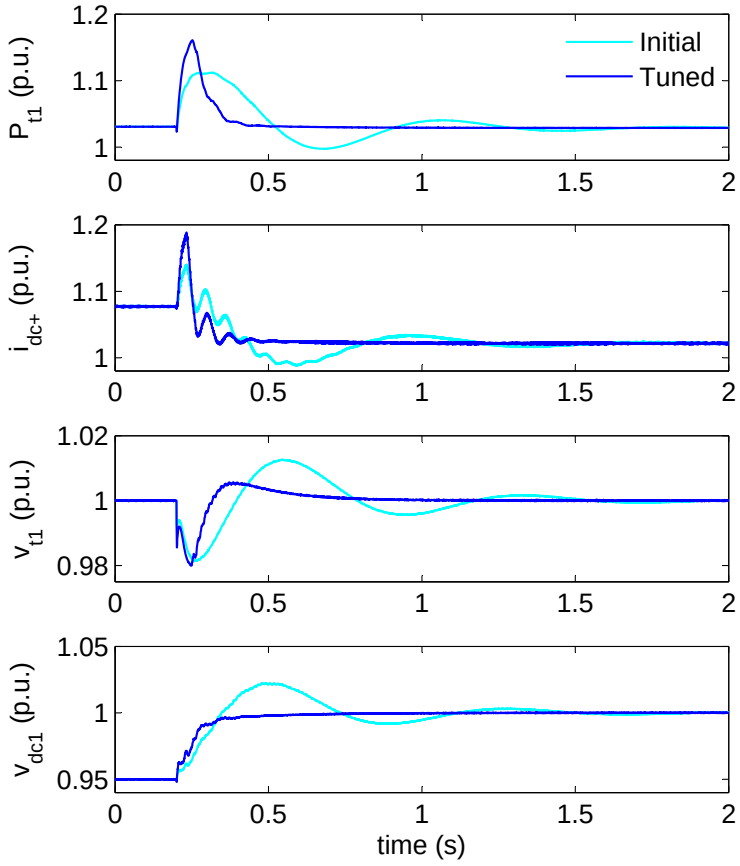

Figure 4.3: Variations of active power, dc current, ac voltage, and dc voltage for a step change in dc voltage reference at 0.2 s

Step Change in Active Power

At the rated voltage conditions, the ac system at terminal2 was set to receive 450 MW (0.9 p.u.) power. A step change of 0.1 p.u. was applied to the power reference of terminal2 to bring the transmitted power to the rated value. The EMT simulation results for the above disturbance are shown in Figure 4.4. It can be observed that the results of the case with tuned controller gains show improved settling time in ac and dc quantities. In addition, the large overshoots seen in both active power and dc current are eliminated.

The results provided in Figures 4.3 and 4.4 prove that the test system with tuned controller gains produces acceptable results for step changes. However, it is also required to investigate the efficacy of the tuned gains when the test system is subjected to large disturbances such as power ramp-up and three phase faults.

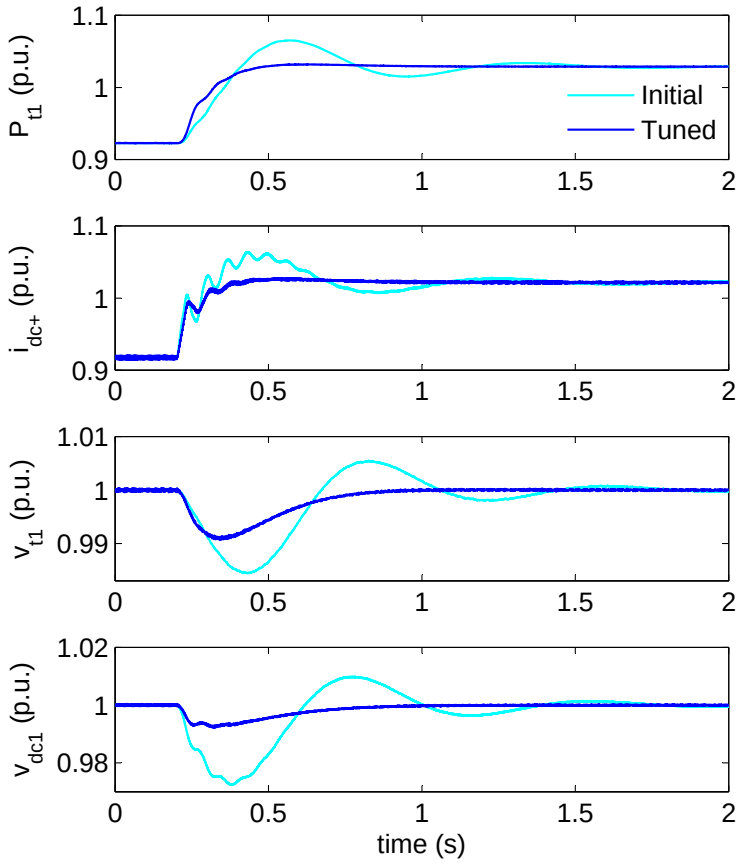

Figure 4.4: Variations of active power, dc current, ac voltage, and dc voltage for a step change in active power reference at 0.2 s

Quick Power Ramp-Up

The test system was set to transfer power from terminal1 to terminal2 at rated ac and dc voltages and the initial power was set to zero. The power order of terminal2 was changed from 0 to 1.0 p.u. at 4 p.u./s to reflect a quick power ramp-up. Time-

domain simulation results corresponding to the power order change with initial and tuned controller gains are compared in Figure 4.5.

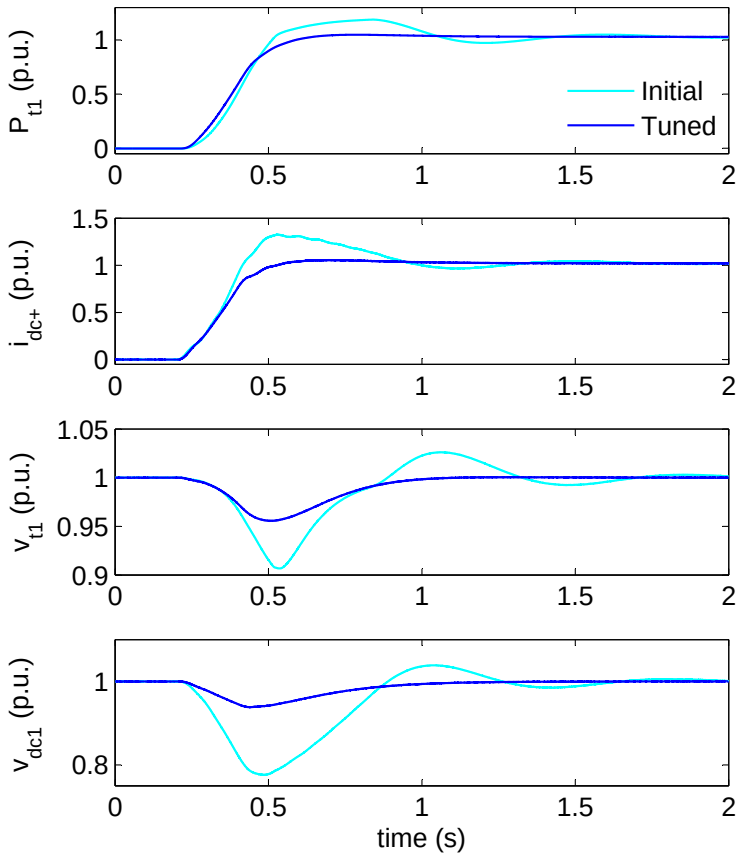

Figure 4.5: Variations of active power, dc current, ac voltage, and dc voltage for a power order change at 0.2 s

It can be observed that the voltage dips in ac and dc voltages are reduced with tuned gains. In addition, the overshoot observed in power and dc current are eliminated. Moreover, the settling time of ac and dc quantities are significantly improved.

Three Phase Faults

Among ac faults, the three phase to ground faults are considered the most severe fault. To explore the system performance for the worst case scenario, three phase faults with

a duration of 10 cycles and negligible impedance were applied to ac terminals one at a time. Time-domain simulation results for faults at terminal1 and terminal2 are shown in Figures 4.6 and 4.7 respectively.

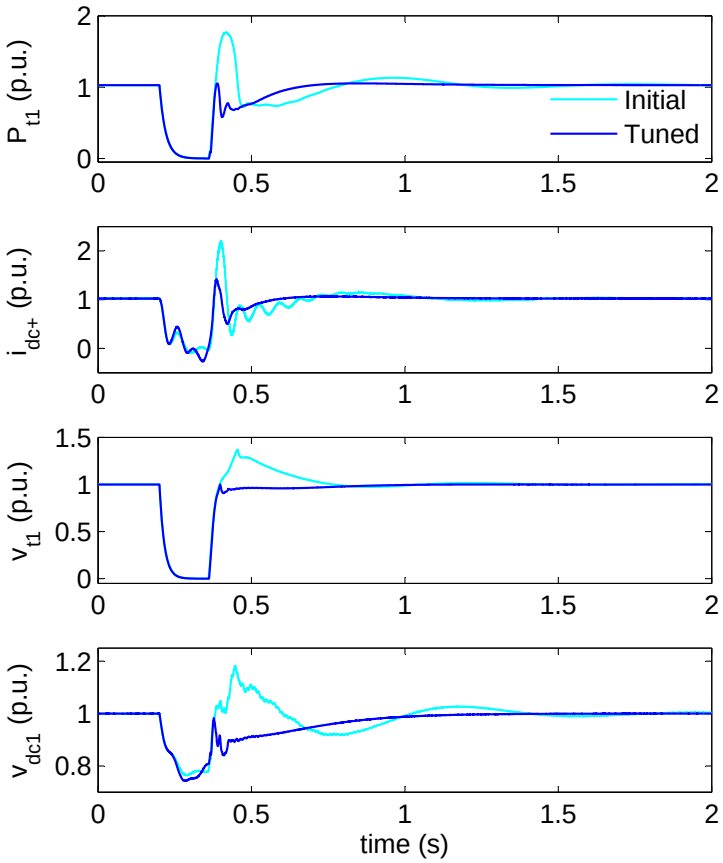

Figure 4.6: Variations of active power, dc current, ac voltage, and dc voltage for a three phase fault on terminal1 at 0.2 s

It can be observed that the simulation results with tuned gains show improved settling time and damping. Although the overshoots in power and dc current (for the fault at terminal2) are a little higher compared to the simulation with initial gains, the overall performance is better with the tuned gains.

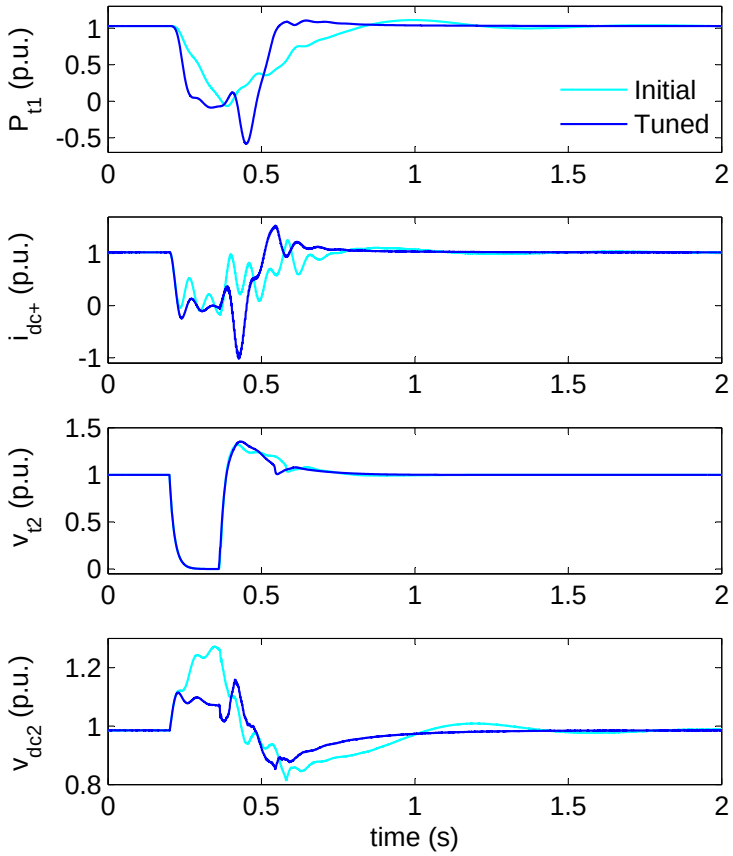

Figure 4.7: Variations of active power, dc current, ac voltage, and dc voltage for a three phase fault on terminal2 at 0.2 s

The time-domain simulation results shown in Figures 4.5-4.7 show that the tuned controller parameters give acceptable performance for large transients including three phase to ground faults.

It must be noted that unsymmetrical faults such as single phase and two phase faults are not studied in this thesis. It is because of the fact that unsymmetrical faults require special controllers such as negative sequence controller and they are not modelled in the test system. In addition, these special controllers need to be tuned by exploring time-domain responses of the system for such disturbances and such controller tuning is out of the scope of this thesis.

4.6 Steps to Tune Controllers of an MMC-VSC System

- **Step-1**: Develop a small-signal model of the MMC-VSC system under study including dynamics of the ac system, dc system, converter (including arm inductor and losses), and control system (including control-loops, measuring delays, and PLL). It would be important to validate the small-signal model against a non-linear EMT simulation model of the test system.

- **Step-2**: Use initial estimated values for the controller parameters and perform small-signal stability assessment to identify the low damped oscillatory modes as well as the sensitive aperiodic modes. In addition, perform the participation factor analysis to classify modes into electrical resonances and controller modes.

- **Step-3**: Chose sufficient number of operating points to cover the possible operating regions of the MMC-VSC system. The small-signal model is valid in the operating region close to the operating point that is used to develop the model.

- **Step-4**: The damping improvements of electrical resonances through controllers are limited. Therefore, the required damping of these modes have to be set carefully. Similarly, set the required damping for controller modes and required negative values for aperiodic modes.

- **Step-5**: Formulate the frequency-domain objective function considering all operating conditions and the required performance criteria.

- **Step-6**: Apply the controller tuning procedure proposed in this thesis to tune PI-controller parameters. It must be noted that the optimization problem is general so that any meta-heuristic method that can handle large number of variables can be chosen as the optimization method.

- **Step-7**: Evaluate the performance of the tuned controller gains by applying them to the EMT simulation model of the test system. Apply a wide range of disturbances such as step changes and large transients to test the effectiveness and robustness of the tuned controller gains before using the tuned gains on a practical system.

4.7 Chapter Summary

This chapter proposed a generalized frequency domain controller tuning procedure that can be used to simultaneously tune all PI-controllers in MMC-VSC systems. The steps to solve the developed optimization problem using the simulated annealing technique has been explained. Importantly, it has been identified that the PLL gains have less influence on the system stability compared to the d-q decoupled controller gains. The EMT simulation results with both initial and tuned gains have been compared for a wide range of disturbances such as step changes and large transients. It has been shown that the performance of the test system with tuned gains is superior compared to that of initial gains. Finally, the steps to tune controllers of a given MMC-VSC system are outlined to show how this method can be adopted for practical HVdc projects.

Chapter 5

Important Aspects of Controller Tuning of MMC-VSC Systems

.

Voltage source converters can be connected to weak or passive ac networks to transmit power. However, the transient and small disturbance performance of a VSC system connected to a weak ac network will depend on ac system strength, controller parameters, and dc system. Recent research articles investigate the stability of VSC systems connected to weak ac systems [44, 67, 68, 69]. This chapter is dedicated to examine the suitability of the proposed controller tuning method considering different ac system strengths and measuring delays in instantaneous voltage and current measurements.

5.1 Impact of AC System Strength

To explain the influence of the ac system strength on the stability of MMC-VSC systems, the point-to-point MMC-VSC test system was connected to two ac networks

with SCR of 2.0. At steady state, the SCR of terminal2 was changed from 2.0 to 5.0, 3.0, 1.5, and finally back to 2.0 at 2 s, 4 s, 6 s, and 8 s respectively. The controller gains used for this simulation are the initial controller gains and throughout the simulation, the SCR of terminal1 was kept at 2.0. The EMT simulation results corresponding to above changes in SCRs are shown in Figure 5.1.

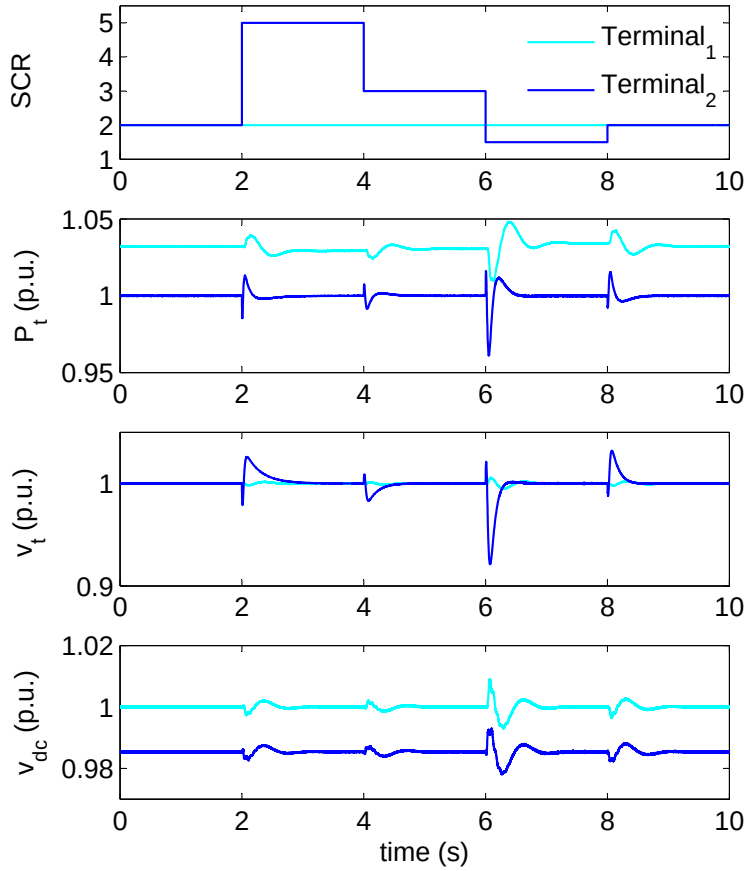

Figure 5.1: Variations of ac and dc quantities for changes in ac system strength

It can be seen from Figure 5.1 that when the system becomes strong (time instances 2.0 s and 4.0 s), the transients are very small and the ac voltage is within ±0.02 p.u. limits of the nominal value. However, when the system becomes weak (at 6.0 s), the transients are large and the ac voltage shows a transient dip to 0.9 p.u.

In addition, it can also be seen that the changes of system strength of one ac system influences the ac and dc quantities of the opposite side. Therefore, it is important to assure that there is no poorly damped modes present in the system. The controller tuning procedure proposed in this thesis improves the damping of poorly damped modes. Therefore, it is possible to have satisfactory performance of MMC-VSC even with weak ac connections.

5.1.1 Short Circuit Ratio Estimation

In VSC controller tuning, the short circuit ratio (SCR) estimation is important as the ac system strength has an influence on the system stability. System strength of an ac system is an accepted measure of the interaction between ac and dc systems in HVdc studies [70]. Typically, the term SCR is used to represent the strength of an ac system in ac-dc studies. Studies in [22, 71] show that the control of a VSC station becomes easy when it is connected to a strong ac bus, whereas a weak ac network connection will result in high temporary over voltages at the network bus, increase the chance of leading to a voltage instability, and result in a long restart time after a shut-down. In previous studies on VSC controller tuning, the SCR information has simply been ignored [72, 73, 31, 32]. However, the system strength has a significant influence on the system stability [22]. In order to include the SCR information in control loop tuning, the first step would be to estimate the system strength of the connected ac system. The available methods to estimate Thévenin equivalent parameters of an ac power system are summarized below.

Estimation of the ac system strength has been a challenging task since 1980s as a problem of finding the Thévenin equivalent parameters of an ac network for voltage stability studies. A number of methods have been proposed to estimate the Thévenin

equivalent parameters of an ac system. A method based on Kalman filter to estimate the Thévenin equivalent parameters is presented in [74]. This method estimates the Thévenin equivalent voltage and a series reactance using voltage, current, and reactive power measurements at the power system node of interest. In [75], the system admittance matrix is calculated using the node voltages from a power-flow solution. Then, the admittance matrix is inverted to find the impedance matrix and also the Thévenin equivalent impedance seen at any node of interest. In [76], local measurements are used to estimate the Thévenin equivalent impedance. To minimize the error in estimation, a least square method is employed in [76]. Phasor measurements are used in [77] to estimate the Thévenin equivalent parameters neglecting the resistive component of the Thévenin impedance. In [78], two consecutive sets of measurements obtained from a phasor measurement unit (PMU) are used to estimate the Thévenin equivalent parameters by applying Tellegen's theorem. An improved method using three PMU measurements to estimate Thévenin equivalent parameters is presented in [79]. The methods discussed above are developed to estimate the Thévenin equivalent parameters of a power system seen from the node of interest. In contrast, in HVdc stability studies, the complete ac system connected to the HVdc terminal is represented using the Thévenin equivalent. In this thesis, a simple technique named as the voltage pulse method is used to estimate the SCR.

Voltage Pulse Method

The ideas presented in literature motivated the use of the ac voltage pulse technique for SCR estimation, which is a modified version of the previous works [76, 77, 79]. This method uses two sets of voltage and current phasors that are measured at the network terminal of a VSC system at two different steady state operating conditions.

One of the main challenges stated in literature regarding the estimation of Thévenin equivalent parameters is that the variation in power caused by the intermittent nature of loads. In dc transmission systems, typically the power flow is controlled by the converter controls. Therefore, the SCR estimation is less complicated in VSC systems. The theory behind this voltage pulse method is simple as explained below.

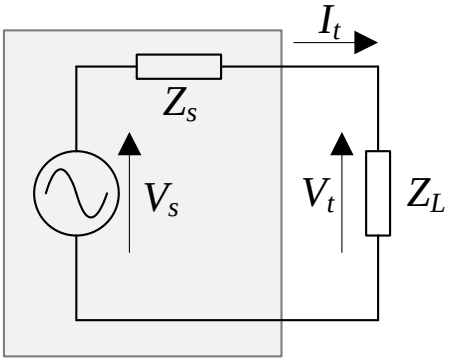

Figure 5.2: A simple electric circuit

Consider an electric circuit as shown in Figure 5.2. The source model represents the ac system seen from dc side at the network terminal and the load (Z_L) represents the dc system seen from ac side at the same network terminal. Table 5.1 shows the phasor measurements of voltages and currents at two different operating conditions and the angles are measured with respect to a common reference. In a practical power system, the common reference could be the voltage phasor of a strong bus.

Table 5.1: Steady state phasor measurements

Operating Point	**Voltage**	**Current**
OP1	$V_{t1}\angle\theta_{v1}$	$I_{t1}\angle\theta_{i1}$
OP2	$V_{t2}\angle\theta_{v2}$	$I_{t2}\angle\theta_{i2}$

It has to be noted that the first operating point (OP1) corresponds to the nominal operating condition of the system. The second operating point (OP2) is obtained by changing the terminal ac voltage (V_t) by a small amount for a small period. Assuming that the source voltage (V_s) is a constant during the small period in which the terminal voltage (V_t) is changed, Equations (5.1) and (5.2) can be written for the two operating conditions OP1 and OP2 respectively.

$$V_s = V_{t1}\angle\theta_{v1} + Z_s \times I_{t1}\angle\theta_{i1} \tag{5.1}$$

$$V_s = V_{t2}\angle\theta_{v2} + Z_s \times I_{t1}\angle\theta_{i2} \tag{5.2}$$

By equating V_s in above equations, the source impedance (Z_s) can be written as given by Equation (5.3).

$$Z_s = -\left(\frac{V_{t1}\angle\theta_{v1} - V_{t2}\angle\theta_{v2}}{I_{t1}\angle\theta_{i1} - I_{t2}\angle\theta_{i2}}\right) \tag{5.3}$$

Using this source impedance, the SCR can be calculated by substituting the known values of the rated line-line RMS value of the terminal voltage (V_t) and the rated dc power (P_{dc}) in Equation (5.4).

$$SCR = \frac{\left(V_t^2/Z_{th}\right)}{P_{dc}} \tag{5.4}$$

This method of SCR estimation require voltage and current measurements to be taken at two different operating conditions. However, in a practical power system, it is not recommended to change the operating point too far from the desired steady state operating condition. Therefore, a very small pulse (0.02 p.u.) is applied to the ac voltage reference ($V_{t(r)}$) for a small period of time (100 ms) to change the operating

point of the MMC-VSC test system by a small amount for a short time period. This SCR estimation method is successfully modelled in the EMT model of the MMC-VSC test system.

Performance Evaluation of Voltage Pulse Method

To evaluate the performance of the SCR estimation method proposed in this thesis, the test system is simulated with different ac system strengths and at each setting, the SCR is estimated. The SCR value is set by using proper values for the Thévenin source impedance. Table 5.2 shows the maximum percentage error calculated for 10 estimations for each SCR setting. It can be seen that the maximum error is close to 1 %. Therefore, this method provides a good estimation of SCR that can be used for VSC controller tuning purpose.

Table 5.2: Maximum percentage error in SCR estimation with constant Thévenin voltage

Actual SCR	**Estimated SCR**	**Percentage Error (%)**
1.5	1.502	0.13
2.0	2.021	1.05
2.5	2.501	0.04
3.0	3.003	0.10
4.0	4.042	1.05
5.0	5.015	0.30

The results shown in Table 5.2 are obtained by assuming a constant Thévenin source voltage. However, when representing an actual ac power system using a Thévenin equivalent, the Thévenin equivalent voltage cannot be assumed as a con-

stant. Therefore, to evaluate the performance of the estimation method under fluctuating source voltage conditions, 3% and 5% (worst case) voltage fluctuations are applied to the Thévenin equivalent voltage. The voltage fluctuation is generated using a white noise generator (with a mean of 0 and a standard deviation of 1). For each SCR setting 10 readings are taken and the calculated percentage error in estimation are shown in Table 5.3.

Table 5.3: Maximum percentage error in SCR estimation considering fluctuation in Thévenin voltage

SCR	**Maximum Percentage Error (%)**	
	3 % Fluctuation in Voltage	**5 % Fluctuation in Voltage**
1.5	2.8	3.9
2.0	2.7	7.5
2.5	5.0	10.0
3.0	6.1	9.1
4.0	7.3	9.3
5.0	5.3	17.0

It can be observed that the estimation accuracy reduces when the SCR increases. However, in this thesis, the SCR is estimated to categorize the ac systems into strong or weak. It is because, the controller gains tuned for a strong system can be used when the ac system is moderately strong and above (SCR$\geq$2.0) and the controller gains have to be changed when the ac system becomes weak (SCR$\leq$2.0). Therefore, the estimation accuracy obtained using the voltage pulse method is sufficient to design the control system for MMC-VSC systems.

5.1.2 Tuning of Controllers Considering Weak to Strong AC Systems

It was shown through both EMT simulation results and eigenvalue analysis results that the performance of an MMC-VSC system depends on the stregnth of the ac system connected to its terminals. The effect of ac system strength on controller tuning is studied by considering different ac systems such as a weak system (SCR=1.5), a moderately strong system (SCR=2.0), strong systems (SCR=3.0, 5.0), and a very strong system (SCR=20.0). The controller parameters for each SCR systems were tuned separately using the controller tuning technique proposed in **Chapter 4**. Table 5.4 shows the initial and tuned controller parameters for different ac systems.

The performance of the tuned controller parameters is evaluated by applying them to the EMT simulation model of the test system. The simulation results and the observations are summarized below.

5.1.3 Performance of Tuned Controller Gains with Weak AC Systems

To explain the efficacy of the proposed controller tuning method, the tuned controller gains for the MMC-VSC test system with weak ac networks (SCR=1.5 on both sides) is considered in this section. Simulation results with initial and tuned gains for different disturbances are compared to show the efficacy of the proposed controller tuning procedure.

Table 5.4: Tuned PI-controller gains for different SCR

MMC	PI	Gain	Initial Gains	Tuned Controller Gains			
				SCR 1.5	SCR 2.0	SCR 3.0	SCR 5.0
MMC1	PLL1	K_P	50.0	51.0	50.9	50.4	49.7
		K_I	250.0	236.8	249.4	249.4	255.6
	v_{dc1}	K_P	2.0	5.5	9.4	8.1	7.8
		K_I	20.0	24.1	40.9	35.1	35.2
	V_{t1}	K_P	1.0	1.8	2.7	0.8	0.5
		K_I	20.0	99.8	23.8	24.1	28.2
	i_{t1d}	K_P	1.0	0.4	1.2	1.1	1.2
		K_I	100.0	24.0	101.8	101.8	101.6
	i_{t1q}	K_P	1.0	2.3	1.3	0.6	1.2
		K_I	100.0	107.6	102.8	98.0	100.3
MMC2	PLL2	K_P	50.0	50.2	50.8	49.7	49.4
		K_I	250.0	251.1	249.5	250.7	247.7
	P_{t2}	K_P	1.0	0.1	0.6	0.8	1.1
		K_I	20.0	8.5	12.7	13.2	16.5
	V_{t2}	K_P	1.0	3.3	1.1	0.1	0.1
		K_I	20.0	34.5	12.7	20.5	27.4
	i_{t2d}	K_P	1.0	0.5	0.8	1.0	0.8
		K_I	100.0	67.4	92.9	101.6	93.4
	i_{t2q}	K_P	1.0	0.7	0.9	1.0	1.5
		K_I	100.0	102.2	98.9	101.0	94.4

Step Change in Active Power

The test system was set to deliver 450 MW (0.9 p.u.) power to the terminal2 at rated ac and dc voltages. At steady state, the power order to MMC2 was changed to 1.0 p.u. by applying a step change of 0.1 p.u. The time-domain simulation results with initial and tuned gains are compared in Figure 5.3. It can be seen that there is a low

frequency oscillation in ac and dc quantities when initial gains are used. It is because, with the initial gains, there were low damped modes such as the dc link resonance (seen in dc current) and the dc voltage controller mode. However, in the response with tuned gains, the low frequency modes are well damped and the overshoots and sharp voltage dips are eliminated. In addition, the tuned gains improved settling times.

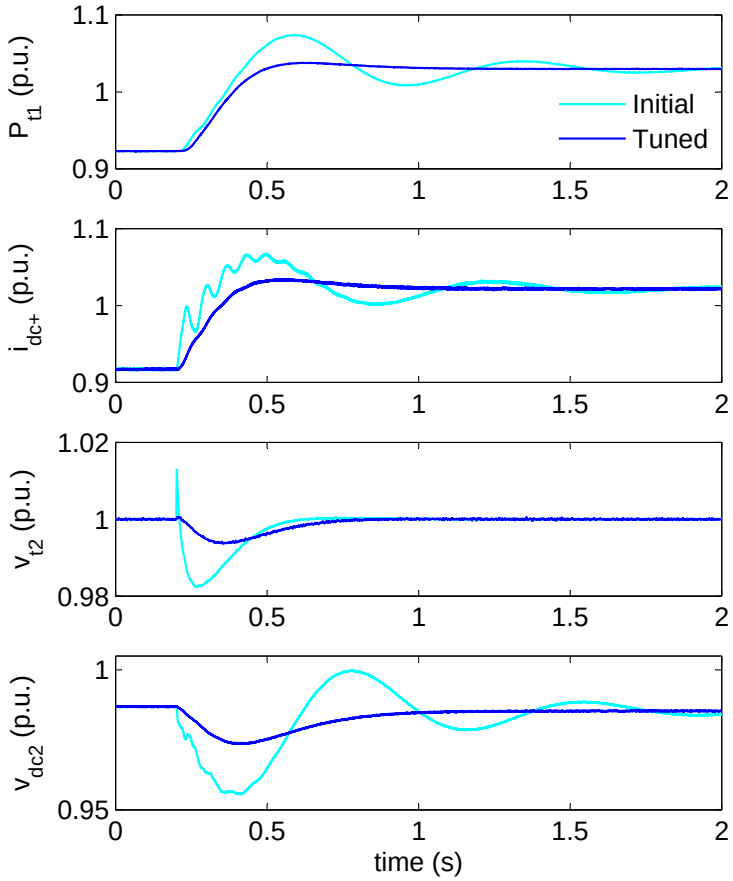

Figure 5.3: Variations of active power, dc current, ac voltage, and dc voltage for a step change in reference power of terminal2 at 0.2 s (SCR1=SCR2=1.5)

Three Phase to Ground Fault

At steady state, when the rated power was transmitted from terminal1 to terminal2, a three phase to ground fault with a duration of 10 cycle was applied at terminal2. The EMT simulation result corresponding to the above fault is shown in Figure 5.4. It can be observed that with initial gains the response of power and dc current show undesirable oscillations. In addition, the ac voltage shows very high post transient over voltage. The response with tuned gains is more satisfactory with well damped oscillations and improved settling time. Importantly, the post fault ac over voltage is eliminated.

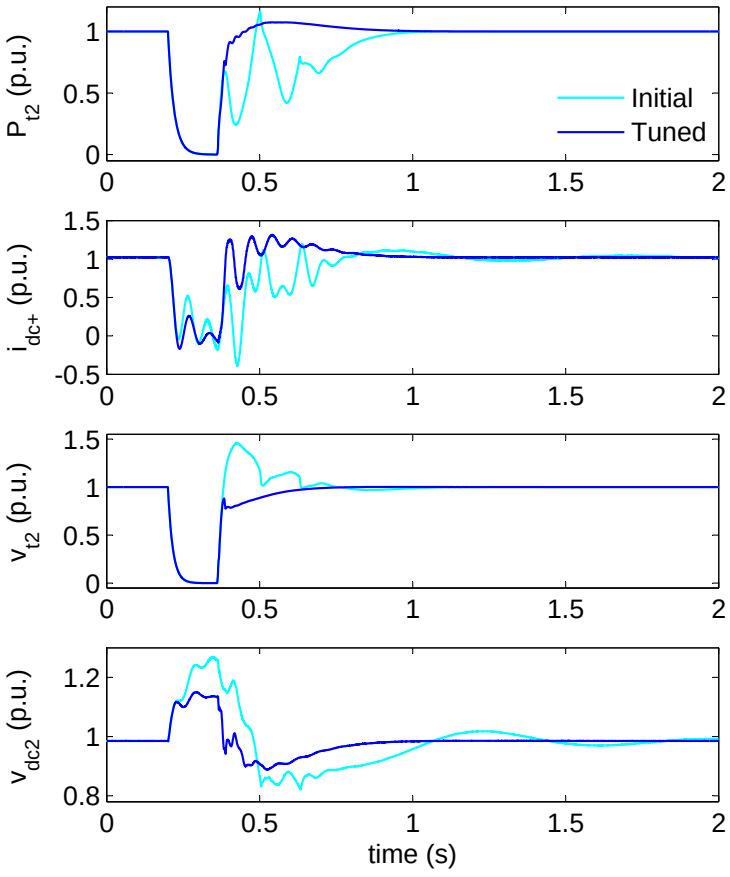

Figure 5.4: Variations of active power, dc current, ac voltage, and dc voltage for a three phase fault at terminal2 at 0.2 s (SCR1=SCR2=1.5)

5.1.4 Performance Comparison of Tuned Controller Gains for Weak to Strong AC Systems

The tuned gains for ac systems with SCRs of 1.5, 2.0, 3.0, 5.0, and 20.0 are compared in this section to show that similar performance of MMC-VSC system can be obtained with different ac systems, if the controller gains are properly tuned. A sufficient number of time-domain simulation studies were conducted to verify the transient and small-signal stability performances. To support the claim, a small disturbance and a large disturbance are discussed in this section.

When the ac system is strong, the outer-loop PI-controller, that produces the q-axis current reference, will be selected to control the reactive power. The reactive power control is selected as a strong ac system acts as a stiff grid to hold the terminal ac voltage. In contrast, when the ac system becomes weak, the outer-loop controller is set to control the terminal ac voltage. The reactive power controller also can be tuned using the controller tuning method proposed in this paper. In addition, it was observed that when an ac system becomes strong, a set of controller gains can be found that gives acceptable performance for a range of strong SCRs. Therefore, the controller gains tuned for SCR=5.0 is used to simulate the system with SCR=20.0 to show that when the ac system is strong, the controller gains can be kept the same.

Step Change in DC Voltage

At steady state, when the ac system at terminal2 was supplied with the rated power of 500 MW at 0.95 p.u. dc voltage, a step increase of 0.05 p.u. was applied to the dc voltage reference of terminal1 to bring the dc voltage to its rated value. The time-domain simulation results of the MMC-VSC test system with different ac systems ranging from weak (SCR=1.5) to very strong (SCR=20.0) are compared in Figure

5.5. It can be seen that the performance of different SCR systems are similar and acceptable. In addition, it can be noted that the ac voltage of the system connected to SCR=20.0 is almost a constant even during the disturbance. This observation explains that the ac voltage controller is not required for MMC-VSC systems when connected to strong ac networks.

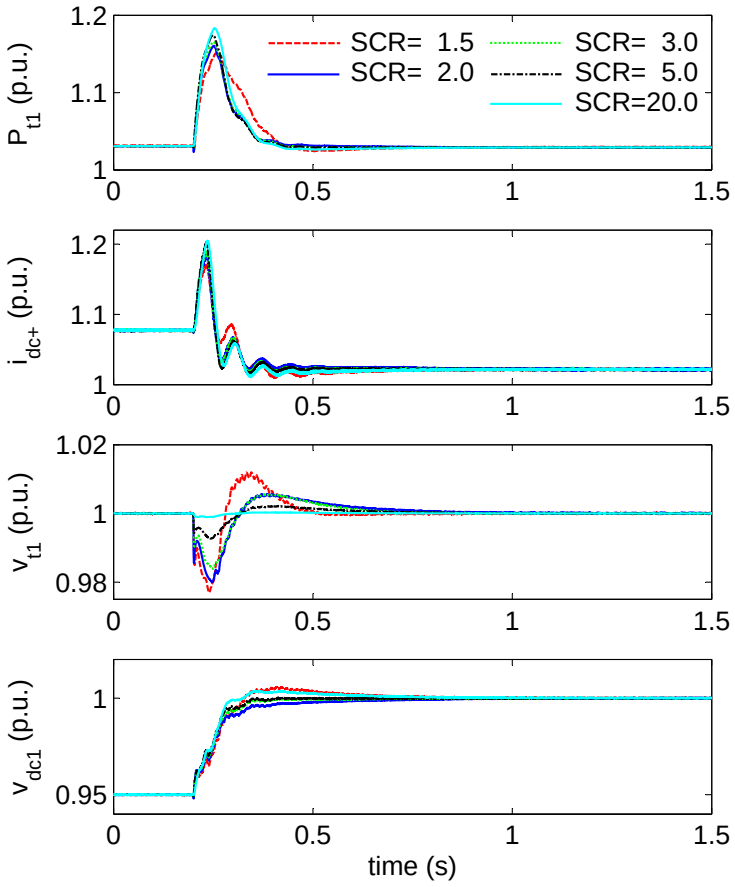

Figure 5.5: Variations of active power, dc current, ac voltage, and dc voltage for a step change in dc voltage of terminal1 at 0.2 s

Power Order Change

To study the response for a large transient, the power order of terminal2 was changed from 0 to 1.0 p.u. at 0.2 s. The time-domain simulation results of MMC-VSC system

connected to different ac systems are compared in Figure 5.6. It can be seen that the behaviour of ac and dc quantities for various SCR are similar and variations are within the acceptable range. Even for this large transient, it can be noticed that the change in ac voltage is negligible for the case with SCR=20.0.

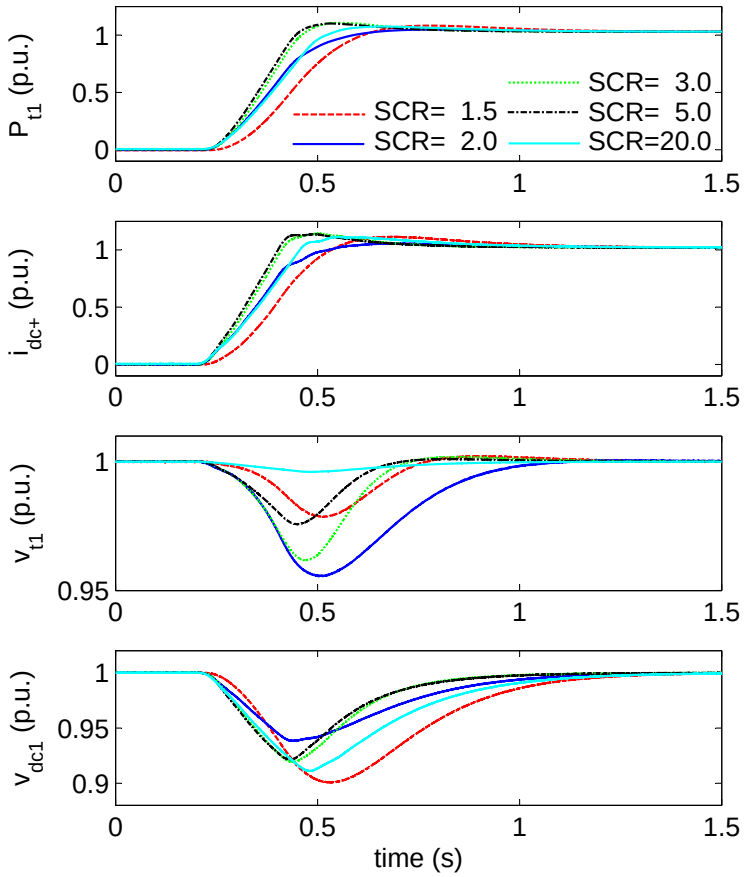

Figure 5.6: Variations of active power, dc current, ac voltage, and dc voltage for a power order change to terminal2 applied at 0.2 s

5.1.5 Tuning of Controllers Considering both Strong and Weak AC Systems

In Section 5.1.2, the ac systems connected to both terminals were selected to have same system strength. However, it is unlikely that both ac systems will have the same

SCR in practical HVdc systems. Therefore, to reflect a practical situation, different possible combinations of strong and weak ac systems are considered for controller tuning. A strong ac system with an SCR of 3.0 and a weak ac system with an SCR of 1.5 are considered for this exercise. Four cases; case-1: SCR1=3.0|SCR2=3.0, case-2: SCR1=3.0|SCR2=1.5, case-3: SCR1=1.5|SCR2=3.0, and case-4: SCR1=1.5|SCR2=1.5 are the different possibilities with these two SCR values. These cases are selected to cover all possible operating scenarios. The MMC1 is selected as the rectifier with dc voltage control and the MMC2 is chosen as the inverter with active power control. The proposed controller tuning method is applied to tune the controller gains for each case and the tuned gains are given in Table 5.5.

It can be noticed that the initial controller gains selected were the same for all cases. However, due to the difference in system strengths, the tuned sets of gains show considerable changes. Importantly, it can be witnessed that when the dc voltage controlling side (terminal1) becomes weak (cases 3 and 4), the d-axis controller gains have to be slowed down to retain the stability of the system. However, the PLL gains did not show much deviation from the initial values for all four cases.

The performance of the tuned VSC system under above mentioned operating scenarios were evaluated using EMT simulations. In order to demonstrate that the parameters tuned for a strong ac system is not suitable under a weak ac system condition, all cases were also simulated with tuned parameters of case-1 (set-1) and compared against the individually tuned cases (set-2). EMT simulation results for some major disturbances are summarized.

Table 5.5: Tuned PI-controller gains for different cases

MMC	**PI**	**Gain**	**Initial**	**Optimized Gains for (SCR1/SCR2)**			
				Case-1 3.0/3.0	**Case-2 3.0/1.5**	**Case-3 1.5/3.0**	**Case-4 1.5/1.5**
MMC1	PLL1	K_P	50	50.4	50.5	51.4	51.0
		K_I	250	249.4	249.7	239.7	236.8
	v_{dc1}	K_P	2	8.1	6.6	5.2	5.5
		K_I	20	35.1	27.1	23.1	24.1
	V_{t1}	K_P	1	0.8	1.1	1.5	1.8
		K_I	20	24.1	26.5	99.7	99.8
	i_{t1d}	K_P	1	1.1	1.1	0.4	0.4
		K_I	100	101.8	103.3	37.9	24.0
	i_{t1q}	K_P	1	0.6	1.4	2.4	2.3
		K_I	100	98.0	97.3	103.2	107.6
MMC2	PLL2	K_P	50	49.7	50.9	50.1	50.2
		K_I	250	250.7	248.3	256.3	251.1
	P_{t2}	K_P	1	0.8	1.1	0.1	0.1
		K_I	20	13.2	20.7	6.8	8.5
	V_{t2}	K_P	1	0.1	1.4	0.1	3.3
		K_I	20	20.5	22.4	42.8	34.5
	i_{t2d}	K_P	1	1.0	1.0	0.3	0.5
		K_I	100	101.6	96.5	25.3	67.4
	i_{t2q}	K_P	1	1.0	1.0	0.5	0.7
		K_I	100	101.0	103.5	107.7	102.2

Quick Power Reversal

To reflect the power reversal operation, the power order of terminal2 was changed from -1.0 p.u. to 1.0 p.u. with a rate of 5 p.u./s at 4.5 s and then at 10.5 s the power order was changed back to -1.0 p.u. The EMT simulation results for the above power transients are shown in Figure 5.7 for cases 1-4.

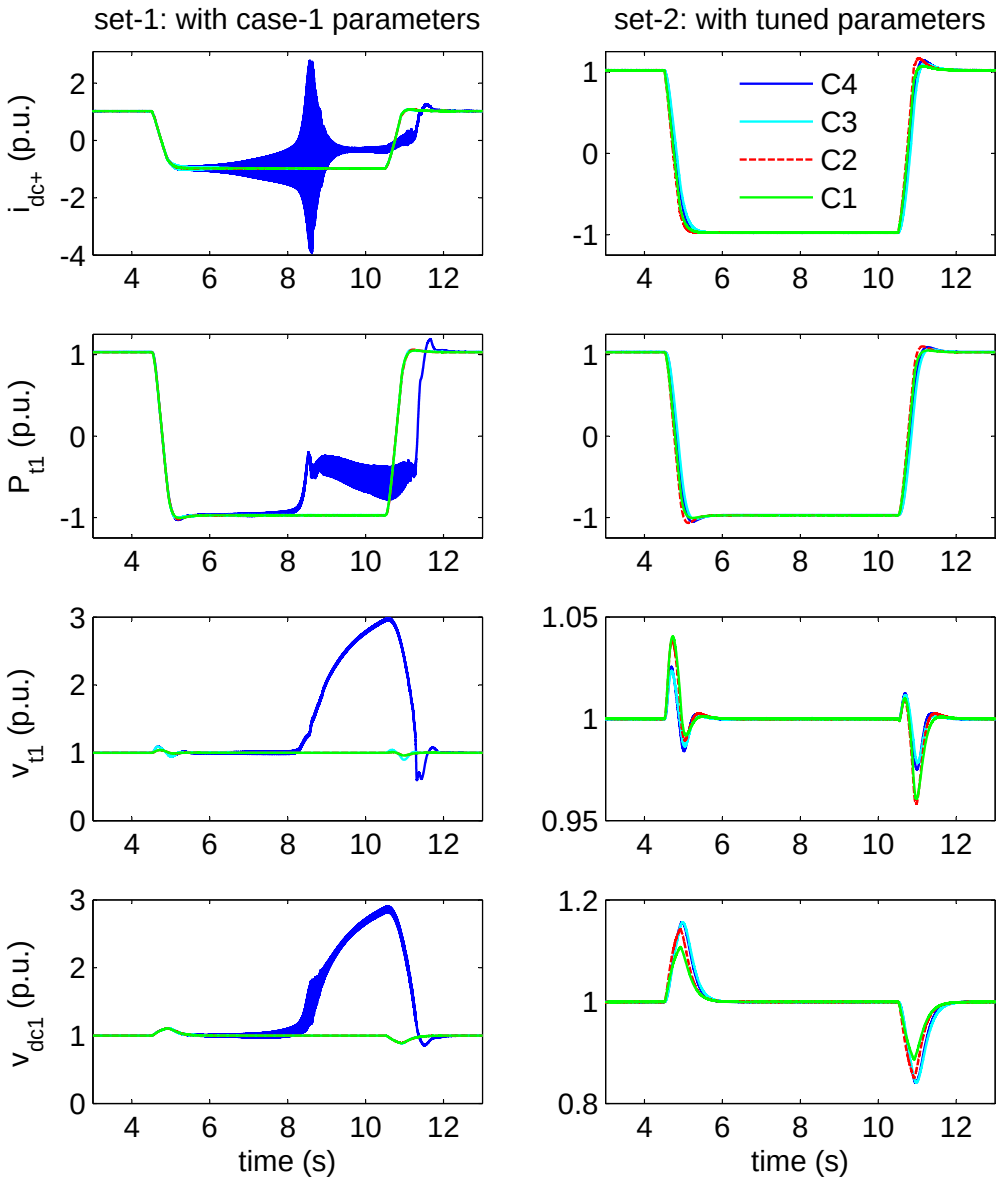

Figure 5.7: EMT simulation results of dc current, active power, ac voltage, and dc voltage for quick power reversal (C1: case-1, C2: case-2, C3: case-3, and C4: case-4)

It can be observed from Figure 5.7 (a) that the case-4 of set-1 (SCR1=1.5, SCR2=1.5) is unstable with large oscillations in dc currents and huge over voltages when the power is reversed. This is because the controller gains used for this simulation were tuned for a strong system (SCR=3.0) and hence they are too fast for a

system with weak ac network connections. In contrast, the simulation results shown in Figure 5.7 (b) illustrates that the system is stable for the same power reversal operation as the controller gains were tuned considering the actual SCR information. Similar performances can be obtained under all possible ac system conditions with properly tuned controller gains.

Three Phase to Ground Fault

A three phase to ground fault with negligible impedance (fault duration of 5 fundamental cycles) was applied to the inverter side ac terminal of the test system. The simulation results for all four cases are shown in Figure 5.8. It can be observed from Figure 5.8 (a) that case-2 and case-4 of set-1 (in both cases, the SCR1=1.5) show undesirable over-voltages. In addition, the settling time is also high. However, Figure 5.8 (b) shows more satisfactory fault performance of the system with considerably damped oscillations. Importantly, the large post fault transients observed in power, ac voltage, and dc voltages in both case-2 and case-4 are reduced with the set of gains tuned for an MMC-VSC system considering different ac system strength.

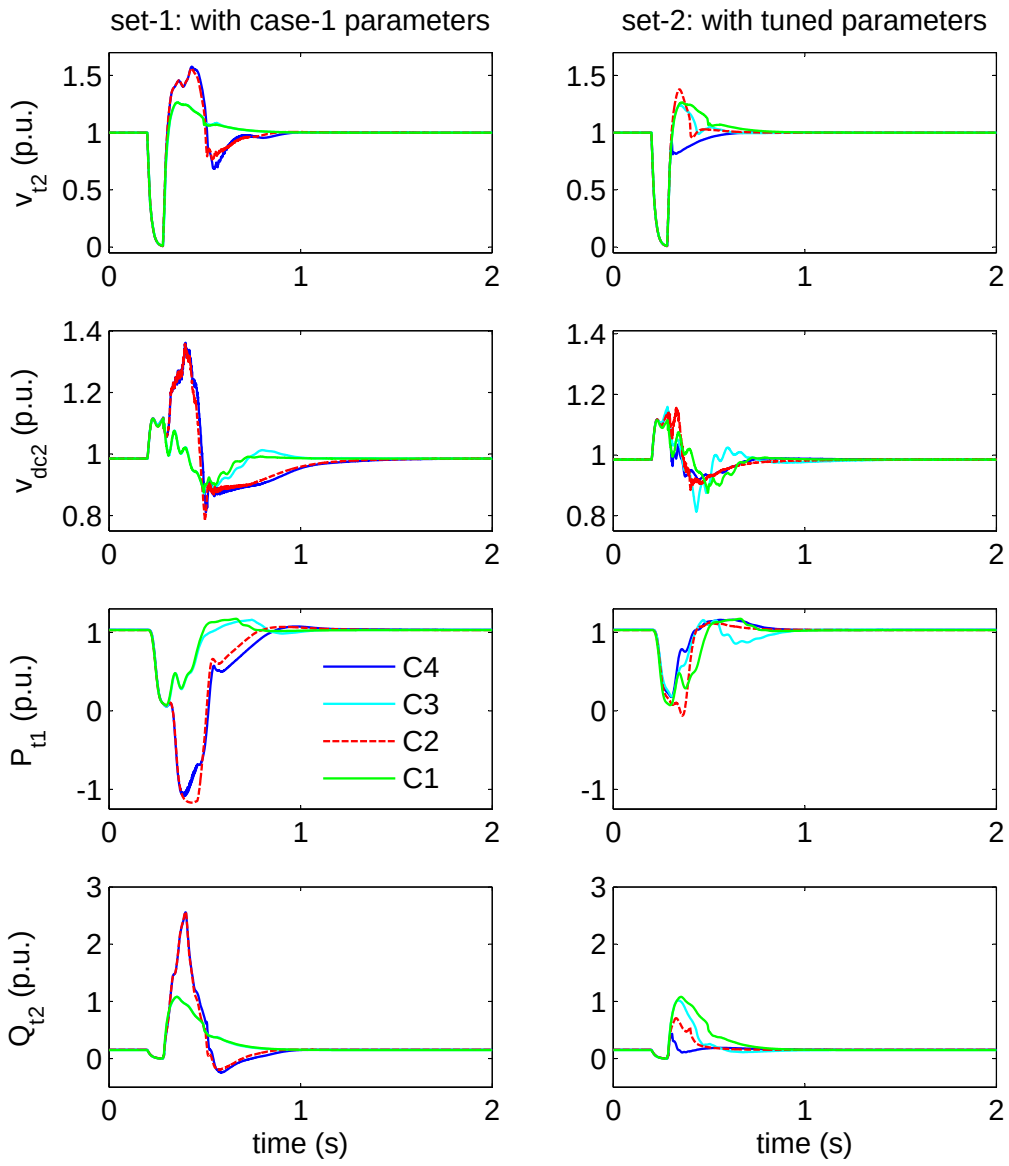

Figure 5.8: EMT simulation results of ac voltage, dc voltage, active power, and reactive power for a three phase fault at terminal2 (C1: case-1, C2: case-2, C3: case-3, and C4: case-4)

5.2 Impact of Measuring Delays

In practical systems, measuring transducers are used to measure instantaneous currents and voltages. In addition, it is required to separate these measurements into

positive and negative sequence components in order to treat unbalanced conditions. These operations introduce delays in instantaneous currents and voltages. It is shown in **Chapter 3** that the delays in instantaneous measurements can affect the stability of MMC-VSC systems. In addition, it is shown that the poorly damped modes introduced by the measuring delays can lead the MMC-VSC system to instabilities. Therefore, it is important to tune controller gains considering effects of time delays in instantaneous measurements. This is done by applying the proposed controller tuning method to the upgraded small-signal model developed in **Chapter 3**.

It was observed that the oscillatory modes introduced by the delays in d-q voltages cannot be improved much by adjusting controller gains as it highly depends on the delay time-constant. Therefore, the required damping for modes 10 and 11 were set to 15 %. In addition, it was also noted that the damping improvement of the dc resonance through the controllers is limited. Therefore, the damping requirement for the dc resonance was set to 15 %. Moreover, it was observed that the damping of modes 2 and 4 depend on the delay time-constants. Therefore, the damping requirement for those modes were set to 25 %. The damping requirements for the other modes were set to 80 %. Then, by applying the proposed controller tuning method, the controller gains corresponding to all 4 cases were obtained. The initial and tuned controller parameters are given in Table 5.6. Then, the tuned controller gains were applied to the EMT model of the test system and two large transients were studied as described in the following section.

5.2.1 Quick Power Reversal

A quick power reversal operation was studied. The power reference to terminal2 was changed from -1.0 p.u. to 1.0 p.u. with a rate of 5 p.u./s at 3 s and then at 6 s the

Table 5.6: Tuned PI-controller gains for different cases considering the measuring delays

MMC	**PI**	**Gain**	**Initial**	**Optimized Gains for (SCR1/SCR2)**			
				Case-1 3.0/3.0	**Case-2 3.0/1.5**	**Case-3 1.5/3.0**	**Case-4 1.5/1.5**
MMC1	PLL1	K_P	50	50.4	50.0	52.7	51.9
		K_I	250	249.2	250.0	246.8	242.1
	v_{dc1}	K_P	2	5.2	5.5	6.3	6.5
		K_I	20	20.8	21.7	26.8	27.5
	v_{t1}	K_P	1	1.2	0.9	1.2	1.2
		K_I	20	24.5	29.4	99.0	99.0
	i_{t1d}	K_P	1	0.9	1.0	1.3	1.3
		K_I	100	97.0	106.5	31.9	31.2
	i_{t1q}	K_P	1	0.7	0.7	1.2	1.3
		K_I	100	94.8	99.1	88.8	99.3
MMC2	PLL2	K_P	50	50.0	50.1	50.7	50.7
		K_I	250	249.6	256.7	249.3	248.7
	P_{t2}	K_P	1	0.4	1.1	0.1	0.1
		K_I	20	19.8	14.2	8.4	10.0
	v_{t2}	K_P	1	0.9	1.1	1.4	3.5
		K_I	20	21.5	22.7	32.1	32.8
	i_{t2d}	K_P	1	0.9	1.0	0.8	1.0
		K_I	100	97.1	104.5	76.4	68.0
	i_{t2q}	K_P	1	0.7	1.4	0.7	1.4
		K_I	100	95.9	104.0	101.0	104.2

power order was changed back to -1.0 p.u. at the same rate. The EMT simulation results obtained for the power reversal are shown in Figure 5.9. It can be observed that the performances of the MMC-VSC system for all four cases are similar and acceptable.

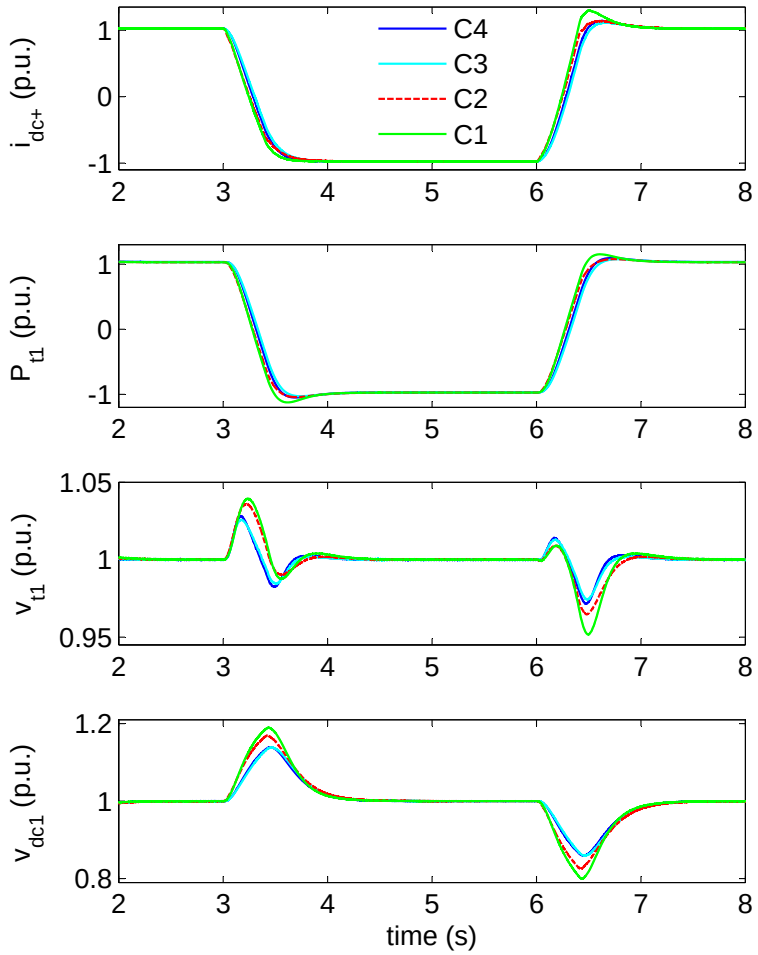

Figure 5.9: EMT simulation results of dc current, active power, ac voltage, and dc voltage for quick power reversal (C1: case-1, C2: case-2, C3: case-3, and C4: case-4)

5.2.2 Three Phase to Ground Fault

A three phase fault with negligible impedance and 5 cycle duration was applied to the inverter (terminal2) ac terminal. The EMT simulation results of all 4 cases are shown in Figure 5.10. It can be observed that the performance of the MMC-VSC system for a three-phase fault at the inverter is acceptable with the tuned controller gains.

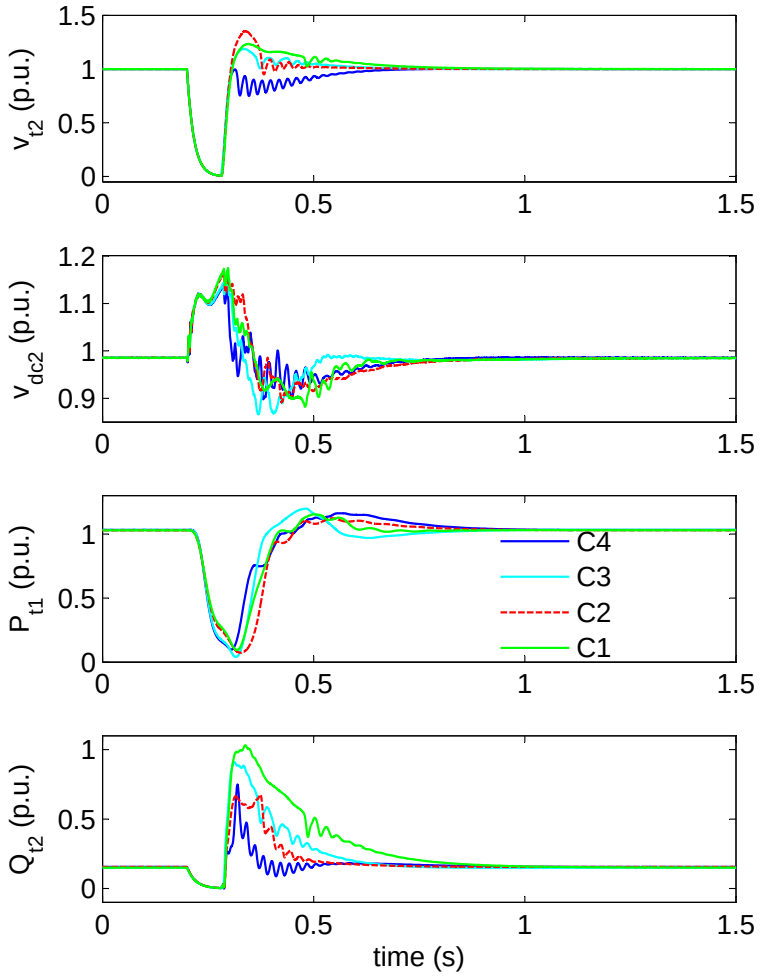

Figure 5.10: EMT simulation results of ac voltage, dc voltage, active power, and reactive power for a three phase fault at terminal2 (C1: case-1, C2: case-2, C3: case-3, and C4: case-4)

5.3 Discussion on Computation Time for Controller Tuning

The performance of the proposed controller tuning algorithm is evaluated by calculating the average time taken to simultaneously tune all PI-controllers in the test system. Different ac system strengths ranging from weak to strong systems are considered and the performance requirements are set as the same. For each ac system, the average time taken to tune controllers on a general purpose computer (with 4

Table 5.7: Average computation time

Short circuit ratio (SCR)	**Average computation time**
5.0	less than a minute
3.0	∼2 minutes
2.0	∼5 minutes
1.5	∼30 minutes

cores) are given in Table 5.7. It can be observed that the proposed controller tuning technique takes only a few minutes to simultaneously tune all PI-controllers of the MMC-VSC system connected to ac systems with SCR values higher than 2.0. From the results provided in Table 5.7, it is clear that the proposed controller tuning is more suitable to simultaneously tune converters in a dc grid compared to the time-domain simulation based optimization techniques proposed in [22] and [80].

5.4 Guidelines for MMC-VSC Control System Design

PI-controllers of any given MMC-VSC system can be simultaneously tuned using the controller tuning procedure presented in **Chapter 4** of this thesis. In addition, based on the experience gained from controller tuning, non-linear EMT simulations, and small-signal stability assessment of MMC-VSC systems, a number of key points that need to be considered in designing control system of MMC-VSC systems are summarized below.

1. Measurement delays may have a significant impact on the stability of VSC systems connected to weak ac grids. Therefore, it is necessary to properly model the delays associated with measuring transducers and filters. In addition, the selection of very high PLL gains will result unstable operation as poorly damped modes introduced by measuring delays are sensitive to PLL gains.

2. The analysis done in this thesis confirms that it is important to model the VSC system in detail including the dynamics of ac system, dc system, d-q control loops, measuring delays, and PLL, in order to assess the stability accurately.

3. The gains of active power, dc voltage, and d-axis current controllers have to be reduced if the MMC-VSC system is connected to weak ac grids. When the ac system is weak, the power transfer capability to the ac system is limited. Therefore, it is essential to slow down the control actions of power and dc voltage controllers. In addition, the gains of d-axis current controllers have to be reduced to act in-accordance with outer-loop controllers.

4. A weak ac system is not able to maintain the terminal voltage at 1.0 p.u. Therefore, the ac voltage controller gains have to be increased to maintain the ac bus voltage when the ac system is weak. A similar observation is reported in [51].

5.5 Chapter Summary

This chapter discussed the influence of ac system strength and measuring delays in instantaneous quantities on the stability of MMC-VSC systems. The controller tuning considering different ac system strengths is discussed. Then, the controller tuning is done considering both different ac systems and the effect of measuring delays in d-q voltage and currents. A number of EMT simulation results are presented to show the efficacy of the proposed controller tuning technique. In addition, the computation

time required to simultaneously tune the controllers of the test system is briefly discussed. Finally, important guidelines for MMC-VSC control system design are summarized.

Chapter 6

Conclusions, Contributions, and Future Work

.

6.1 General Conclusions

A generalized frequency-domain controller tuning procedure for MMC-VSC systems has been presented in this thesis. The gain tuning problem has been formulated as a mathematical optimization problem in such a way that most meta-heuristic optimization methods are candidates for solving it. In this thesis, the simulated annealing method has been successfully applied. It has been shown that the proposed tuning method can be applied to simultaneously tune controller parameters of of a point-to-point MMC-VSC test system. In addition, the tuned PI-controller parameters have been rigorously tested by performing a wide range of EMT simulations on a real-time digital simulator. The controller tuning procedure proposed in this thesis is generic and can be adapted for any type of dynamic devices in power systems.

The impacts of gains and time-constants of MMC-VSC control system units such as d-q decoupled control loops, measurement transducers, and phase-locked loops on the stability and dynamic performance has been investigated. It is shown that the measuring delays in instantaneous d-q frame voltages and currents can introduce poorly damped oscillatory modes. In addition, it is shown that these poorly damped modes can make the MMC-VSC system unstable if very high PLL gains are used. Moreover, it is also shown that properly tuned d-q decoupled controller parameters can assure the stability of an MMC-VSC with weak ac connections even after being subjected to large transients such as three phase to ground faults and emergency full power reversal. Finally, based on the understanding of the test system, a set of guidelines that needs to be considered in the planning stage of an MMC-VSC system is summarized.

The research was started with developing the following models of a point-to-point MMC-VSC system, which are essential to use the controller tuning procedure proposed in this thesis.

- Electromagnetic transient (EMT) model with the typical control system including d-q decoupled controller, circulation current suppression controller, and basic protection is developed using the real-time digital simulator (RTDS).
- Linearized state-space model consisting dynamics of the ac system, dc system, control system, PLL, arm inductor, converter losses, measurement filters, and measuring delays in instantaneous voltages and currents is modelled from scratch, coded using the MATLAB software, and validated against the EMT simulation model.

6.2 Contributions

The main contributions of the thesis are summarized below,

- A generalized frequency domain controller tuning procedure for simultaneous tuning of converter controls is introduced. This novel technique is applicable to tune controller parameters of any MMC-VSC system. In this thesis, this generalized frequency domain controller tuning method is used to simultaneously tune all PI-controllers of the test system.
- The gain tuning problem is formulated as an optimization problem in-terms of frequency-domain stability related attributes and the objective function is general. Therefore, any suitable meta-heuristic optimization technique can be applied to find solutions. In this thesis, the simulated annealing method of optimization that can handle a large number of variable and guarantee the global optimum solution is used to solve the problem.
- Important guidelines to design the control system of an MMC-VSC system are proposed. The guidelines include the selection of PI-controller parameters, measuring time-constants, and PLL gains.

The key contributions of this thesis are published in reputed journals and conference proceedings.

Transaction Papers

1. S. Arunprasanth, U.D. Annakkage, C. Karawita, and R. Kuffel,"Generalized Frequency Domain Controller Tuning Procedure for VSC Systems,"*IEEE Trans. Power Del.*, vol. 31, no. 2, pp 732-742, Oct. 2015.

Conference Papers

1. S. Arunprasanth, U.D. Annakkage, C. Karawita, and R. Kuffel,"Performance Evaluation of the Generalized Controller Tuning Procedure for MMC-VSC Systems,"*presented at the IEEE PES General Meeting*, Boston, MA, USA, Jul. 2016.

2. S. Arunprasanth, U.D. Annakkage, C. Karawita, and R. Kuffel,"Generalized Frequency Domain Controller Tuning Procedure for VSC Systems,"*presented at the IEEE PES General Meeting*, Boston, MA, USA, Jul. 2016.

3. S. Arunprasanth, U.D. Annakkage, C. Karawita, and R. Kuffel, "A Generic Point-to-Point MMC-VSC System for Real-Time and Off-Line Simulation Studies,"*presented at the Int. Conf. Power Syst. Transients (IPST)*, Cavtat, Croatia, Jun. 2015.

4. S. Arunprasanth, U.D. Annakkage, C. Karawita, and R. Kuffel, "Small-Signal Stability Modelling and Analysis of an MMC-VSC System,"*presented at the CIGŔE Canada Conf. Power Syst.*, Winnipeg, MB, Canada, Sep. 2015.

6.3 Future Work

Based on the experience gained throughout the work done in this thesis and the knowledge on present work that are being carried out in different parts of the world, a list of possible future directions of this work are outlined below.

- This thesis utilized the simulated annealing optimization technique to solve the gain tuning problem that was formulated as a frequency-domain optimization problem. However, one can also try with different optimization techniques such

as particle-swarm optimization, genetic algorithm, ant-colony algorithm, or non-linear simplex to solve the optimization problem and compare any advantages.

- In this thesis, the application of the proposed controller tuning method to tune controllers of a point-to-point MMC-VSC system is shown. The application of the proposed controller tuning procedure to a multi-terminal system is similar and simple as there are advanced small-signal modelling tools available at present. Therefore, the tuning of multi-terminal MMC-VSC system using the proposed method incorporating small-signal modelling software can be another future direction.

- It was observed and reported in this thesis that measuring delays in instantaneous d-q currents and voltages introduce poorly damped modes that lead an MMC-VSC system into unstable operation when it is connected to weak ac networks. However, the researcher believes that a corrective action such as delay compensation could improve the stability of the overall system. Therefore, such an investigation could be a possible direction to be explored.

- A method to estimate short circuit ratio (SCR) of an ac system using the voltage pulse method is investigated in this thesis. In addition, it was also observed and reported that the controller gains have to be changed when the ac system becomes weak (SCR$\leq$2.0). However, further investigation would be required to accurately determine the strength of practical ac power systems.

Appendix A

Additional Information

A.1 Generation of AC Voltage Using Voltage Source Converters

The 2-level VSC was very common when the VSC technology was first considered for the HVdc applications [81]. However, due to poor harmonic performance and high losses, 3-level and multi-level VSCs were introduced. The evolution of VSC converter technology is shown in Fig. A.1. The 2-level VSC can produce two voltage levels ($+V_{dc}$ and $-V_{dc}$). The realization of a sine wave using a 2-level VSC is shown in Fig. A.1 (a). It can be seen that the ac output wave contains harmonics. Then, the 3-level VSC is shown in Fig. A.1 (b) and the realized output voltage is more close to the reference wave compared to the 2-level VSC output as three voltage levels ($+V_{dc}$, $-V_{dc}$, and 0) are used. However, still the harmonic performance is not improved a lot and needs harmonic filters which is an added cost. The more advanced type VSC known as the MMC is shown in Fig. A.1 (c). The basic building block of an MMC is known as a sub-module (SM) and an MMC is constructed by cascading a number

of SM in series as shown in Fig. A.1 (c). In contrast to the harmonic performance of conventional 2-level and 3-level VSCs, the waveform generated by an MMC is very close to the reference sine wave [82].

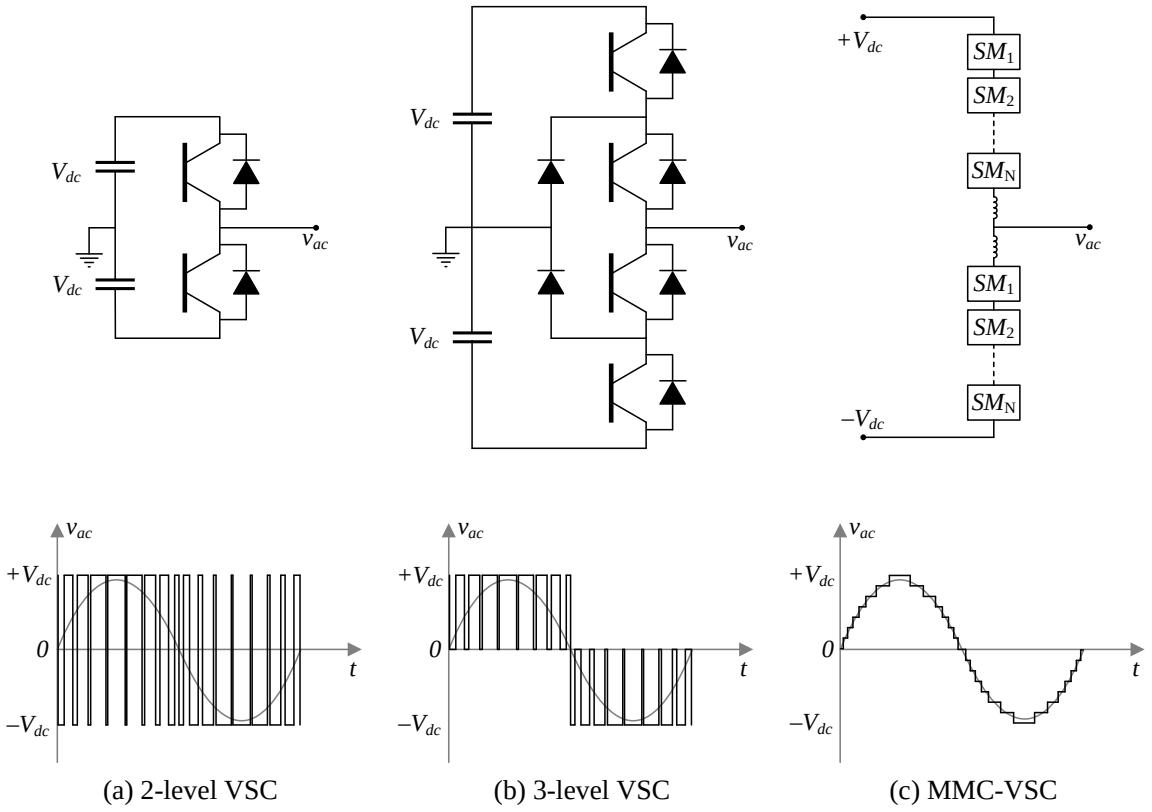

(a) 2-level VSC (b) 3-level VSC (c) MMC-VSC

Figure A.1: Evolution of VSC technology

A.2 Introduction to the RTDS Simulators

The RTDS simulator is a specially designed hardware based on parallel processing techniques to conduct power system transient simulation studies in real-time by solving the *Dommel's* EMT simulation algorithm [83]. Multiple racks of RTDS hardware allows simulation of large power systems by splitting it into subsystems, each of which is solved on individual racks. Each rack of RTDS consists of a Giga Transceiver Work-

station Interface (GTWIF) card that handles the communication between the RTDS simulator and host computers and a number of processor cards to simulate the behaviour of the test system.

The graphical user interface developed for the RTDS simulator is known as RSCAD. The Draft module in RSCAD has a master library consists of generic components to construct simulation cases. The constructed circuit is then compiled to generate the simulation code needed to run the case using the RSCAD RunTime module. RunTime module in RSCAD allows the user to interact with their simulation by changing switch states and set points. Power system transients can be recorded and displayed in RunTime plots and also slow varying signals can be continuously monitored using meters. RSCAD has separate modules to create transmission lines (T-Line module) and cables (Cable module). RSCAD conversion tool allows the conversion of cases from PSS/E to RSCAD and also from MATLAB Simulink to RSCAD. Finally the C-Builder module allows user to create user defined models [84, 85, 86].

A.3 Open Loop Test on PLL Gains

A synchronous reference frame (SRF) PLL is supplied with a balanced three phase ac voltage as shown in Fig. A.2. Then, the supply frequency was changed in steps from 60 Hz to 59.5 Hz, to 60.5 Hz, and back to 60 Hz at 0.2 s, 0.7 s, and 1.2 s respectively. The response of PLL tracked frequency for different PLL gains are plotted in Fig. A.3. It can be seen that the response of PLL is very slow and undesirable when the PLL gains are very low (K_P=10, K_I=50). On the other hand, the PLL response does not improve a lot when the PLL gains are very high ($K_P > 50$, $K_I > 250$). The conclusion from this open-loop test is that selection of suitable PLL gains (not very low and not very high) will results good performance of the system. However, it is

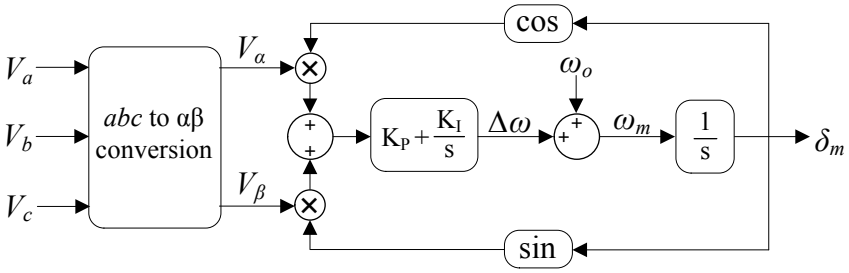

Figure A.2: Model of SRF-PLL for open loop test

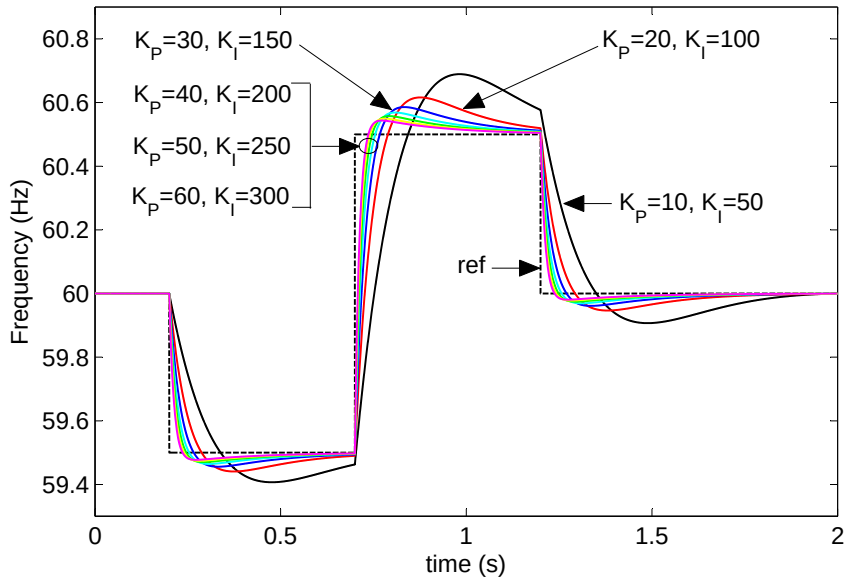

Figure A.3: Response of PLL for step changes in input frequency

not complete to draw general conclusions based on the open loop test. Therefore, a close loop test based on the small-signal model is presented in Section 3.4.2.

Bibliography

[1] M. Milligan, B. Frew, B. Kirby, M. Schuerger, K. Clark, D. Lew, P. Denholm, B. Zavadil, M. O'Malley, and B. Tsuchida, "Alternatives no more: Wind and solar power are mainstays of a clean, reliable, affordable grid," *Power and Energy Magazine, IEEE*, vol. 13, no. 6, pp. 78–87, Nov. 2015.

[2] N. Hingorani, "Flexible ac transmission," *Spectrum, IEEE*, vol. 30, no. 4, pp. 40–45, Apr. 1993.

[3] S. Cole and R. Belmans, "Transmission of bulk power," *IEEE Ind. Electron. Mag*, vol. 3, no. 3, pp. 19–24, Sep. 2009.

[4] T. Hammons, D. Woodford, J. Loughtan, M. Chamia, J. Donahoe, D. Povh, B. Bisewski, and W. Long, "Role of hvdc transmission in future energy development," *IEEE Power Eng. Rev.*, vol. 20, no. 2, pp. 10–25, Feb. 2000.

[5] D. A. Woodford, "Hvdc transmission," *Manitoba HVDC Research Centre*, pp. 400–1619, Mar. 1998.

[6] J. Arrillaga, Y. H. Liu, and N. R. Watson, *Flexible Power Transmission: The HVDC Options*. John Wiley & Sons, Jan. 2007.

[7] J. Renedo, A. Garcia-Cerrada, and L. Rouco, "Active power control strategies for transient stability enhancement of ac/dc grids with vsc-hvdc multi-terminal systems," *IEEE Trans. Power Syst.*, vol. PP, no. 99, pp. 1–10, Jan. 2016.

[8] A. Yazdani and R. Iravani, *Voltage-Sourced Converters in Power Systems: Modeling, Control, and Applications*. John Wiley & Sons, Feb. 2010.

[9] A. Nami, J. Liang, F. Dijkhuizen, and G. Demetriades, "Modular multilevel converters for hvdc applications: Review on converter cells and functionalities," *IEEE Trans. Power Electron.*, vol. 30, no. 1, pp. 18–36, Jan. 2015.

[10] Y. Yang, X. Yang, F. Qian, L. Li, G. Wu, S. Lin, and M. Liu, "Effect of 800 kv yun-guang ultra hvdc transmission system on voltage profile in guangdong power grid and corresponding enhancement measures," in *2010 IEEE PES Innovative Smart Grid Technologies Conference Europe (ISGT Europe)*, pp. 1–5, Oct. 2010.

[11] W. Long and S. Nilsson, "Hvdc transmission: Yesterday and today," *IEEE Power and Energy Mag.*, vol. 5, no. 2, pp. 22–31, Mar. 2007.

[12] O. Peake, "The history of high voltage direct current transmission," *Australian Journal of Multi-Disciplinary Engineering*, vol. 8, no. 1, pp. 47–55, Sep. 2010.

[13] U. Axelsson, A. Holm, C. Liljegren, K. Eriksson, and L. Weimers, "Gotland hvdc light transmission—world's first commercial small scale dc transmission," in *Proc. CIRED Conf., Nice, France*, vol. 32, May. 1999.

[14] N. Flourentzou, V. Agelidis, and G. Demetriades, "Vsc-based hvdc power transmission systems: An overview," *IEEE Trans. Power Electron.*, vol. 24, no. 3, pp. 592–602, Mar. 2009.

[15] G. Asplund, K. Eriksson, and O. Tollerz, "Hvdc light, a tool for electric power transmission to distant loads," in *VI SEPOPE Conf., Salvador, Brazil*. Citeseer, May. 1998.

[16] Wikipedia, "List of hvdc projects — wikipedia, the free encyclopedia," 2016, [Online; accessed 26-January-2016]. [Online]. Available: https://en.wikipedia.org/w/index.php?title=List_of_HVDC_projects&oldid=701491127

[17] N. Flourentzou, V. Agelidis, and G. Demetriades, "Vsc-based hvdc power transmission systems: An overview," *IEEE Trans. Power Electron.*, vol. 24, no. 3, pp. 592–602, Mar. 2009.

[18] G. Konstantinou, J. Pou, S. Ceballos, R. Darus, and V. G. Agelidis, "Switching frequency analysis of staircase-modulated modular multilevel converters and equivalent pwm techniques," *IEEE Trans. Power Del.*, vol. 31, no. 1, pp. 28–36, Feb. 2016.

[19] G. Falahi and A. Q. Huang, "Design consideration of an mmc-hvdc system based on 4500v/4000a emitter turn-off (eto) thyristor," in *Proc. IEEE Energy Convers. Congress and Exposition (ECCE)*, pp. 3462–3467, Sep. 2015.

[20] M. Guan and Z. Xu, "Modeling and control of a modular multilevel converter-based hvdc system under unbalanced grid conditions," *IEEE Trans. Power Electron.*, vol. 27, no. 12, pp. 4858–4867, Dec. 2012.

[21] S. Deore, P. Darji, and A. Kulkarni, "Dynamic phasor modeling of modular multi-level converters," in *Proc. 7th IEEE Int. Conf. Ind. Inf. Syst. (ICIIS)*, pp. 1–6, Aug. 2012.

[22] Z. J. Zhou, "Co-ordination of converter controls and an analysis of converter operating limits in vsc-hvdc grids," Ph.D. dissertation, Dept. Elect. and Comput. Eng., The Univ. Manitoba, Winnipeg, Sep. 2013.

[23] G. Kalcon, G. Adam, O. Anaya-Lara, S. Lo, and K. Uhlen, "Small-signal stability analysis of multi-terminal vsc-based dc transmission systems," *IEEE Trans. Power Syst.*, vol. 27, no. 4, pp. 1818–1830, Nov. 2012.

[24] M. A. Perez, S. Bernet, J. Rodriguez, S. Kouro, and R. Lizana, "Circuit topologies, modeling, control schemes, and applications of modular multilevel converters," *IEEE Transactions on Power Electronics*, vol. 30, no. 1, pp. 4–17, Jan. 2015.

[25] C. Schauder and H. Mehta, "Vector analysis and control of advanced static var compensators," *Proc. IEE Gener. Transmiss. Distrib.*, vol. 140, no. 4, pp. 299–306, Jul. 1993.

[26] A. Fuchs, M. Imhof, T. Demiray, and M. Morari, "Stabilization of large power systems using vsc-hvdc and model predictive control," *IEEE Trans. Power Del.*, vol. 29, no. 1, pp. 480–488, Feb. 2014.

[27] C. Bajracharya, M. Molinas, J. A. Suul, T. M. Undeland *et al.*, "Understanding of tuning techniques of converter controllers for vsc-hvdc," in *Proc. Nordic Workshop on Power and Ind. Electron. (NORPIE), Espoo, Finland.* Helsinki Univ. Technol., Jun. 2008.

[28] F. Freijedo, A. Vidal, A. Yepes, J. Guerrero, O. Lopez, J. Malvar, and J. Doval-Gandoy, "Tuning of synchronous-frame pi current controllers in grid-connected converters operating at a low sampling rate by mimo root locus," *IEEE Trans. Ind. Electron.*, vol. 62, no. 8, pp. 5006–5017, Aug. 2015.

[29] L. Mazouz, S. A. Zidi, S. Saadi, M. Khatir, and T. Benmessaoud, "Vsc-hvdc system optimized pi controllers using bacterial foraging algorithm," *J. Electr. Eng.*, vol. 97, no. 3, pp. 205–212, Jan. 2015.

[30] S. Filizadeh, A. Gole, D. Woodford, and G. Irwin, "An optimization-enabled electromagnetic transient simulation-based methodology for hvdc controller design," *IEEE Trans. Power Del.*, vol. 22, no. 4, pp. 2559–2566, Oct. 2007.

[31] L. Wang and N. Ertugrul, "Selection of pi compensator parameters for vsc-hvdc system using decoupled control strategy," in *Proc. 20th Australasian Univ. Power Eng. Conf. (AUPEC)*, pp. 1–7, Dec. 2010.

[32] C. Zhao, X. Lu, and G. Li, "Parameters optimization of vsc-hvdc control system based on simplex algorithm," in *Proc. IEEE Power and Energy Soc. General Meeting (IEEE-PES GM)*, pp. 1–7, Jun. 2007.

[33] A. Goharrizi, R. Singh, A. Gole, S. Filizadeh, J. Muller, and R. Jayasinghe, "A parallel multimodal optimization algorithm for simulation-based design of power systems," *IEEE Trans. Power Del.*, vol. 30, no. 5, pp. 2128–2137, Oct. 2015.

[34] K. Rouzbehi, A. Miranian, A. Luna, and P. Rodriguez, "Optimized control of multi-terminal dc grids using particle swarm optimization," in *Proc. 15th European Conf. Power Electron. Appl. (EPE)*, pp. 1–9, Sep. 2013.

[35] K. Padiyar and N. Prabhu, "Modelling, control, design, and analysis of vsc based hvdc transmission systems," in *Proc. Int. Conf. Power Syst. Technol. (PowerCon)*, vol. 1, pp. 774–779, Nov. 2004.

[36] M. Janaki, R. Thirumalaivasan, and N. Prabhu, "Design of robust controller for vsc based hvdc using genetic algorithm," in *Proc. Int. Conf. Advances in Electr. Eng. (ICAEE)*, pp. 1–6, Jan. 2014.

[37] A. Moharana, J. Samarabandu, and R. Varma, "Fuzzy supervised pi controller for vsc hvdc system connected to induction generator based wind farm," in *Proc. IEEE Electr. Power and Energy Conf. (EPEC)*, pp. 432–437, Oct. 2011.

[38] M. Kumar and N. Srikanth, "Dynamic performance of a fuzzy pi controlled svpwm based hvdc light transmission system," in *Proc. Annual IEEE India Conf. (INDICON)*, pp. 1–5, Dec. 2013.

[39] L. Xu and S. Ahmed-Zaid, "Tuning of power system controllers using symbolic eigensensitivity analysis and linear programming," *IEEE Trans. Power Syst.*, vol. 10, no. 1, pp. 314–322, Feb. 1995.

[40] N. Kshatriya, U. Annakkage, F. Hughes, and A. Gole, "Optimized partial eigenstructure assignment-based design of a combined pss and active damping controller for a dfig," *IEEE Trans. Power Syst.*, vol. 25, no. 2, pp. 866–876, May 2010.

[41] A. Konara and U. Annakkage, "Robust power system stabilizer design using eigenstructure assignment," *IEEE Trans. Power Syst.*, vol. 31, no. 3, pp. 1845–1853, Jun. 2015.

[42] X. Chen, N. Pahalawaththa, U. Annakkage, and C. Kumble, "Output feedback tcsc controllers to improve damping of meshed multi-machine power systems," *IEE Proc. Gener. Transmiss. Distrib.*, vol. 144, no. 3, pp. 243–248, May 1997.

[43] X. Chen, N. Pahalawaththa, U. Annakkage, and C. Kumble, "Design of decentralised output feedback tcsc damping controllers by using simulated annealing," *IEE Proc. Gener. Transmiss. Distrib.*, vol. 145, no. 5, pp. 553–558, Sep. 1998.

[44] J. Zhou, H. Ding, S. Fan, Y. Zhang, and A. Gole, "Impact of short-circuit ratio and phase-locked-loop parameters on the small-signal behavior of a vsc-hvdc converter," *IEEE Trans. Power Del.*, vol. 29, no. 5, pp. 2287–2296, Oct. 2014.

[45] W. Wang, A. Beddard, M. Barnes, and O. Marjanovic, "Analysis of active power control for vsc-hvdc," *IEEE Trans. Power Del.*, vol. 29, no. 4, pp. 1978–1988, Aug. 2014.

[46] P. Kundur, N. J. Balu, and M. G. Lauby, *Power system stability and control*. McGraw-hill New York, Jan. 1994.

[47] J. Beerten, S. D Arco, and J. Suul, "Identification and small-signal analysis of interaction modes in vsc mtdc systems," *IEEE Trans. Power Del.*, vol. 31, no. 2, pp. 888–897, Aug. 2015.

[48] S. Anbuselvi, R. Devi, P. Somasundaram, and T. Nargunadevi, "Small signal stability analysis of power system with vsc based hvdc link employing phase angle control," *Int. Review on Modelling and Simulations*, vol. 5, no. 5, Oct. 2012.

[49] S. Arunprasanth, U. D. Annakkage, C. Karawita, and R. Kuffel, "A generic point-to-point mmc-vsc system for real-time and off-line simulation studies," in *Proc. Int. Conf. Power Syst. Transients (IPST), Cavtat, Croatia*, Jun. 2015.

[50] G. Pinares and M. Bongiorno, "Modeling and analysis of vsc-based hvdc systems for dc network stability studies," *IEEE Trans. Power Del.*, vol. 31, no. 2, pp. 848–856, Jul. 2015.

[51] H. Ding, S. Fan, J. Zhou, Y. Zhang, and A. Gole, "Parametric analysis of the stability of vsc-hvdc converters," in *Proc. 11th IET Int. Conf. AC and DC Power Transmiss.*, pp. 1–6, Jul. 2015.

[52] N. Chaudhuri, R. Oliveira, and A. Yazdani, "Stability analysis of vector controlled modular multilevel converters in linear time periodic framework," *IEEE Trans. Power Electron.*, vol. 31, no. 7, pp. 5255–5269, Jul. 2016.

[53] S. Arunprasanth, U. Annakkage, C. Karawita, and R. Kuffel, "Small-signal stability modelling and, analysis of an mmc-vsc system," in *Proc. CIGRÉ Canada Conf. Power Syst., Winnipeg, MB, Canada*, Sep. 2015.

[54] C. Karawita and U. Annakkage, "Multi-infeed hvdc interaction studies using small-signal stability assessment," *IEEE Trans. Power Del.*, vol. 24, no. 2, pp. 910–918, Apr. 2009.

[55] C. Du, M. H. J. Bollen, E. Agneholm, and A. Sannino, "A new control strategy of a vsc-hvdc system for high-quality supply of industrial plants," *IEEE Trans. Power Del.*, vol. 22, no. 4, pp. 2386–2394, Oct. 2007.

[56] C. Du, E. Agneholm, and G. Olsson, "Comparison of different frequency controllers for a vsc-hvdc supplied system," *IEEE Trans. Power Del.*, vol. 23, no. 4, pp. 2224–2232, Oct. 2008.

[57] M. Gibbard, N. Martins, J. Sanchez-Gasca, N. Uchida, V. Vittal, and L. Wang, "Recent applications of linear analysis techniques," *IEEE Trans. Power Systems*, vol. 16, no. 1, pp. 154–162, Feb. 2001.

[58] A. M. Lyapunov, "Stability of motion-english translation," *Academic Press Inc.*, 1967.

[59] U. Gnanarathna, A. Gole, and R. Jayasinghe, "Efficient modeling of modular multilevel hvdc converters (mmc) on electromagnetic transient simulation programs," *IEEE Trans. Power Del.*, vol. 26, no. 1, pp. 316–324, Jan. 2011.

[60] H. Saad, J. Peralta, S. Dennetière, J. Mahseredjian, J. Jatskevich, J. A. Martinez, A. Davoudi, M. Saeedifard, V. Sood, X. Wang, J. Cano, and A. Mehrizi-Sani, "Dynamic averaged and simplified models for mmc-based hvdc transmission systems," *IEEE Trans. Power Del.*, vol. 28, no. 3, pp. 1723–1730, Jul. 2013.

[61] A. J. Far and D. Jovcic, "Small-signal dynamic dq model of modular multilevel converter for system studies," *IEEE Trans. Power Del.*, vol. 31, no. 1, pp. 191–199, Feb. 2016.

[62] N. Chaudhuri, R. Oliveira, and A. Yazdani, "Stability analysis of vector-controlled modular multilevel converters in linear time-periodic framework," *IEEE Trans. Power Electron.*, vol. 31, no. 7, pp. 5255–5269, Jul. 2016.

[63] M. Gibbard, N. Martins, J. J. Sanchez-Gasca, N. Uchida, V. Vittal, and L. Wang, "Recent applications of linear analysis techniques," *IEEE Trans. Power Syst.*, vol. 16, no. 1, pp. 154–162, Feb. 2001.

[64] S. Kirkpatrick, M. P. Vecchi *et al.*, "Optimization by simulated annealing," *Science*, vol. 220, no. 4598, pp. 671–680, May 1983.

[65] S. Kirkpatrick, "Optimization by simulated annealing: Quantitative studies," *J. Statistical Physics*, vol. 34, no. 5–6, pp. 975–986, Mar. 1984.

[66] N. Metropolis, A. W. Rosenbluth, M. N. Rosenbluth, A. H. Teller, and E. Teller, "Equation of state calculations by fast computing machines," *The J. Chemical Physics*, vol. 21, no. 6, pp. 1087–1092, Jun. 1953.

[67] S. Arunprasanth, U. Annakkage, C. Karawita, and R. Kuffel, "Generalized frequency domain controller tuning procedure for vsc systems," *IEEE Trans. Power Del.*, vol. 31, no. 2, pp. 732–742, Oct. 2015.

[68] Y. Huang, X. Yuan, J. Hu, and P. Zhou, "Modeling of vsc connected to weak grid for stability analysis of dc-link voltage control," *IEEE J. Emerging and Sel. Topics in Power Electron.*, vol. 3, no. 4, pp. 1193–1204, Apr. 2015.

[69] Y. Huang, X. Yuan, J. Hu, P. Zhou, and D. Wang, "Dc-bus voltage control stability affected by ac-bus voltage control in vscs connected to weak ac grids," *IEEE J. Emerging and Sel. Topics in Power Electron.*, vol. 4, no. 2, pp. 445–458, Jun. 2016.

[70] "Ieee guide for planning dc links terminating at ac locations having low short-circuit capacities," *IEEE Std 1204-1997*, 1997.

[71] L. Zhang, L. Harnefors, and H. Nee, "Modeling and control of vsc-hvdc links connected to island systems," *IEEE Trans. Power Syst.*, vol. 26, no. 2, pp. 783–793, May 2011.

[72] C. Bajracharya, "Control of vsc-hvdc for wind power," Ph.D. dissertation, Dept. Elect. Power Eng., Norwegian Univ. Science and Tech., Sweden, Jun. 2008.

[73] J. Suul, M. Molinas, L. Norum, and T. Undeland, "Tuning of control loops for grid connected voltage source converters," in *Proc. 2nd IEEE Power Energy Conf., Johor Baharu, Malaysia*, pp. 797–802, Dec. 2008.

[74] K. Ohtsuka, S. Yokokawa, H. Tanaka, and H. Doi, "An equivalent of multi-machine power systems and its identification for on-line application to decen-

tralized stabilizers," *IEEE Trans. Power Syst.*, vol. 4, no. 2, pp. 687–693, May 1989.

[75] A. Chebbo, M. Irving, and M. Sterling, "Voltage collapse proximity indicator: Behaviour and implications," *IEE Proc. Gener. Transmiss. Distrib.*, vol. 139, no. 3, pp. 241–252, May 1992.

[76] K. Vu, M. Begovic, D. Novosel, and M. Saha, "Use of local measurements to estimate voltage-stability margin," *IEEE Trans. Power Syst.*, vol. 14, no. 3, pp. 1029–1035, Aug. 1999.

[77] S. Corsi and G. Taranto, "A real-time voltage instability identification algorithm based on local phasor measurements," *IEEE Trans. Power Syst.*, vol. 23, no. 3, pp. 1271–1279, Aug. 2008.

[78] I. Smon, G. Verbic, and F. Gubina, "Local voltage-stability index using tellegen's theorem," *IEEE Trans. Power Syst.*, vol. 21, no. 3, pp. 1267–1275, Aug. 2006.

[79] S. Abdelkader and D. Morrow, "Online tracking of thevenin equivalent parameters using pmu measurements," *IEEE Trans. Power Syst.*, vol. 27, no. 2, pp. 975–983, May 2012.

[80] A. Y. Goharrizi, R. Singh, A. M. Gole, S. Filizadeh, J. C. Muller, and R. P. Jayasinghe, "A parallel multimodal optimization algorithm for simulation-based design of power systems," *IEEE Transactions on Power Delivery*, vol. 30, no. 5, pp. 2128–2137, Oct. 2015.

[81] B. Andersen, L. Xu, and K. Wong, "Topologies for vsc transmission," in *AC-DC Power Transmission, 2001. Seventh International Conference on (Conf. Publ. No. 485)*, Nov. 2001, pp. 298–304.

[82] B. Gemmell, J. Dorn, D. Retzmann, and D. Soerangr, "Prospects of multilevel vsc technologies for power transmission," in *Proc. IEEE/PES Transmiss. Distrib. (T&D) Conf. Exposition*, pp. 1–16, Apr. 2008.

[83] H. Dommel, "Digital computer solution of electromagnetic transients in single- and multiphase networks," *IEEE Trans. Power App. Syst.*, vol. PAS-88, no. 4, pp. 388–399, Apr. 1969.

[84] R. Kuffel, J. Giesbrecht, T. Maguire, R. Wierckx, and P. McLaren, "Rtds-a fully digital power system simulator operating in real-time," in *Proc. WESCANEX 95. Commun., Power, and Comput. Conf.*, vol. 2, pp. 300–305, May 1995.

[85] R. Kuffel, J. Giesbrecht, T. Maguire, R. Wierckx, and P. McLaren, "Rtds-a fully digital power system simulator operating in real-time," in *Proc. First Int. Conf. Digital Power Syst. Simulators (ICDS '95.)*, pp. 19–24, Apr. 1995.

[86] R. Kuffel, J. Giesbrecht, T. Maguire, R. Wierckx, and P. McLaren, "Rtds-a fully digital power system simulator operating in real-time," in *Proc. Int. Conf. Energy Management and Power Del. (EMPD '95.)*, vol. 2, pp. 498–503, Nov. 1995.